Engineered Science

REVIEW PAPER View Article Online

Recent Advances in Resistive Switching Materials and Devices: From Memories to Memristors

Gang Liu,[1] Yu Chen,[2,*] Shuang Gao,[1] Bin Zhang,[2] Run-Wei Li[1,*] and Xiaodong Zhuang[3]

Resistive switching devices have not only been considered as an emerging candidate for the next generation information storage technology, but also demonstrated great potential for in-memory computing systems with greatly enhanced computation capability. This review focuses on the recent advances in resistive materials and devices. We first describe the electric field-induced filamentary conduction model that accounts for the resistive switching behavior observed in inorganic materials, as well as the novel electric field-engineering strategy that is used to optimize the device structure and the memory performance. The alternative ways of using organic and hybrid materials to construct resistive switching devices are then illustrated. By tuning the charge transfer interaction and solid state electrochemical redox properties in small molecules, polymer, metal-organic framework and organic-inorganic hybrid perovskite materials, bistable and multibit memories, as well as the biomimicking memristors have been fabricated. Finally, we discuss the future development of the resistive switching materials and devices, aiming to clarifying the key issues that hinders its practical applications.

Keywords: Resistive switching; Memory; Memristor; Information storage; Information processing

Received 19 September 2018**, Accepted** 28 October 2018

DOI: 10.30919/es8d779

1. Introduction

As the cornerstone of the modern information technology, the development of memory devices with high speed, large capacity, long life time, low power consumption and ease of operation characteristics is beneficial for the fast revolution of the digital world.[1,2] Due to the limitation of the state-of-the-art semiconductor manufacturing technology, modern computer systems usually adopt the hierarchy of volatile and non-volatile storage, as well as the von Neumann architecture in which the microprocessors and the data storage devices exist individually,[3] to achieve the optimal trade-off between the computation performance and the costs.[4] However, shuttling information between the microprocessor and different levels of the memory hierarchy usually incurs significant latency and power consumption.[5] Thus, it is an urgent task to develop novel information storage techniques based on new materials and new mechanisms to overcome the von Neumann bottleneck problem and to enhance the computers' capability when dealing with more and more complicated tasks.

Resistive random access memory (RRAM) is an emerging information storage technology that shows current switching with large ON/OFF ratio in metal/insulator/metal (MIM) sandwich structures (Fig. 1a).[6] With the advantages of simple structure and fabrication process, high storage density and compatibility with CMOS technology,[7,8] RRAM devices can be tightly integrated with the microprocessor in the same chip to shorten the inter-level vias path and lower the access latency.[9] Since Year 2009, International Technology Roadmap for Semiconductors (ITRS) has selected RRAM as one of the most emerging candidates for the next generation memory technology.[10] Very recently, it is also demonstrated that the memristor devices, with the incremental change of device resistance and a relatively lower ON/OFF ratio in a similar MIM structure, can be used for in-memory computing applications (Fig. 1b).[11]

Over the past decade, great efforts have been devoted to the design, fabrication and properties-tuning of resistive switching materials.[12-14] A series of inorganic and organic materials have been developed to achieve high-performance resistive switching memory and memristor applications.[15-54] In this account, we will briefly review the recent research progress of the inorganic resistive switching materials, followed by the organic memory and memristor materials. Finally, a short perspective of the future development of the resistive switching materials, which may attract considerable amount of interest in both the industrial and academic communities, is addressed at the end of this article.

2. Inorganic Resistive Switching Materials and Devices

2.1 Resistive Switching Mechanisms in Inorganic Materials

In the early stage of RRAM research, it was proposed and widely accepted that the resistive switching behavior closely relies on the transport and electrochemical reactions of mobile cations or anions in inorganic metal oxide insulating layers to form filamentary

[1]*Key Laboratory of Magnetic Materials and Devices Ningbo Institute of Materials Technology and Engineering Chinese Academy of Sciences, Ningbo, 315201, China*
[2]*Key Laboratory for Advanced Materials Institute of Applied Chemistry School of Chemistry and Molecular Engineering East China University of Science and Technology 130 Meilong Road, Shanghai 200237, China*
[3]*College of Chemistry and Chemical Engineering Shanghai Jiaotong University 800 Dongchuan Road, Shanghai 200240, China*
***E-mail:** runweili@nimte.ac.cn ; chentangyu@yahoo.com*

Gang Liu

Gang Liu *is currently a full Professor at the Ningbo Institute of Materials Technology and Engineering, Chinese Academy of Sciences. After receiving his Ph.D. degree from the National University of Singapore in 2010, he worked as a research associate at the Nanyang Technological University and then as a research fellow at the National University of Singapore from January 2010 to August 2012. In August 2012, he joined the CAS Key Laboratory of Magnetic Materials and Devices of NIMTE. His research interests include the design and fabrication of resistive switching materials, as well as their applications in electronics and optoelectronics.*

Shuang Gao

Shuang Gao *is currently an Assistant Professor at the Ningbo Institute of Materials Technology and Engineering (NIMTE), Chinese Academy of Sciences (CAS). He received the B.S. degree from University of Science and Technology Beijing (USTB) in 2011 and then the Ph.D. degree from Tsinghua University in 2016. His current research interests are mainly memristive materials and devices for wearable electronics and novel logic-in-memory as well as neuromorphic computing applications.*

Run-Wei Li

Run-Wei Li *is currently a full professor at the Ningbo Institute of Materials Technology and Engineering (NIMTE), the Chinese Academy of Sciences (CAS) and the director of CAS Key Laboratory of Magnetic Materials and Devices. After receiving his Ph.D. degree from the Institute of Physics, CAS in July 2002, he worked as a JSPS research fellow at the Osaka University. In September 2003, he moved to the Kaiserslautern University as an Alexander von Humboldt research fellow. Since March 2008, he has been "One Hundred Talents" professor of CAS. His research work is mainly focused on the functional materials and devices for new types of storage and sensors.*

Yu Chen

Yu Chen *is a full professor at East China University of Science and Technology in Shanghai. He received his Ph.D. in Organic Chemistry under the direction of Prof. Dr. Zu-En Huang at Fudan University in July 1996. Since 1996 he has been a member of the Department of Chemistry at Fudan University wherein he spent 1.5 years earning his Associate Professor's position. Starting from February 2000, he took four-month German language Course in Geothe Institute at Schwaebisch Hall as an Alexander von Humboldt language scholar. He then joined Prof. Dr. Michael Hanack's group at the Institute of Organic Chemistry, University of Tuebingen, as an Alexander von Humboldt research fellow and as a research associate. At the end of October 2002, he moved to the Department of Materials Science and Engineering, University of Washington at Seattle, USA, and worked with Prof. Dr. Alex K. Y. Jen as a research associate. In February 2004, he joined the Professor Dr. Osamu Ito's group at the Institute of Multidisciplinary Research for Advanced Materials, Tohoku University at Sendai (Japan) as a research scientist of CREST, JST. He has published 210 papers, reviews and communications, of which more than 160 papers were published in the international peer-review journals such as Chem. Soc. Rev., Prog. Mater. Sci., Angew. Chem. Int. Ed., J. Am. Chem. Soc., Adv. Mater., Adv. Funct. Mater., Mater. Horizons, Chem. Mater. and others. His main research interests include organic synthesis; Organic and/or polymeric functional materials designed for nonlinear optics, OLED/PLED, organic solar cells, molecular memory devices; fullerene chemistry; phthalocyanine chemistry; and photo-induced electron transfer processes of conjugated polymers.*

Bin Zhang

Bin Zhang *is currently an associate professor at East China University of Science and Technology (ECUST). He obtained his B. S. degree in Applied Chemistry and Ph.D degree in Advanced Materials Processing and Manufacturing in 2008 and 2013, respectively, both from ECUST under the supervision of Prof. Yu Chen. Then he worked as a research fellow in Prof. En-Tang Kang's group at the National University of Singapore from May 2013 to July 2015. In September 2015, he joined the Institute of Applied Chemistry at ECUST. His current research interests focus on the surface modification of 2D materials, design and preparation of electroactive functional materials for memristor.*

Xiaodong Zhuang

Xiaodong Zhuang*, a synthetic material chemist, is presently a full professor of Shanghai Jiao Tong University in China. He is the founding deputy editor-in-chief of PhysChem, and serves as editorial board member for several scientific journals. Zhuang's research interests include rational designed two dimensional soft materials and carbon-rich porous materials for energy storage and conversion, e.g. metal-air batteries, supercapacitors, and catalytic carbon dioxide conversion, hydrogen evolution reaction, oxygen reduction reaction, etc. So far, he has published more than 130 peer reviewed papers with citations over 5800 times and h-index of 38.*

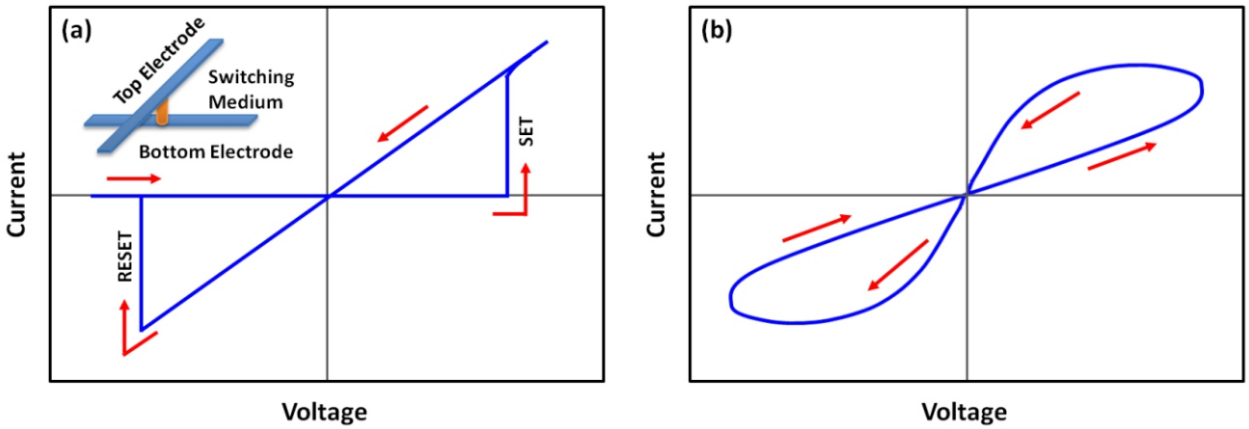

Fig. 1 Resistive switching behavior with (a) digital- (abrupt) and (b) analog- (incremental) type of changes in the current-voltage (I-V) characteristics of the electrode/insulator/electrode structured devices (inset of a).

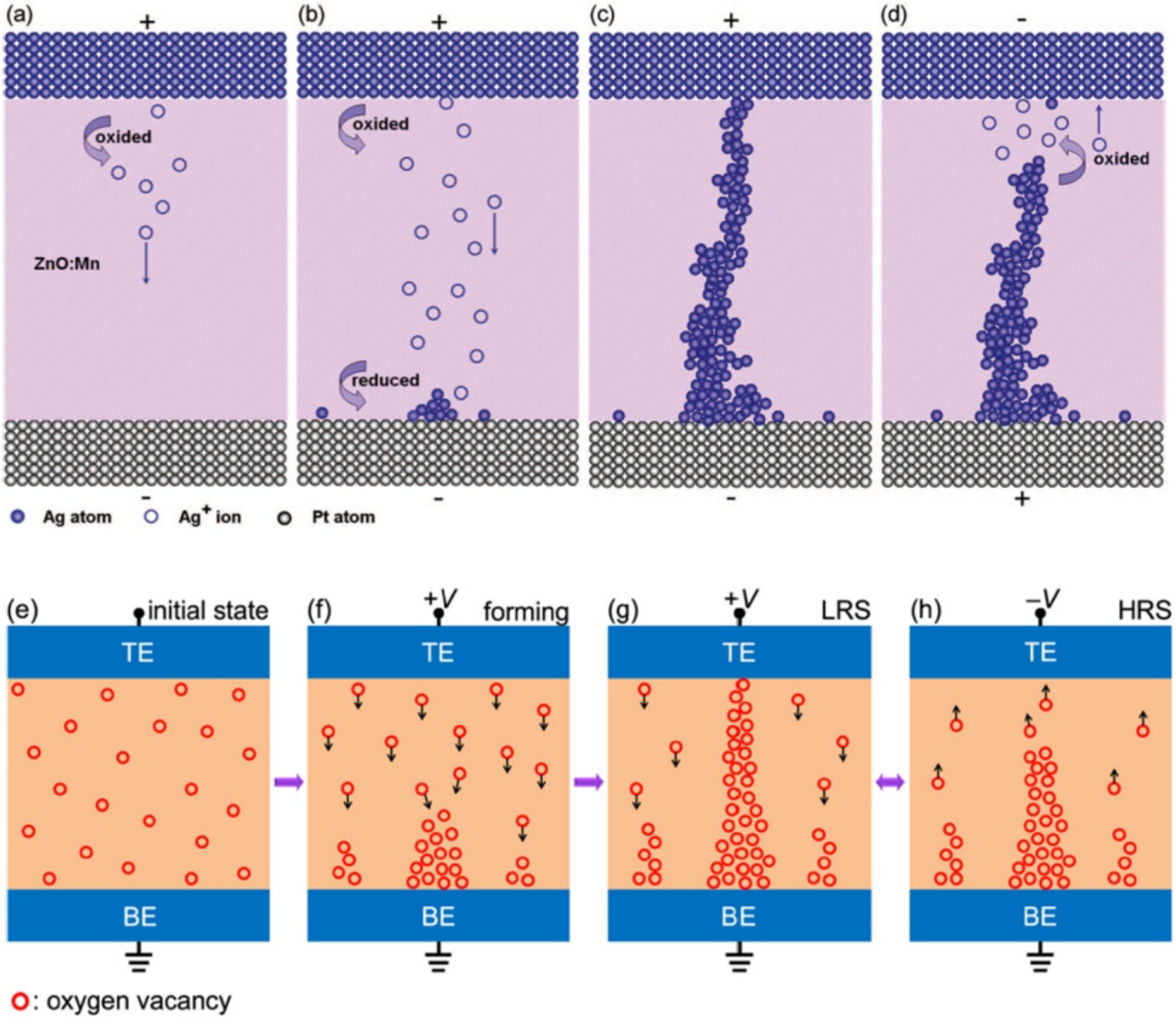

Fig. 2 Schematic illustration of the resistive switching mechanisms of the (a-d) electrochemical metallization (ECM) devices and the (e-h) valence change memory (VCM) systems. Reproduced with permission from Ref 8 and 104.

conductive pathways, the reversible generation and annihilation of which modulate the device conductance/resistance significantly.[55-57,12-14] Various ionic conducting or insulating materials, starting from $RbAg_4I_5$, AgI, Cu_2S, to SiO_2, ZnO, HfO_2, TiO_2, Ta_2O_5 and etc, are involved in intensive studies of the conductive filament evolution kinetics and the device functionality.[58-62] When approaching nanoscale, both the material performance and system properties of the resistive switching cells are significantly modulated by quantum effects, excess surface free energy of atoms or atomic clusters, and nonlinear mesoscopic transport phenomena owing to the confinement of the devices in both the vertical and lateral directions. In order to establish a theoretical relationship that links the ionic based resistive switching characteristics and the redox activities, R. Waser and I. Valov adopted the nanobattery model with non-equilibrium states to understand the dynamic behavior of the nanoscale resistive switching memories and categorize the devices into electrochemical metallization systems and the valence change systems.[7,63-66] The electrochemical metallization (ECM) devices are also called conductive bridging (CB) cells, wherein the electrochemical metal deposition and dissolution is employed purposely to induce the resistive switching.[67,68] Such devices are usually constructed from an electrochemically active metal electrode, a solid electrolyte layer and an electrochemically inert counter electrode (Figs. 2a-d). Under positively biased voltage or electric field, Ag, Cu, or Ni electrode metals can be anodically ionized, dissolved and injected into the electrolyte insulator. The cations migrate across the insulating layer under the action of the high electric field (generally 10^8 V/m) and are reduced into metallic atoms by the electrons injected from the counter electrode through a cathodic metallization reaction. Depending on the mobility of the cation inside the solid electrolyte, the reduction of the ions and nucleation of the metal atomic clusters can occur either at the surface of the inert electrode or inside the insulating later, giving rise to conical shaped conductive filaments pointing towards the anode or cathode respectively. In case that the electrochemically active metal electrodes are missing in the electrode/insulator/electrode sandwich structure, the migration of oxygen anions (vacancies) and the reduction of the native metal ions inside the insulating layer may also lead to the formation of elemental metal or conductive metal suboxide filaments and resistive switching characteristics (Figs. 2e-h). Since such switching behaviors involves the valence changes of the native metal ions that constitute the insulating layer, the corresponding devices are defined as valence change memories (VCM).[69-73]

Resistive switching phenomena in the ECM and VEM devices involves complex interplay between the physical, electrochemical and thermochemical processes of ionic species either occurring in the bulk insulator or at its interface with electrodes. Mechanistic insights into the nanoscale switching processes therefore play a crucial role in spurring the technological development of the devices, and are key factors to their further design and optimization. In order to probe the underlying processes and dynamics of resistive switching in details, plenty techniques based on imaging, spectroscopy, scanning probe and electrical approaches have been used and evaluated. In comparison, the electron beam and nanotip-based microscopy techniques demonstrates high spatial resolution for observing the morphological or microstructural variation, while the spectroscopic approaches are more suitable for determining the compositional and valent properties.[74-78]

The formation and evolution dynamics of the conductive filaments can be visualized directly by imaging techniques including optical microscopy,[79] scanning electron microscopy (SEM)[75,80] and transmission electron microscopy (TEM),[72,75,76,81] with detailed information on the filament number, geometry, microstructure and chemical composition that are essential to understanding the switching mechanism in resistive switching devices. Due to the random formation of small size conductive filaments buried in confined space of the insulating layer, special care should be paid to conduct the microscopic observation at the precise switching region with sufficiently high resolution. It is noteworthy that currently there does not exist an ideal imaging technology that is capable of peering into a real, unmodified resistive switching device with sufficient spatial resolution to resolve the involved physical processes. In practice, modification to a real device, or building of a custom analog, has to be arranged to improve the imaging access, leading to inevitable differences to what is happening in real case. These differences can be critical in understanding the underlying mechanism of the imaged devices, or even changes their final functions. Thus, special care should be taken to conduct the imaging

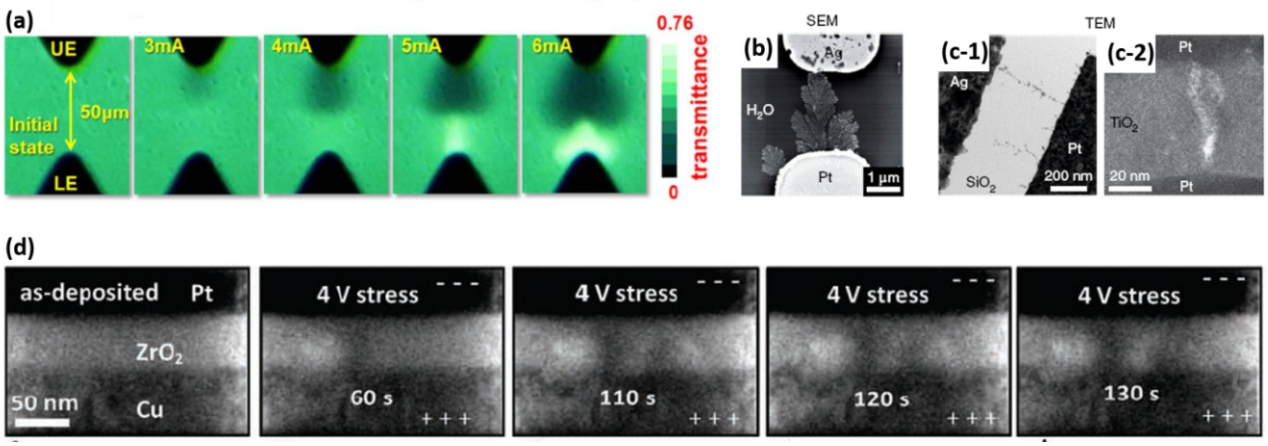

Fig. 3 Direct observation of conducting filaments in resistive switching memories. (a) Optical microscopy imaging of W_2O_5 filaments in an Au/WO_{3-x}/Au device with a planar configuration. (b) SEM observation of Ag filaments in an Ag/H_2O/Pt structure. (c-1) Bright-field TEM observation of Ag filaments in an Ag/SiO_2/Pt memristor and (c-2) dark-field TEM observation of an oxygen-deficient Magnéli filament in TiO_2-based VCM cells. (d) Dynamic growth of the conductive filament as visualized with a series of TEM images in an Cu/ZrO_2/Pt structure. Reproduced with permission from Refs 72, 75, 80, 101 and 105.

experiment, and compromise is necessary between the ideal real device and the sample for imaging.[82-100] The ease-of-operation and low-cost nature allow the optical microscopy a good choice for monitoring the relatively wider filaments with the dimension of several hundred nanometers to micrometers, and is usually applied to device with lateral structure and thus longer conductive filaments. For instance, the electric field-induced migration of oxygen species and the subsequent redox activities may not only lead to resistive switching characteristics, but also result in conductive filaments with electrochromic behavior that can be visually discriminated from the background color and readily captured by photo microscope. In 2014, Shang *et al* for the first time visualized the evolution of conductive filament directly by *in-situ* optical image technique based on the color-conductivity dependence of tungsten oxide in an Au/WO_{3-x}/Au planar structure (Fig. 3a).[79,101] As the device dimension scales down, electron beam based SEM and TEM observation are required to provide a much higher (e.g. 10^2 to 10^4 time compared with the optical microscopy) spatial resolution, while the formation of Ag dendrites have been recorded using SEM in Ag/H_2O/Pt (Figure 3b) and TEM in Ag/SiO_2/Pt planar structures (left panel of Fig. 3c), respectively.[75,80] More importantly, the evolution dynamics of the conductive filaments and intermediate states of resistive switching are also monitored through *in-situ* TEM observation.[74,75,80,81,102-106] Liu *et al* directly fabricated a complete Ag(or Cu)/ZrO_2/Pt resistive switching device on the platform of a tungsten probe used in TEM observation through a dual-beam focused ion beam (FIB) system, with which the device thickness and lateral size are reduced to allow the entire switching layer and its structural changes to be monitored at high magnification and at real time (Fig. 3d).[105] By using the dark-field imaging by diffracted electrons, Hwang *et al* successfully recorded the oxygen vacancy (V_o) conductive filaments in TiO_2-based VCM cells that are difficult to be visualized under the commonly adopted bright-field imaging (right panel of Fig. 3c).[72] In addition, the distinct crystalline structure or orientation of the V_o filament, such as the Magnéli phase buried in the rutile matrix, was also recorded for the first time. Such important information is crucial for understanding outstanding endurance of many oxide based memories, and facilitates in the future design and optimization of high-performance devices.[103,107]

Collecting and analyzing the electrons excited or transmitted from the samples under high energy beam illumination, the spectroscopic approaches including energy dispersive X-ray spectroscopy (EDS), electron energy loss spectroscopy (EELS) and X-ray photoelectron spectroscopy (XPS) are capable of identifying the composition, bonding and/or oxidative state, electronic structure and local environment of the conductive filaments inside the

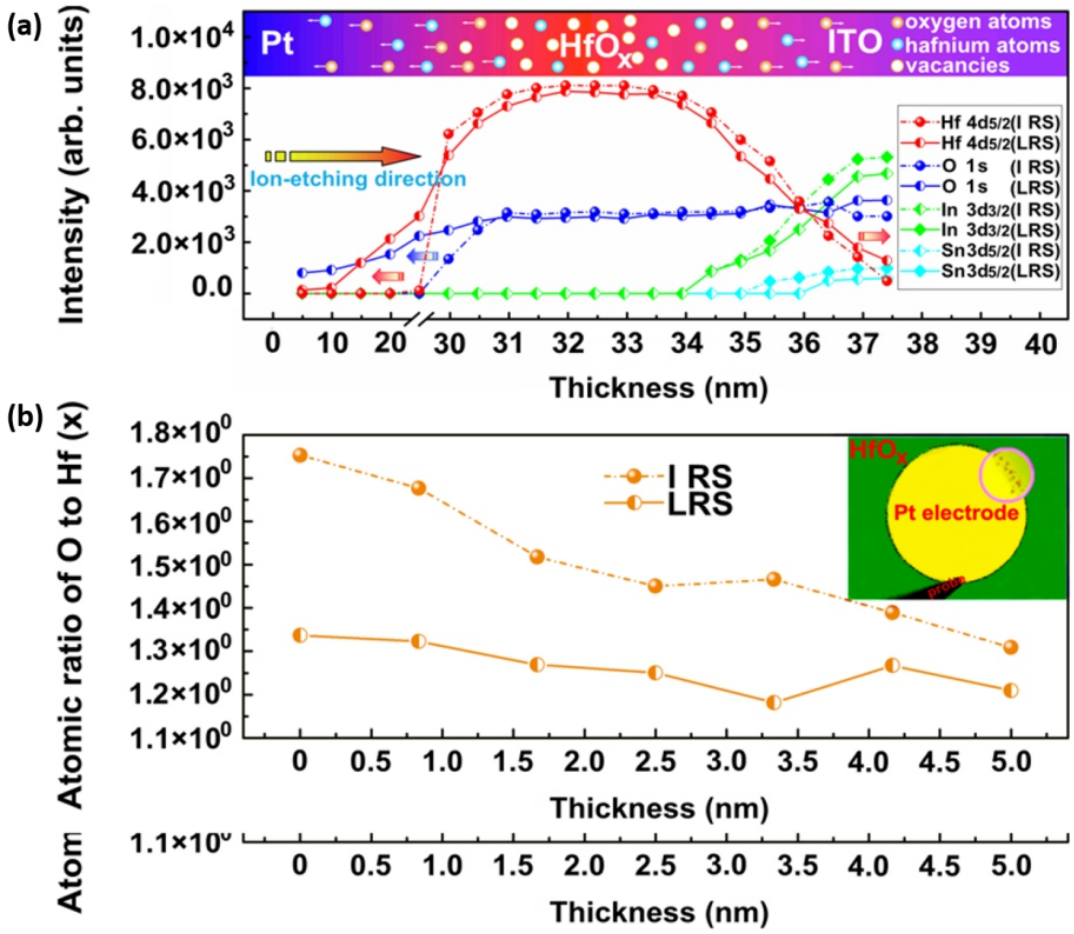

Fig. 4 (a) Distribution of the constituent elements and (b) the O:Hf ratio of the Pt/HfO_x/ITO structure in the initial and low resistance states, respectively. The data sets are retrieved from the XPS depth-profiling of the switching device. Inset of (b) shows the optical microscopic image of the Pt circular electrode after 10 consecutive switching cycles showing the minor degradation of the electrode edges. Reproduced with permission from Ref 23.

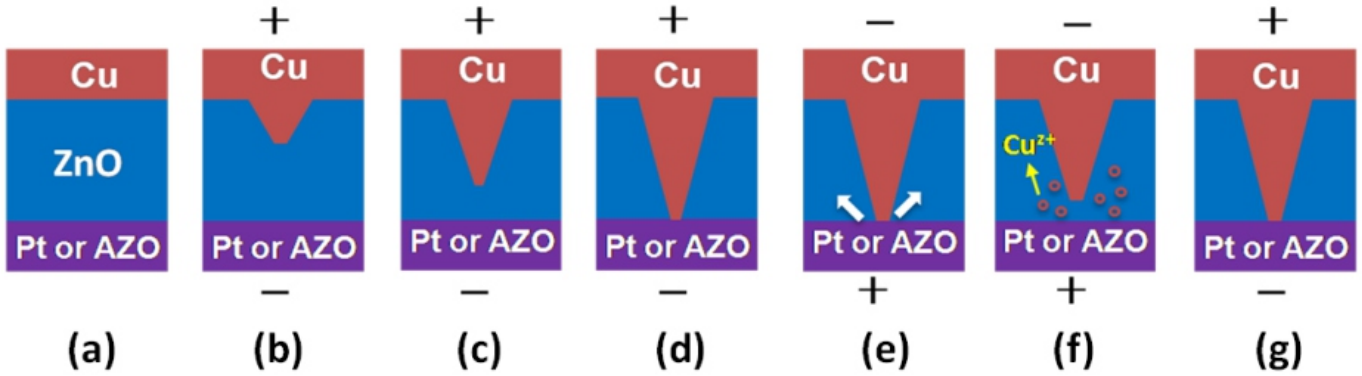

Fig. 5 Schematic illustration of evolution process of the metallic conduction filaments, including (a) the pristine state, (b-d) growth of the filament towards the cathodes, (e,f) annihilation and (g) regeneration of the nanoscale conducting filaments. Reproduced with permission from Ref 18.

insulating layers through spectral, linescan and depth profiling measurements.[58,75,76,78,102,104,108-112,23,48] Among these methods, the EDS[58,75,78,102,104,109] and EELS[76,108,110,113,114] are sensitive to heavier and lighter elements, respectively, and are thus usually used *in-situ* with high-resolution TEM observation to further probe the structural, chemical and environmental properties of the cation and anion based resistive switching devices. Shang *et al* employed ion-etching treatment and XPS depth-profiling analysis on Pt/HfO_x/ITO cells in their initial high resistance state (IRS) and low resistance state (LRS) to monitor the chemical composition change of the switching layer (Fig. 4).[23,112] It is observed that the non-lattice oxygen anions of the non-stoichiometric hafnium oxide can migrate under the electric fields towards the electrodes, resulting in the decrease of oxygen content in the switching thin film. After transition to the LRS, the O:Hf atomic ratio of the bulk film decreases significantly, which suggest that the migration of oxygen ions dominates the formation and rupture of conductive filaments. The LRS hafnium oxide film has an increased concentration of Hf^0 and $HfO_{1.22}$ components, confirming that elemental hafnium and conductive hafnium suboxide participate in the formation of the conductive filaments in the HfO_x switching layer.

Parallelly, fundamental electrical measurements, in conjunction with the energy band diagram of the memory devices, can be used to probe the resistive switching phenomena. Peng *et al* constructed resistive switching devices with the asymmetric sandwich structure of Cu/ZnO/Pt and Cu/ZnO/Al-doped ZnO (AZO), and investigated the relationship between the OFF-state I-V curve and the device energy band diagram.[18] It was found that the revolution of the conducting filament and the observed resistive switching phenomena probably consists of four stages, for instance, the (1) electric field-induced oxidization of the electrode metal atoms to cations, (2) directed migration of the cations towards the cathodes, (3) reduction of the cations to metal atoms at the counter electrode and (4) growth, annihilation and regeneration of the nanoscale conducting filaments (Fig. 5). The conducting filament rupture and rejuvenation usually occur at the cathode, i.e., ZnO/Pt (or AZO) interface, with its shape being conical where the wider and narrower ends are formed at the anodic (Cu) and cathodic (Pt or AZO) interfaces, respectively. By monitoring the local conducting properties of the switching layer through C-AFM technique, it is revealed that the migration of ions and formation of conducting filaments occur at the grain boundaries,[19,116-118] and the operation voltage and the speed of the RRAM devices are both closely related to the grain size, concentration of the mobile cations and their distances to the grain boundaries. With these comprehensive understanding on the variety of mobile ions, their respective migration paths, dynamics and redox activities, a semi-quantitative model has been established to provide universal guidance for developing high-performance resistive switching materials and devices.

2.2 Inorganic Resistive Switching Materials and Memory Devices

The most widely explored application of the resistive switching phenomena is the nonvolatile bistable memories. Over the past two decades, great efforts and plenty of work have been made on resistive switching memories. Herein we are not going into a comprehensive review on this area, since there are already many good review articles and books that can be referred to.[119-122] only a few examples of high-performance inorganic resistive switching materials and their application in information storage are re-evaluated.

Due to the large dielectric constant of around 25,[123] hafnium oxide is considered as a promising candidate replace the silicon oxide gate insulator in field-effect transistors or charge-storage dielectric in DRAM capacitors,[124] while the wide band-gap of approximately 6 eV offers a transparent optical window over the IR to deep-UV (10 μm ~200 nm) solar irradiation spectrum.[126] By incorporating high-κ hafnium oxide into resistive switching memories, the leakage current can be effectively suppressed by reducing the grain boundary leaking paths of polycrystalline films,[127] consequently giving rise to an even thinner switching layer with both function density. The optical transparency and thermal stability (melting point approaching 2800 °C) also make hafnium oxide highly reliable against thermal shock when used in specific occasions.[128] Upon selecting the high κ hafnium oxide (HfO_x) of ~5 nm as switching layer and indium-tin oxide (ITO) as the electrode, Shang *et al* demonstrated by the low-temperature transport measurements that the electric field-induced migration of oxygen ions can lead to the aggregation of metallic hafnium into nanoscale conduction channels (Fig. 6).[23] By deliberately optimizing the thin film depositing process, the as-obtained HfO_x layer carries amorphous-nano crystalline mixed structure and roughened interface at the ITO bottom electrode, which in turn generate uniformly distributed local electric field in the switching layer. As a result, the ITO/ HfO_x/ITO device is forming-free, with its variation coefficient of the programming voltage being less than 4.3%. The device can be switched for more than 10^7 cycles, and the ON/OFF ratio only

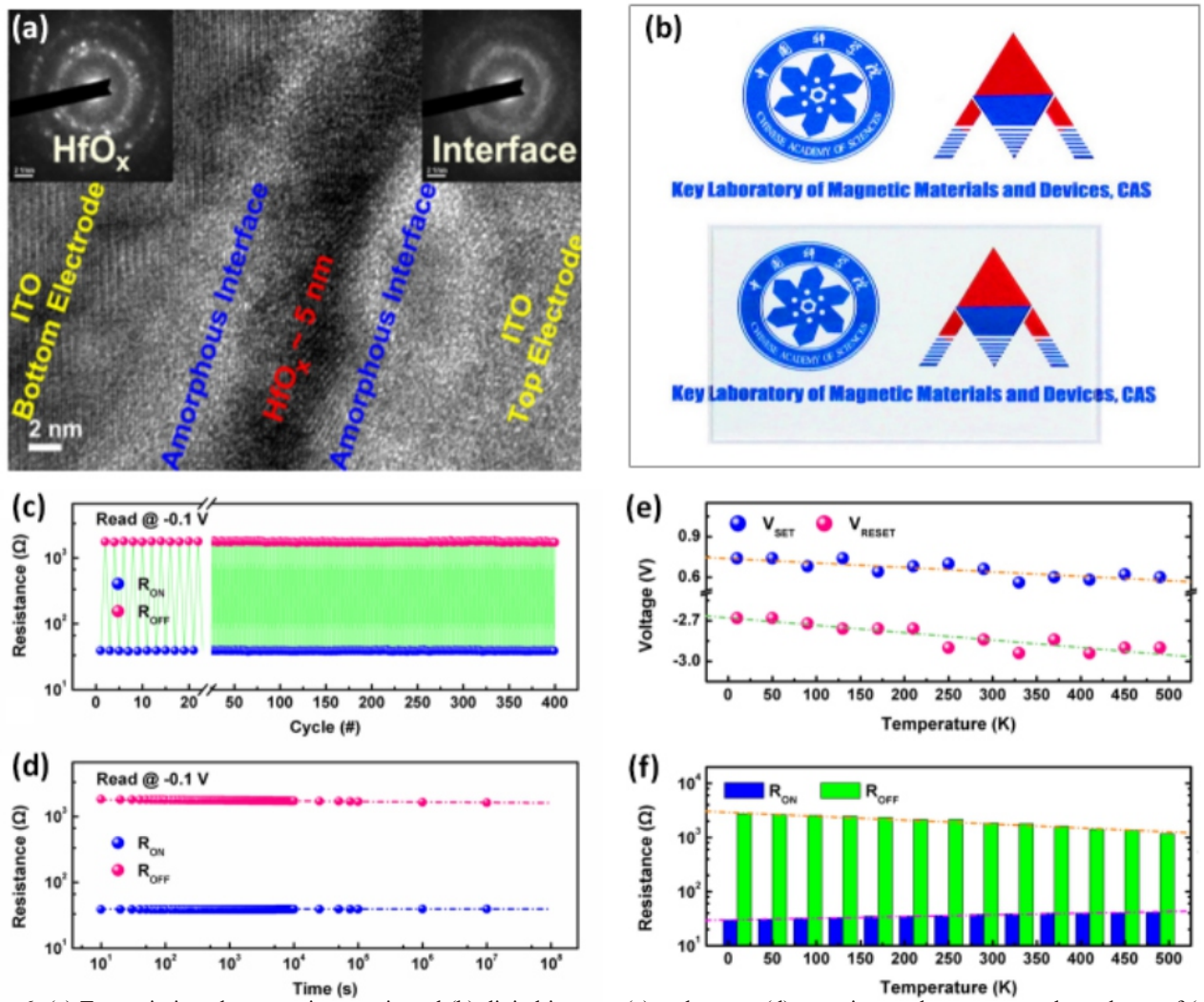

Fig. 6 (a) Transmission electron microscopic and (b) digital images, (c) endurance, (d) retention, and temperature dependence of (e) the switching voltage and ON/OFF state resistances of the ITO/HfO_x/ITO device. Reproduced with permission from Ref 23.

decays for ~17.6% after ten years of operation. Moreover, the all-oxide structure demonstrates promising optical transparency in the near ultraviolet-visible-near infrared spectrum (200 nm ~ 2000 nm) of the solar irradiation, and remains stable in the broad temperature range of 10 K- 490 K (or ± 240 °C), therefore allowing its usages under severe working conditions, e.g., in outer space and etc.

The elaborate evolution of conducting filament *via* local ion motion and electrochemistry in atomic-scale region of the resistive switching material may on the other hand generate atomic point contact (APC) structures showing quantized conductance (QC).[129-139] The stepwise development of device conductance in the unit of G_0 = 77.5 uS, associated with atomic reconfiguration and one-dimensional confinement of electrons during transport in the quantum constriction of APC,[140-142] greatly decorates the bistable resistive switching features of memory devices and directly engenders higher memory density through multibit storage. For instance, by regulating the electric field inside the switching medium to control the migration of metal ions, Zhu *et al* are capable to construct APC nanostructures in the ZnO based resistive switching devices and for the first time observed room-temperature quantized conductance phenomena at the critical state of the filament formation and annihilation.[20] With the unit of $G_0 = 2e^2/h$, where e is an electron charge and h is the Planck's constant, the conductance of the Nb/ZnO/Pt device shows stepwise increases from G_0 to $8G_0$ when swept in the positive biased SET process (Fig. 7a). Further analysis of hundreds of I-V curves shows that most of the conductance changes occur at the integer multiples of G_0, suggesting that discrete quantum channels are formed in the devices (Fig. 7b). Due to the bipolar resistive switching characteristics of the Nb/ZnO/Pt device, quantized decrease of the device conductance in the integer multiples of G_0 is also observed during the RESET process. Hence, multibit memory can be made possible to enhance the storage density of the memory devices upon effective modulation of the revolution of the monoatomic chains in the switching medium. With niobium (a high temperature superconducting metal) as the top electrode, the local distribution of the conducting channel on the nanoscale and the ON state superconducting feature of the device are investigated, confirming that the observed room-temperature quantized conductance is arising from the artificial metallic nanostructure (Fig. 7c). Moreover, when magnetic electrodes such as cobalt are used, significant tunneling magnetoresistance arising from the controllable formation of Co filaments are also observed in resistive switching Co/ZnO/Fe structures (Fig. 7d).[21]

In order to achieve ultrahigh storage density with resistive

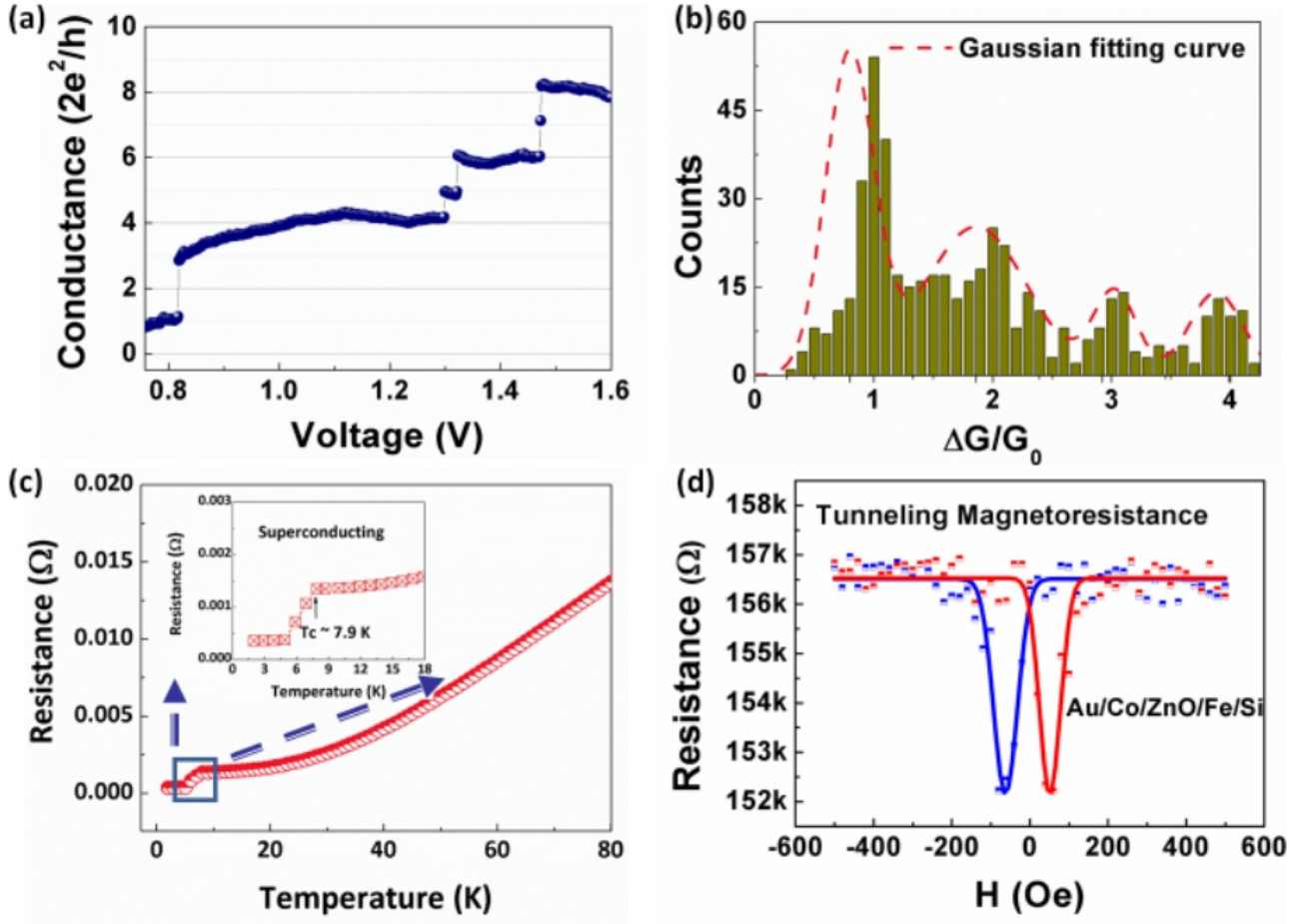

Fig. 7 (a) Resistive switching behavior of the Nb/ZnO/Pt device showing quantized conductance. (b) Histogram of the conductance change ΔG. Dotted lines shows the Gaussian fitting curve of the histogram. (c) Temperature dependence of the device resistance showing superconducting behavior. (d) Tunneling magnetoresistance behavior of the Co/ZnO/Fe device. Reproduced with permission from Refs 20 and 21.

switching memories, the devices are usually arranged in two-dimensional crossbar array and stacked into three-dimensional chips, in which the sneak path currents from the neighboring LRS cells during reading or writing a designated HRS cell can severely impede the proper operation of the array.[143-145] Several access devices, including transistors, diodes and etc have been utilized to solve this circuit issue at each cross point of the array,[146,147] while the two-terminal thin film based selector devices distinguish themselves with easy integration with the resistive switching memory. Owing to the reversible transition between the metallic and insulating states (MIT) and the concomitant threshold resistive switching behavior, vanadium dioxide (VO_2) appears a promising candidate for selector devices.[148] However, the heat- or electric-field-induced VO_2 MIT occurs mostly as an in-plane random 2D percolative behavior through the entire sample,[148] while the inhomogeneous coexistence and cascading evolution of multiple transitioning nanodomains of the tetragonal metallic and monoclinic insulating phases usually lead to avalanche multistep jumps in the transition with much reduced sharpness and uniformity.[149,150] In order to reduce the transition parameter fluctuation for practical applications, Xue et al succeeded in developing one-dimensional VO_2 nanochannel directly *via* electrical-field induced ion migration in V_2O_5 thin film devices for the first time.[151] A reliable MIT behavior with a sharp turn-on voltage slope of <0.5 mV dec^{-1}, fast switching speed of 17 ns, low energy consumption of 8 pJ and low variability of <4.3% is demonstrated in the VO_2 nanochannel device. High-resolution TEM observation and first principles calculation verify that the observed outstanding electrical properties can be attributed to the confinement of MIT in the electroformed VO_2 nanochannel in V_2O_5 thin films. The series connection of the present device with a Pt/HfO_2/Pt/memory cell can ensure the correct reading of the memory for 10^7 cycles continuously, therefore demonstrating its potential use in high-density crossbar memory arrays.

To further lowering the OFF state current and increase the selectivity of the selector for very large scale crossbar arrays, Yang *et al* employed engineered materials by doping fast diffusive species into the dielectric to improved the I-V nonlinearity and transition slope.[152-155] Two types of metal–insulator–metal (MIM) structures, asymmetric Pd/HfO_x/Ag and symmetric Pd/Ag/HfO_x/Ag/Pd crosspoint stacks, were prepared and demonstrates extremely high selectivity of 10^{10}, steep turn on slope of <1 mV dec^{-1}, high endurance beyond 10^8 cycles, and fast ON/OFF switch speed within 75/250 ns (Fig. 8). In particular, the symmetric Pd/Ag/HfO_x/Ag/Pd exhibits an interesting symmetric bidirectional threshold switching behavior, and functions as a reliable selector when being stacked on top of a Pd/Ta_2O_5/TaO_x/Pd resistive switching memory. Microscopic analysis of a nanoscale device reveals the tunneling current between the discontinuously distributed Ag nanostructures over the hafnium

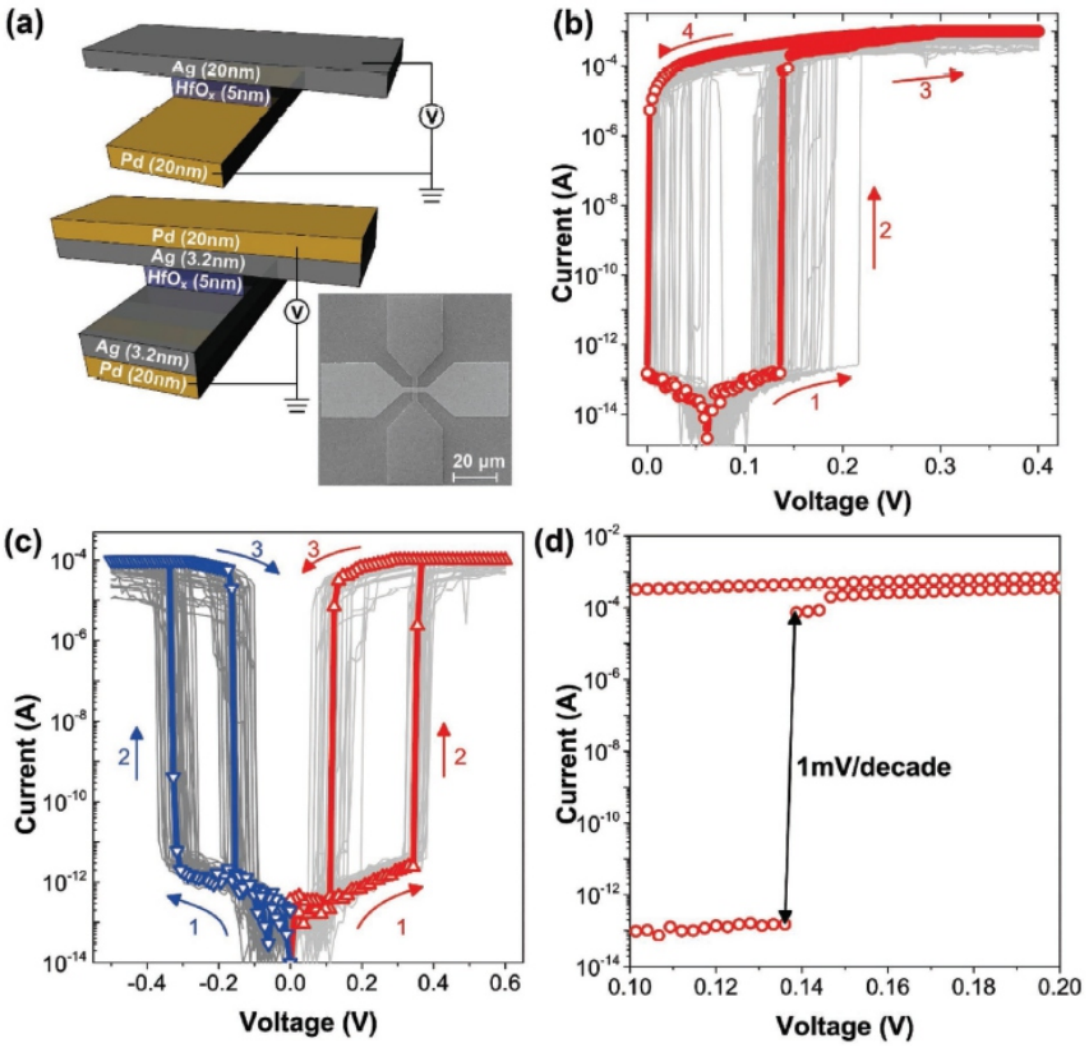

Fig. 8 HfO_x-based threshold switching devices showing large ON/OFF ratio and steep transition slope. (a) Schematics of the asymmetric and symmetric device structures. The inset shows an SEM image of the crosspoint device. (b) The DC I–V characteristic of the asymmetric Pd/HfO_x/Ag selector yields a selectivity of 10^{10}. (c) Consecutive 50 cycles of DC voltage sweep with positive biasing followed by 50 cycles of DC sweep with negative biasing on the symmetric Pd/Ag/HfO_x/Ag/Pd showing bidirectional threshold switching behavior with an ON/OFF ratio of 10^8. (d) Device shows an ON switching slope of ≈1 mV dec^{-1}. Reproduced with permission from Ref 134.

oxide matrix, together with the noticeable structural deformation and new appearance of nanocrystalline *m*-HfO_2 account for the observed ultrahigh selectivity in the Pd/HfO_x/Ag and Pd/Ag/HfO_x/Ag/Pd threshold switching devices. In the meanwhile, Liu *et al* also found that the employment of impermeable graphene layer with controlled defect dimensions to control the injection path and amount of silver cations into the switching matrix, the formation of discontinuous Ag nanostructures can also be achieved in Ag/structural defective graphene/SiO_2/Pt structured devices with low OFF state current of 10^{-12} A, a selectivity of 5×10^8, and a sharp switching slope of 1 mV dec^{-1} (Fig. 9).[156,157] Further increasing in the defect size while maintain the small numbers of defects that are deliberately controlled in the graphene layer, small numbers of strong Ag conductive filaments can be formed under low compliance current through CF distribution centralizing, therefore offering a simple yet effective approach to solving the current-retention dilemma that the CF stability deteriorates greatly with decreasing compliance current. When the impermeable graphene is moved from the Ag/SiO_2 interface to the SiO_2/Pt interface, the over injection of the silver cations into the bottom electrode layer can be effectively hindered, therefore eliminating the miss negative-SET behavior during the normally reset process and enhancing the reliability of the memory devices.

2.3 In-Memory Computing with Inorganic Resistive Switching Materials and Devices

In 1971, circuit theorist Leon Chua at UC Berkeley envisioned that there must be a fourth circuit element beyond the resistor, capacitor and inductor to correlate the electric charge and magnetic flux, when reexamining the symmetry relationship between the six mathematical relations that correlate the four fundamental circuit variables of electric current *i*, voltage *v*, charge *q* and magnetic flux φ.[158,159] He named the element as memristor (memory-resistor), with its behavior defined by

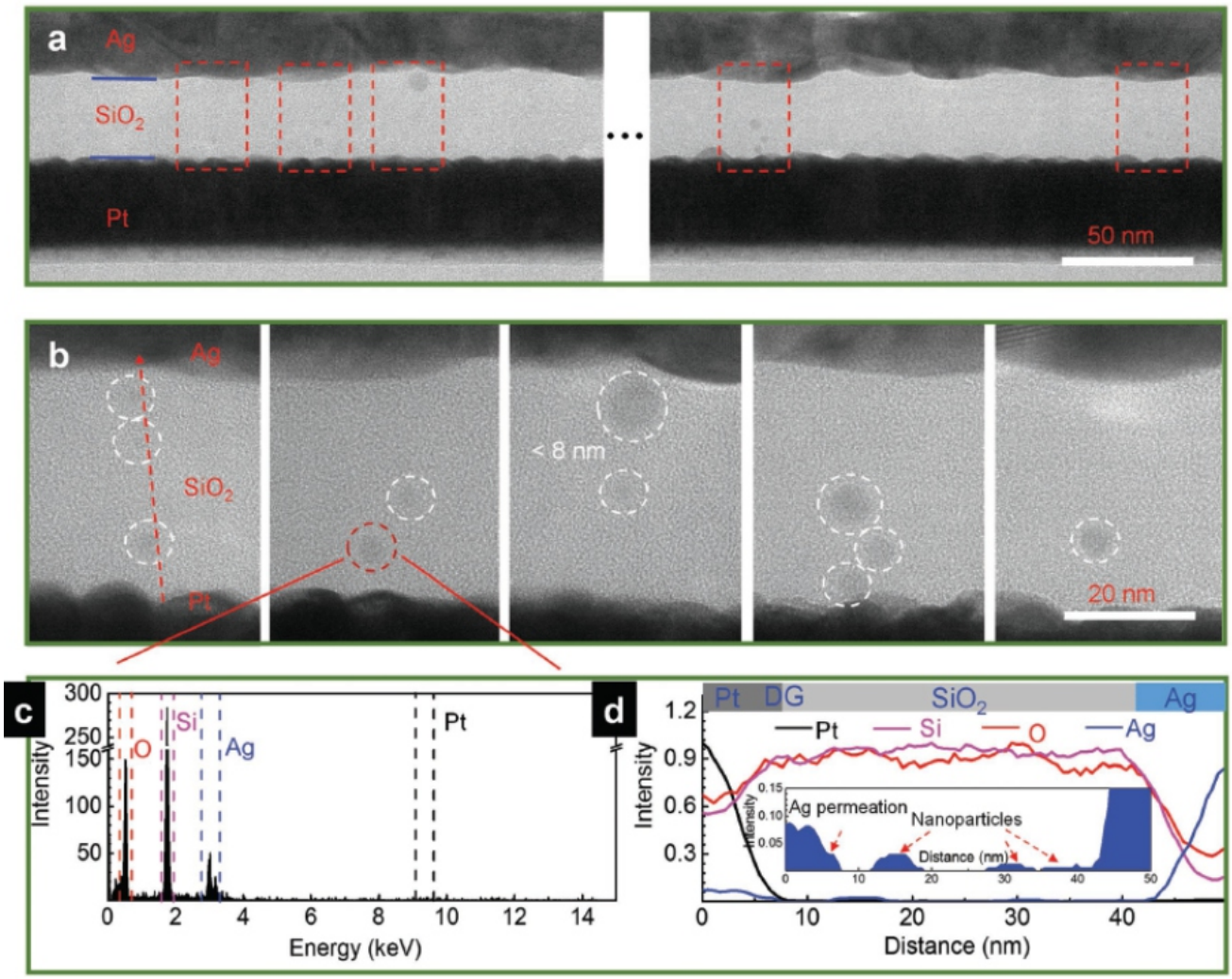

Fig. 9 HRTEM and EDS tests of the Ag/structural-defective graphene/SiO_2/Pt device after threshold switching operations under 500 μA compliance current. (a) TEM image of the two discontinuous parts of the device, in which several nanoparticle groups are marked by red dashed squares. (b) Enlarged HRTEM images of the discrete nanoparticles in (a) with 1-8 nm diameters. c) EDS element analysis of the nanoparticle marked by red dashed circle in (b). (d) Normalized EDS line scan of Pt, Si, Ag, and O elements at the discontinuous nanoparticle CF marked by the red dashed arrow in (b) while the inset shows the enlarged line scan of the Ag peak intensity. Reprint with permission from Ref 137.

the following equations:

$$i = G(w, v)\, v \tag{1}$$

$$\frac{dw}{dt} = f(w, v) \tag{2}$$

where w can be one or one set of internal state variable(s), G G is the generalized conductance that depends on the internal states of the device, and f is a function of time. As a nonlinear device whose internal state variable w (for instance q) and device conductance are time integrals of the instantaneous state (w) and input v, memristor naturally exhibits a history dependent I-V characteristic that cannot be simply duplicated with any combination of the resistors, capacitors and inductors. Experimentally, a memristor should have an electrode/insulator/electrode sandwich structure, which is exactly the same as that of resistive switching memories. Such devices have not been physically implemented untill 2008, when researchers at HP Lab announced the first memristor made from titanium oxide.[160] Plenty of efforts followed to investigate the memristive behaviors of various materials ranging from metal oxides, amorphous silicon, nitrides, sulphides, iodides, selenides, tellurides, chalcogenides, and etc.[25,72,73,161-166]

The original definition of memristor was further extended by Leon Chua in 2011, whereas all two-terminal systems with a frequency-dependent and pinched hysteretic loop confined to the first and third quadrants of the I-V plane are memristors.[167-169] With this broadened definition, it is immediately realized that resistive switching memories are particular digital cases of the memristors that exhibit binary conductance states. Characterized by the continuous and incremental change of device conductance or resistance, memristors with analog-type switching behaviors have recently triggered the research campaign of the novel in-memory computing paradigm including neuromorphic computation and logic applications.[11,170-184] Nonconventional computing architectures constructed from memristors can potentially offer great computing capability through massive parallelism at extremely low energy

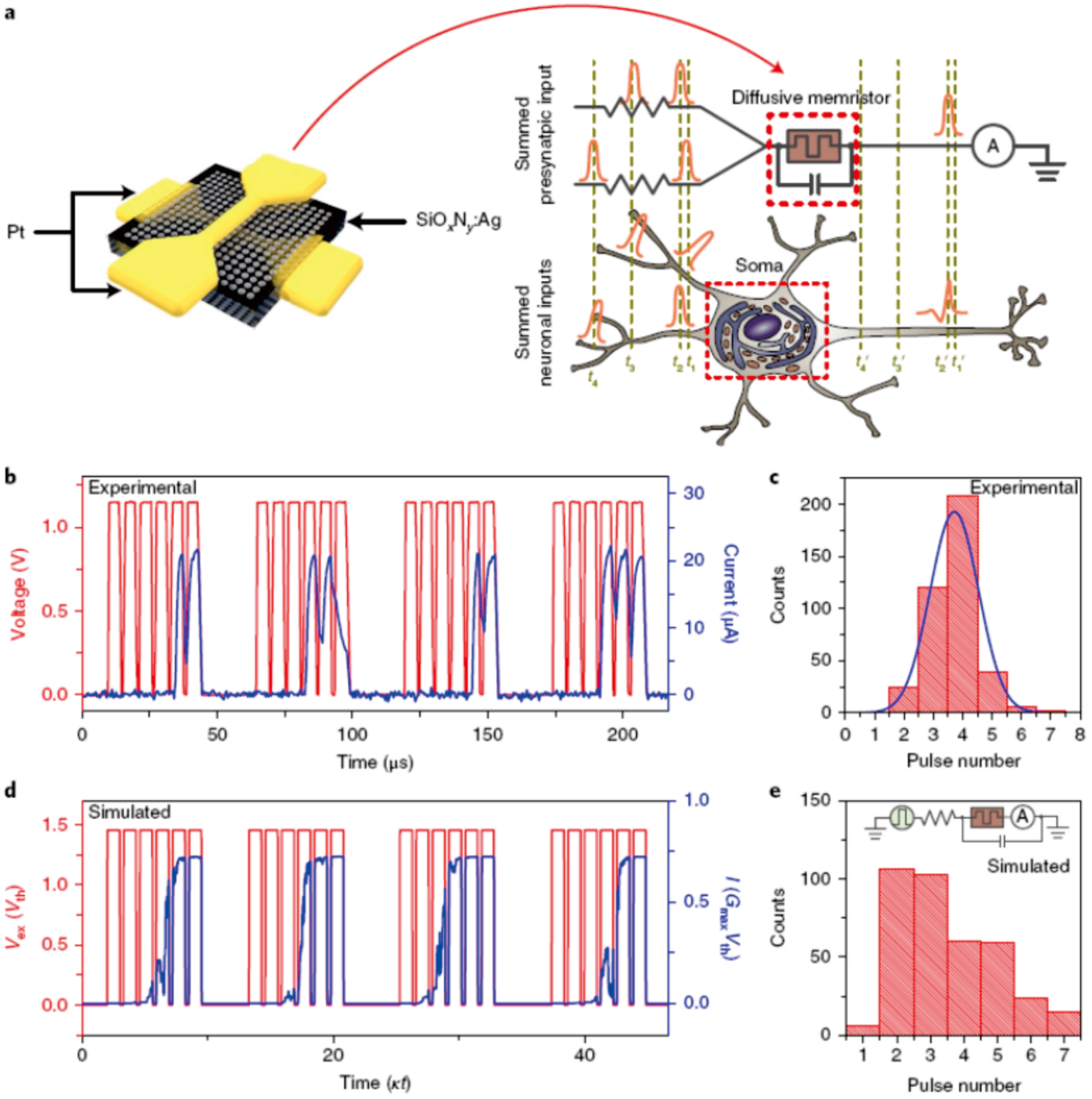

Fig. 10 Diffusive memristor artificial neuron. (a) Schematic illustration of a crosspoint diffusive memristor, which consists of a SiO_xN_y:Ag layer between two Pt electrodes. The artificial neuron receives software-summed presynaptic inputs *via* a pulsed voltage source and an equivalent synaptic resistor (20 μS conductance in this case). Both the artificial and biological neurons integrate input stimuli (orange) beginning at t_1 and fire when the threshold condition is reached (i.e. at t_2'). The integrated signal decays over time such that input stimuli spaced too far apart will fail to reach the threshold (i.e. the delay between t_3 and t_4). (b) Experimental response of the device to multiple subthreshold voltage pulses followed by a rest period of 200 μs (only 20 μs is shown for convenience). The device required multiple pulses to reach the threshold and 'fire'. (c) Histogram of the number of subthreshold voltage pulses required to successfully fire the artificial neuron (red) compared with a Gaussian distribution (blue). (d) Simulated response of the device to multiple subthreshold voltage pulses as in b showing similar behavior to experiment, with the resting time between pulse trains chosen to allow the Ag in the device to diffuse back to the OFF state. (Only 10% of the rest period is shown for convenience.) The time is measured in temperature relaxation time, where κ is the heat transfer coefficient. (e) Simulated switching statistics with respect to pulse numbers (within each train), consistent with the experimental results in (c). The inset illustrates the circuit diagram used in the simulation. Reproduced with permission from Ref 164.

consumption and provide suitable solution for the von Neumann bottleneck issue when dealing with data-intensive tasks.

Devices that behave like synapses and neurons in human brains can provide a more efficient approach for the implementation of artificial neural network (ANN) when in comparison with the traditional CMOS devices and circuits. Significant progress has been made over the past few years in building ANNs with resistive switching memristors to emulate the plasticity of biological synapses, by using the tunable device conductance as synaptic weights.[171,185-190] More recently, a few artificial neurons based on memristor have been reported to exhibit signal processing capability through a leaky integrate-and-fire model.[191-193] An artificial neuron can integrate input signals received from the pre-synapses and generates spikes if a threshold has been reached in a defined time duration, or allows the accumulated inputs to decay when the interval is exceeded.[194] The neuron can reinstate its resting (initial low) conductance after firing an input signal successfully through the "leaky" regulation. Xia, Yang and workers sandwiched Ag nanocluster doped SiO_x or SiO_xN_y thin films between two electrodes and fabricated memristive neurons with the stochastic leaky integrate-and-fire dynamics for the first time.[185] The neuron was connected with resistor synapses in series and characterized by recording its I-V response versus time. The temporal behavior of the device exhibits an obvious delay (τ_d) between the arrival of the voltage input and the rise of the current output (Fig. 10), which can be explained by the interaction of the circuit *RC* time constant and the internal dynamics of the Ag nanostructures inside the memristor. When the voltage vanishes, the device conductance relaxes with a characteristics time (τ_r) that return the neuron to its resting state, and is associated with the dissolution of the Ag nanoparticle conducting bridge by the interfacial energy minimization between Ag and the dielectric insulator. When a sequence of sub-threshold voltage pulses that are unable to activate the neuron individually are applied to the device, it fires after a certain number of pulses and emulate the integrate-and-fire function of biological neurons. After the end of the pulse train, the device relaxes to the resting state again. Upon integrating the neurons with nonvolatile memristive synapses to construct artificial neutral works, unsupervised synaptic weight updating and pattern classification function are successfully demonstrated and pave the way to compact, fast and energy efficient in-memory computing applications.

Beyond the data-intensive tasks that requires only low computing precision without deteriorating the performance, there are also "hard" computing tasks that require high precision and accurate solutions such as solving partial differential equations (PDEs) during numerical computation, as well as simulation, prediction and optimization in weather forecasting and economics.[195-199] Since memristor has the abilities of modulating the current flowing through it based on the resistance value and nonvolatily memorizing the device conductance state, it can be used to perform the analogue multiplication operation where the device current can be calculated as the applied voltage times the conductance value. It does not need an additional memory to store the device conductance, and thus can greatly enhance the computation efficiency previously limited by the classical von Neumann architecture. Following Ohm's law and Kirchhoff's current law, a memristive crossbar array can execute "multiply and accumulate" operations in which vector matrix multiplication can be realized in a single readout step. In 2018, Lu and workers designed a complete memristor-based hardware and software system that can perform precision computing tasks, further extending the application scope of in-memory computing with memristor for high-performance computing environments.[184] Experimentally, a 3.5 nm Ta_2O_{5-x} thin layer was used to build memristor devices, which demonstrate low forming voltage of 1.25 V, stable switching characteristics, and narrow distribution (σ<0.1 V) for all programming voltages. The superior device performance allows the Ta_2O_{5-x} based memristors for reliable passive array operations. By using a write-verify feedback method, the device variety has been lowered to <1% for cell-to-cell variation (Fig. 11). Then the 16×3 memristor crossbar array is wire-bonded and integrated onto a printed circuit board to carry out the coefficient matrix storage and vector-matrix multiplication tasks. By using multiple crossbars where each crossbar represents certain number of bits, the precision of memristor devices can be effectively extended. The complete memristor-based hardware and software system can be used to solve the static elliptic Poisson's equation and time evolving hyperbolic PED equations for a classical water wave propagating problem, respectively, as well as a more practical plasma evolution in an inductively coupled plasma reactor system.

The resistive switching devices have also been reported to implement Boonlean logic operations in the same physical space of a memory cell, where the LRS and HRS can be used as binary input and output signals.[11,164,200-202] With one or more resistive switches as the input devices, the evolution of their resistance can implement logic functions such as AND or materials implication (IMP) according to the respective truth tables.[11,202] In order to realize more advanced functions of XOR, addition, multiplication an etc, a large numbers of resistive switching devices and multiple operation steps are usually required, which greatly increase the spatial-temporal complexity of the log-in-memory computation. Over the past few years, great efforts have been devoted to develop resistive switching devices with abundant electrical characteristics, as well as advanced algorithms, that can be used to simplify the logic architecture and minimize the operation steps. Very recently, Ielmini proposed a concept of resistive switching device based stateful neural network that can perform all logic functions with the same network topology.[178] As shown in Fig. 12, the logic circuit is constructed with three resistive switching devices A, B, and C, which are connected to an internal node and three independent voltage supplies of V_A, V_B and V_C, respectively. An additional load resistor L is also involved to connect the internal node to ground. The current passing any resistive switching device or the load resistor can be expressed as $(V_i - V_{int})G_i$, where i is an index of A, B, C, or L, V_L = 0 V, and G_i is the conductance of the ith device. As such, stateful and cascadable logic operations can be enabled, using the nonvolatile resistance state of the devices as the input and output signals. According to Ohm's aw, Kirchhoff's law and the ionic migration within an output device as the highly nonlinear activation function, the neural network can solve all two-input logic operations (except for XOR) within just one step of physical computation. Benefiting from to the nonvolatile nature of the logic variables, the circuit can be extended to the multilayer neural network to realize linearly nonseparable functions in multiple steps, such as XOR operation. 1-bit full adder operation can be completed within two stops through five resistive switching devices, highlighting that the memristor based stateful neural network are capable of running logic computation with high efficiency in terms of space, time and energy.

3. Organic Resistive Switching Materials and Devices

3.1 Resistive Switching Mechanisms in Organic Materials

In addition to metal oxides, chalcogenides, amorphous silicon and

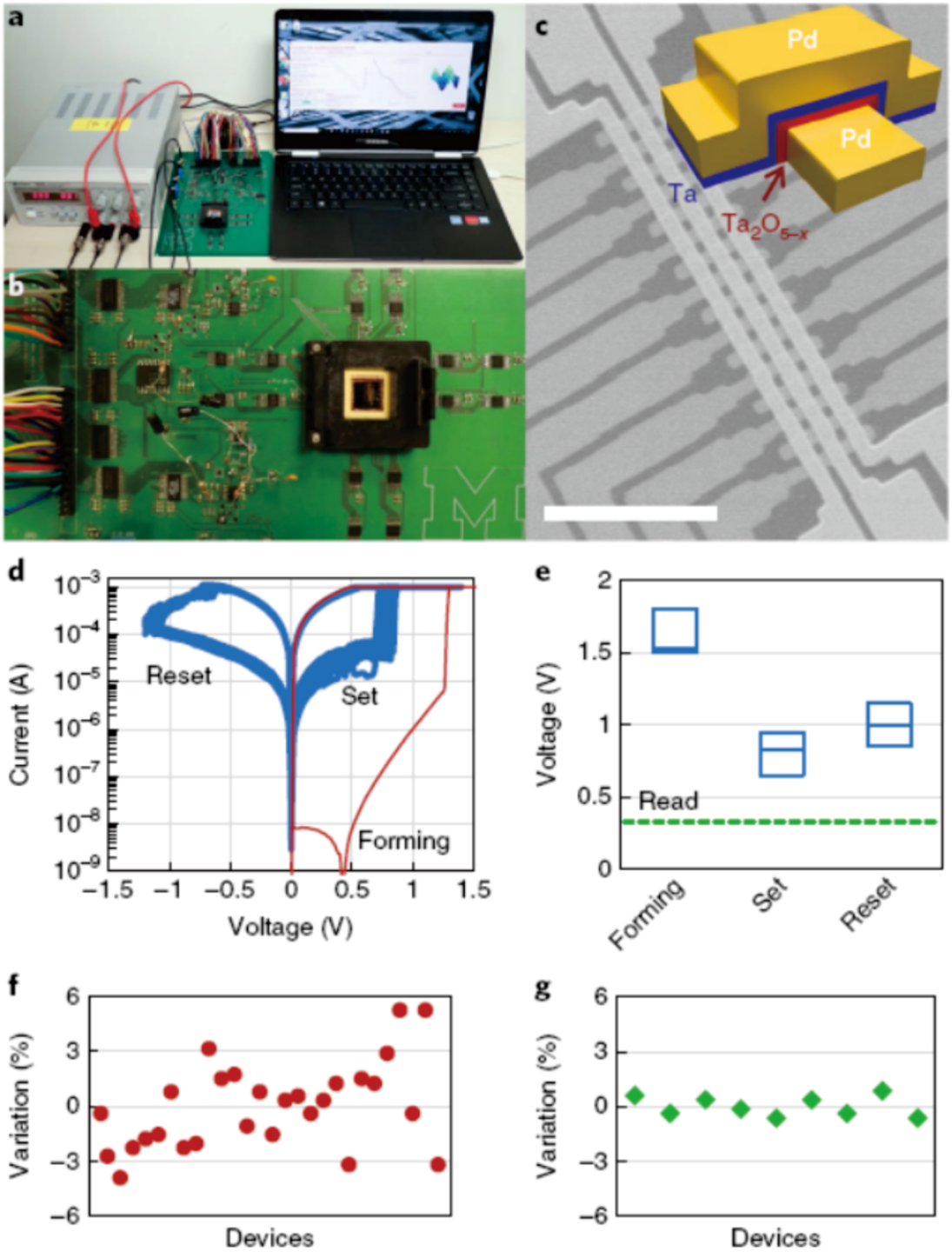

Fig. 11 Hardware set-up and device measurement for a Ta_2O_{5-x} based memristor with precision-extension approach. (a) A photograph of the memristor-based PDE solver system in operation. (b) A photograph of the test board with the mounted memristor crossbar chip. (c) SEM image of the as-fabricated 16×3 crossbar array. Inset shows the device structure of Ta/Ta_2O_{5-x}/Pd. Scale bar: 25 μm. (d) Current-voltage characteristics of the memristor. (e) Pulse measurement results from 26 devices showing narrow distribution of the forming, set and reset voltages. (f) Variation of device conductance obtained from predetermined programming conditions without any feedback mechanism. (g) Reduced conductance variation with the write-verify approach. Reproduced with permission from Ref 165.

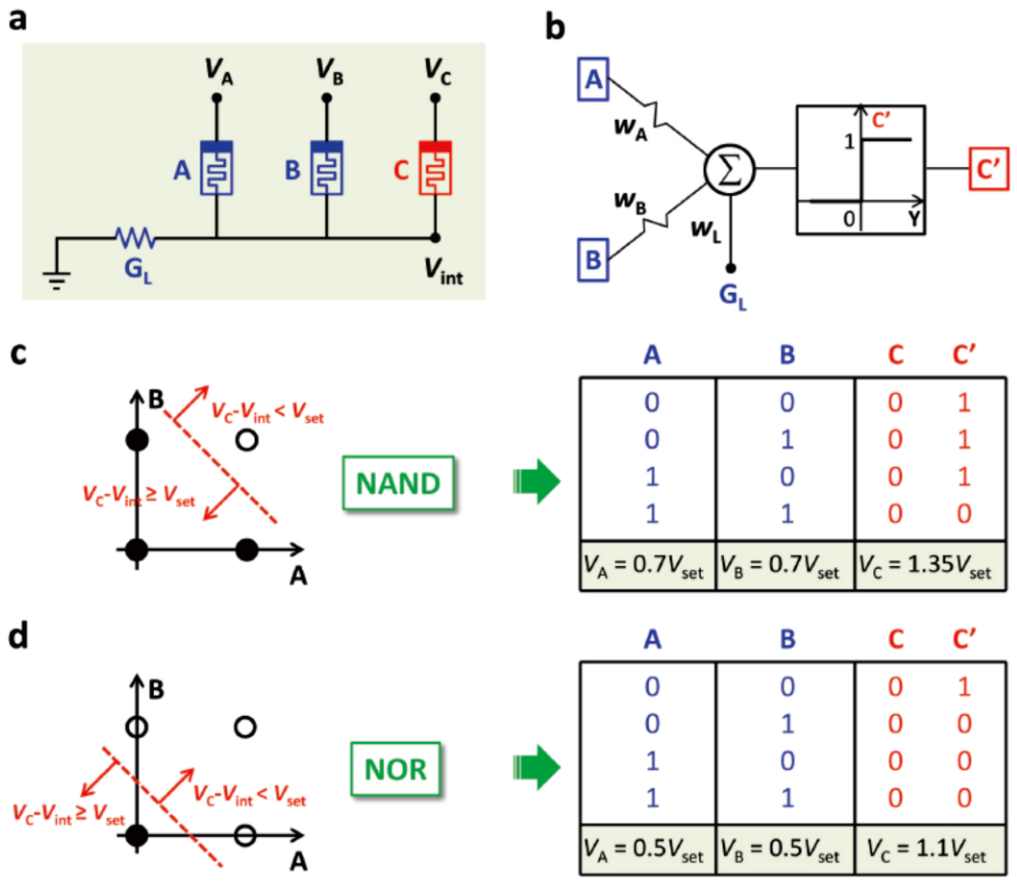

Fig. 12 Fundamental concept of the neural-network-based stateful logic circuit. (a) Resistive switching circuit with two input devices A, B, one output device C,and the load resistor of conductance G_L. (b) Equivalent neural network model for the resistive switching circuit, where conductance states of A and B serve as input variables, the conductance state of C serves as output variable, and the load resistor plays the role of bias in the neural network. (c) and (d) Input/output characteristics and truth table for NAND operation and NOR operation. Full symbols and open symbols correspond to the output state being 1 and 0, respectively. The boundary lines for linear separation of outputs, and the voltage values applied to A, B, and C, to tune the synaptic weights, are also shown. G_L was chosen equal to $1.4G_{LRS}$ for both logic operations. Reproduced with permission from Ref 159.

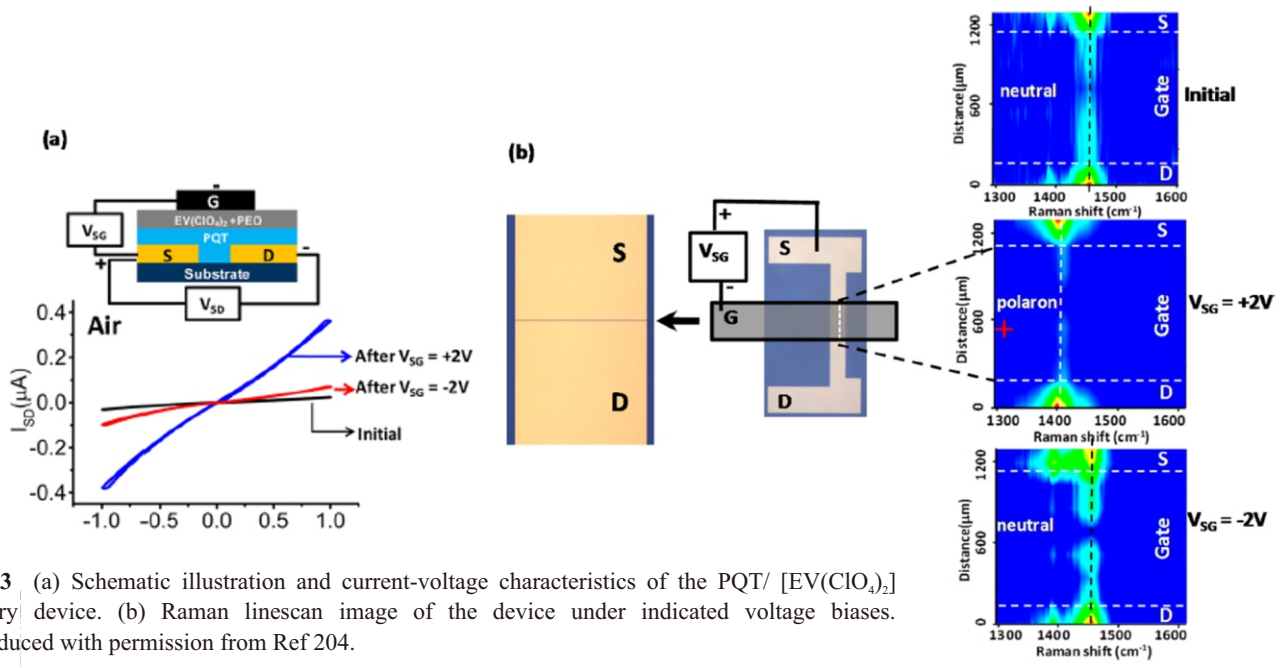

Fig. 13 (a) Schematic illustration and current-voltage characteristics of the PQT/ $[EV(ClO_4)_2]$ memory device. (b) Raman linescan image of the device under indicated voltage biases. Reproduced with permission from Ref 204.

other inorganic materials, individual or package of organic molecules are also capable of storing electrical bits of information through their bistable resistances. Organic small molecules, polymers and hybrid materials usually exhibit features of low-cost potential, easy processability, mechanical flexibility and ductibility, as well as the tunable electronic performance through a molecular design cum synthesis strategy.[26,27] In particular, the solution processing capability of organic materials allows them to be handled *via* dip coating, blade casting, spray coating, spin coating, roller-coating and even ink-jet printing, not only making the more elaborated processes of vacuum deposition of functional thin films eliminable, but allowing the fabrication of flexible memory chips. Extensive studies have been performed on the resistance switching in organic materials, wherein focus has been concentrated on the development of novel materials for memory performance optimization.[28-35]

Electrical conductivity of a material is generally the product of its charge carrier concentration and mobility. Therefore, any mechanism that can make changes in either the carrier concentration or mobility, or both, can lead to changes in the device conductance. Both intrinsic and extrinsic switching mechanisms have been proposed and solidated in organic materials,[29,32,33,51,54,203,216-221] while only those intrinsic mechanisms are of interest to chemists working in this area. In organic resistive switching materials, the intrinsic conductance bistability mainly arises from the charge transfer interaction between the electron donating and accepting moieties,[29,215,216] electrochemical reduction-oxidation (redox) activities,[51,54,217,218] and conformational change of rotatable unities.[32,33,219-221] Due to the lack of advanced characterizing and analyzing tools, less direct physical evidences were available to support the above mentioned models during the initial stage of organic resistive switching research. Identifying the operation mechanism was difficult at that moment, which hindered the development of functional materials and improvement in the device performance (in particular the endurance and retention of the switching devices).[32] Nevertheless, well-established conduction mechanisms, including Ohmic conduction, Schottky emission, thermionic emission, space-charge-limited current, tunneling current, ionic conduction, hopping conduction and etc have been adopted to account for charge transport in each conductance state.[35]

With the advances in the characterizing techniques experienced in the past decade, the switching mechanisms have been more clearly verified through spectroscopic and microscopic approaches. Representative examples include the *in-situ* spectra, linescan and two-dimensional mapping of the Raman and UV-Vis spectroscopy, and high-resolution TEM observations. For instance, the unpaired or lone pair electrons can be removed through chemical or electrochemical oxidation from an electron-rich molecules (e.g. ferrocene, thiophene and triphenylamine), which in turn introduce impurity (radical cation, or, polaron) energy levels into the bandgap and modulates the device conductance significantly *via* intra- and inter-molecular hopping through these charged centers.[51,54,217,222-224] In order to monitor the redox activities causing the resistive switching in organic materials, McCreery *et al* fabricated an analogue of the polythiophene field effect transistor by using soluble and ambient stable poly(3,3‴-didodecylquaterthiophene) (PQT) as the semiconductor channel, and ethylviologen perchlorate [$EV(ClO_4)_2$] as the counter electrode material to complete an electrochemically gated transistor (Fig. 13).[223] The use of additional reducible [$EV(ClO_4)_2$] can provide a counter reaction to support the polymer oxidation and reduction processes, and appropriate counter-ions (e.g. perchlorate) to simultaneously balance the charged form (polarons) of the polymer, giving rise to stabilized redox reaction of PQT and improved retention of the devices. With all the necessary components for a redox memory cell, the device exhibits reversible switching between high and low conductance states with a "write or erase" bias applied through the gate electrode, while a separate readout circuit to monitor the polymer conductance through source-drain currents. Spatial resolved Raman spectroscopy reveals that polarons are formed throughout the polymer layer accompanying the observed resistive switching behavior of the three-terminal device, indicating that thiophene oxidation "propagates" by growth of the conducting polaron form from the source to the drain electrodes. As such, direct physical evidence is obtained through *in-situ* spectroscopic measurements that correlate the device conductance modulation with concurrent electrochemical redox reaction in solid-state organic memory devices.

In the thin films of polymer materials, the loosely packed supermolecular chains in the disordered regions, together with the chain ends and folding, usually act as trapping sites for charge carriers and lead to low conductance of the material.[225] If conformational ordering of the π conjugated moieties (which are effective carrier transport components) can be achieved under the application of external electric field or voltage, higher interchain mobility can be then obtained through the overlapping of related orbitals between two adjacent groups. By controlling the density of conformationally ordered high-conducting regions in thin film devices, bistable and even multilevel resistive switching have been achieved with various organic materials.[32,33,219,221] Due to its ability to transport positive charges (holes), carbazole molecule is widely used in electronic and photochemical applications such as electro-photographic process and in light emitting, photorefractive and photovoltaic devices.[226,217] Lim and coworkers synthesized a series of non-conjugated polymers containing carbazole groups in the pendant groups, and explored their resistive switching characteristics associated with the conformation change effects (Fig. 14). It was observed that without any spacer incorporated between the pendant carbazole moiety and the vinyl backbone, poly(*N*-vinyl carbazole) (PVK) only exhibits a high low conductivity state. The addition of a relatively short ethylacrylate spacer between carbazole and polymer skeleton can give rise to a nonvolatile yet non-erasable resistive switching characteristics in poly(2-(*N*-carba zolyl)ethyl methacrylate) (PMCz), while further increasing the spacer length with a benzyloxyethyl group leads to a volatile switching behavior in poly(9-(2-((4-vinylbenzyl) oxy)ethyl)-9*H*-carbazole) (PVBCz). Since the carbazole group has the tendency to form a partial or full face-to-face conformation with the neighboring carbazole groups to result in extended electron delocalization,[219] the switching effects in PMCz and PVBCz are probably arising from the conformational change of the polymers *via* rotation of the carbazole groups to form a more region-regular arrange under external electric field, similar to that of PVK. In order to visualize the electric field induced conformation ordering of the carbazole containing polymers, high-resolution TEM observation was conducted on all the three polymer thin film devices after being switched to LRS if exists. Compared to the TEM image of a PMCz film in its initial OFF state (Fig. 14b), the ON state images clearly shows ordered micro domains (Figs. 14c&d), which resemble the polycrystalline structures of a PVK film (Figs. 14e&f). The appearance of the ordered structure in the ON state PMCz film suggests that the carbazole pendant groups in PMCz have transformed from a regio-random arrangement to a regio-regular arrangement through the electric field induced conformation change. In comparison, due to the presence of a longer and softer benzyloxyethyl spacer in

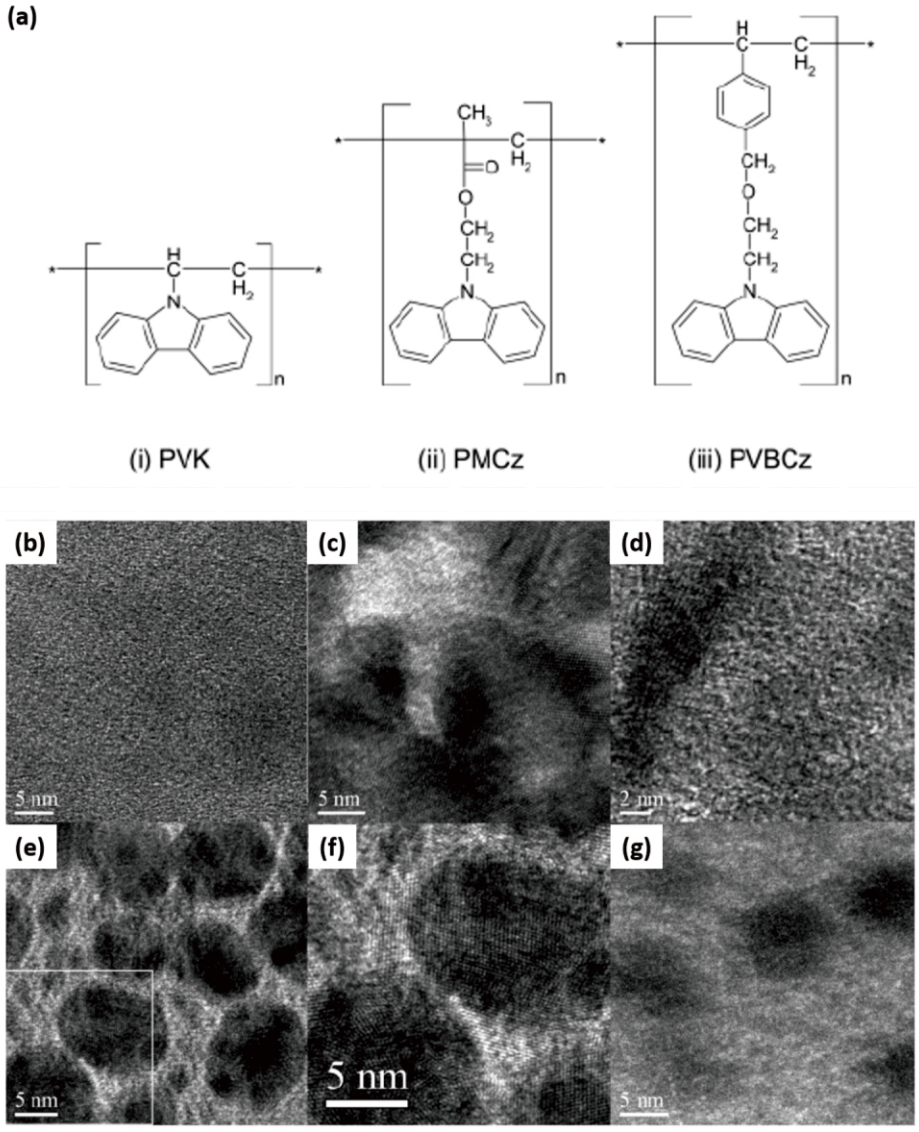

Fig. 14 (a) Molecular structures of poly(*N*-vinyl carbazole) (PVK), poly(2-(*N*-carbazolyl) ethyl methacrylate) (PMCz) and poly(9-(2-((4-vinylbenzyl)oxy)ethyl)-9*H*-carbazole) (PVBCz), respectively. TEM images of (b) an OFF state PMCz film, (c) an ON state PMCz film showing ordered microdomains, (d) an ON state PMCz film with higher magnification, (e) a PVK film, (f) a magnified region in the PVK film, and (g) a PVBCz film, after a voltage sweep from 0 to -4 V and conformation relaxation. Reproduced with permission from Ref 200.

PVBCz, the excited face-to-face conformation of the adjacent carbazole groups can easily relax to its initial randomly oriented configuration after removing the power supply and thus volatile switching nature in the current-voltage characteristics. With the TEM sample preparation time (typically ≥ 1 h) longer than the conformation relaxation time, it was unable to capture any structural ordered micro domains in the TEM images.

By incorporating both electron donating (D) and accepting (A) moieties into the chemical structure, a series of electroactive polymer materials exhibiting resistive switching behaviors have been synthesized successfully.[28-33] The applied electric field can provide the electrons enough energy to be excited from the donor to the acceptor. The as-formed charge transfer (CT) state will not only increase the concentration of the charge carriers, but also enhance their mobility, therefore leading to changes in the materials conductance/resistance. For example, a series of non-conjugated vinyl copolymer of $PTPA_nOXD_m$ was synthesized with different molar ratios of triphenylamine (TPA) donor and oxidiazole (OXD) acceptor chromohpores.[30] When sandwiched between an aluminum and an ITO electrode, the sandwich structures show controllable electrical conductivity behavior, ranging from insulator, write-once-read-many (WORM) type switching, rewritable switching, threshold switching to insulator characteristics with the acceptor concentration decreasing continuously. To gain insights into the molecular geometry and electronic properties of the PTA/POXD homopolymers and $PTPA_nOXD_m$ random copolymers, molecular simulation has been conducted using the density functional theory (DFT) method at B3LYP/6-31G(d) level to calculate the highest occupied molecular orbital (HOMO), lowest unoccupied molecular orbital (LUMO), electrostatic potential (ESP) surfaces and dipole moments of the

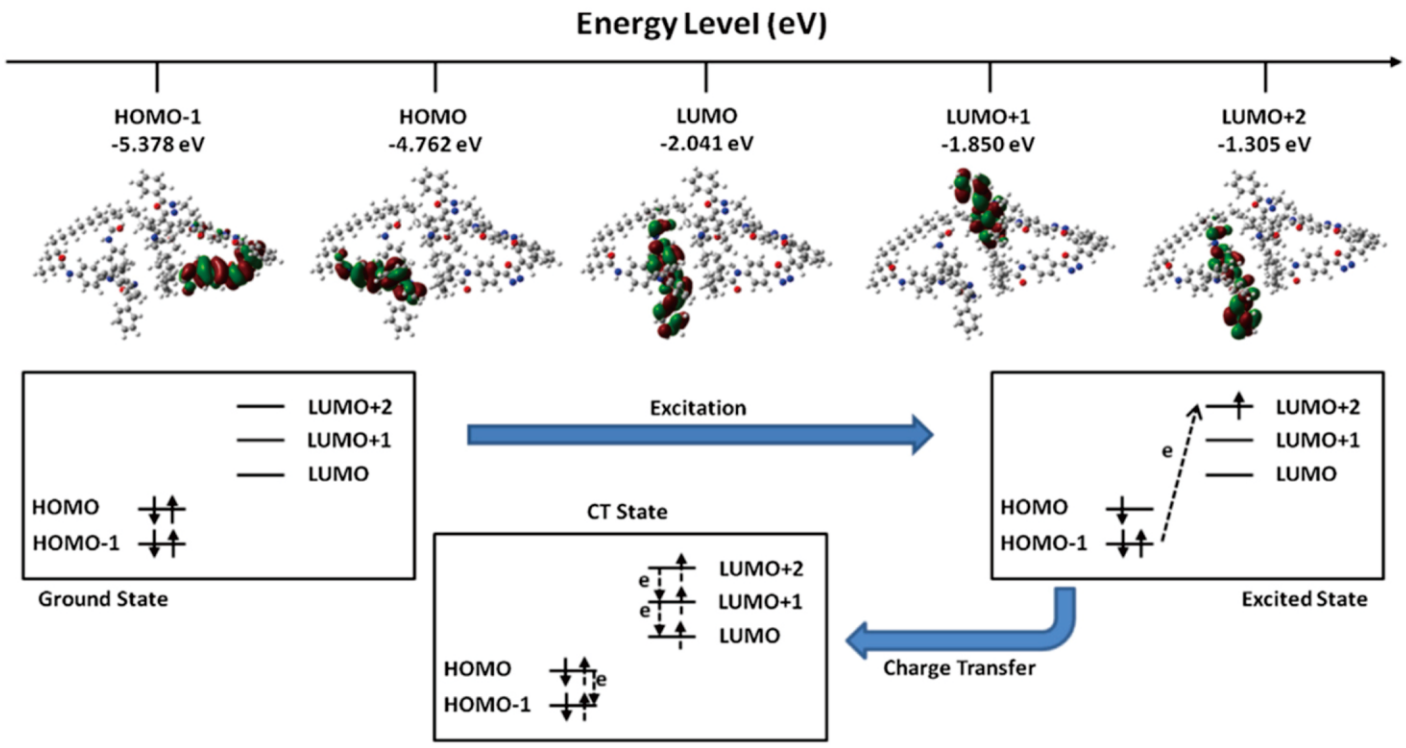

Fig. 15 Plausible electric field-induced electronic transition in polymer materials of $PTPA_1OXD_4$. Reproduced with permission from Ref 30.

pentamers with Gaussian 09 program package. As shown in Fig. 15, the HOMO resides on the first triphenylamine chromophore of the pentamer while the LUMO locates on the oxidiazole moiety next to the D-A interface at which charge transfer occurs. Under high electric field, electrons in the HOMO-1 accumulate sufficient energy and transit into LUMO+2 to give an excited state. Since LUMO, LUMO+1 and LUMO+2 are all distributed in the OXD domain, the electrons excited from HOMO-1 can be further stabilized by delocalization along the four VOXD moieties *via* intramolecular hopping, and relax to a lower excited state. The vacancy in HOMO-1 can be partially compensated by electrons in the HOMO of the triphenylamine donor unity through energy-decay transition. Consequently, a charge transfer state of the $VTPA_1OXD_4$ pentamer has been established. Driven along the direction of the external electric field, the increased amount of charge carriers can lead to an increase in the current flowing through the polymer thin film and switches the device from a low conductivity state to a high conductivity state.

According to the above mentioned mechanisms, special care should be taken when designing proper organic materials for resistive switching memories. Most of the effort on organic switching materials till now lays in the design and synthesis of the molecules with enhanced electrical behavior, while attentions are just recently initialized to improve their mechanical performance simultaneously.[229-231] In the following sections, the recent advances on resistive switching materials of small molecules, polymers based materials, and organic-inorganic hybrid materials are summarized and discussed.

3.2 Organic Small Molecule Resistive Switching Materials and Memory Devices

Organic small molecules usually possess the unique advantages of well-defined structure and high purity when in comparison with organic polymer and hybrid materials, and have attracted great research interest in the field or resistive switching memory in the past two decades.[232,233] Various commercially available semiconducting small molecules, including 2-amino-4,5-imida zoledicarbonitrile (AIDCN), tris-(8-hydroxyquin line) aluminum (Alq_3), N,N′-Di(naphthalen1yl) -N,N′-diphenyl-benzidine (NPB), pentacene and etc, have been explored in the multilayer structure of Al/small molecule/metal nanoclusters/small molecule/Al by Yang *et al*.[234-239] Due to the significant energy difference between the electrode metal and the organic layer, charge injection is greatly limited in the as-fabricated device with low conductivity state. Upon sufficiently high electric field, the metal nanoclusters become polarized, inducing opposite charge carriers at the metal nanocluster/organic molecule interface and lowering the interfacial resistance. As such, the device is switched to the high conductivity state with high ON/OFF ratio of $>10^4$, fast switching speed of <10 ns, endurance of $>10^6$ cycles and even multilevel switching character with data retention $>10^5$ s.[240-244] Nevertheless, due to the involvement of metal nanocluster which requires special care during deposition and intrinsic nature of resistive switching to the choice of organic small molecules, the tunability of the device performance and thus the application scope are largely hindered. With the aim to enable device performance modulation, much attention has been paid to materials with intrinsic resistive switching characteristics *via* rational molecular design strategy.

Introducing electron donor-acceptor structure and charge transfer interaction in organic small molecules is a feasible approach to receive the intrinsic resistive switching behavior through either permanent or reversible formation of conductive charge transfer

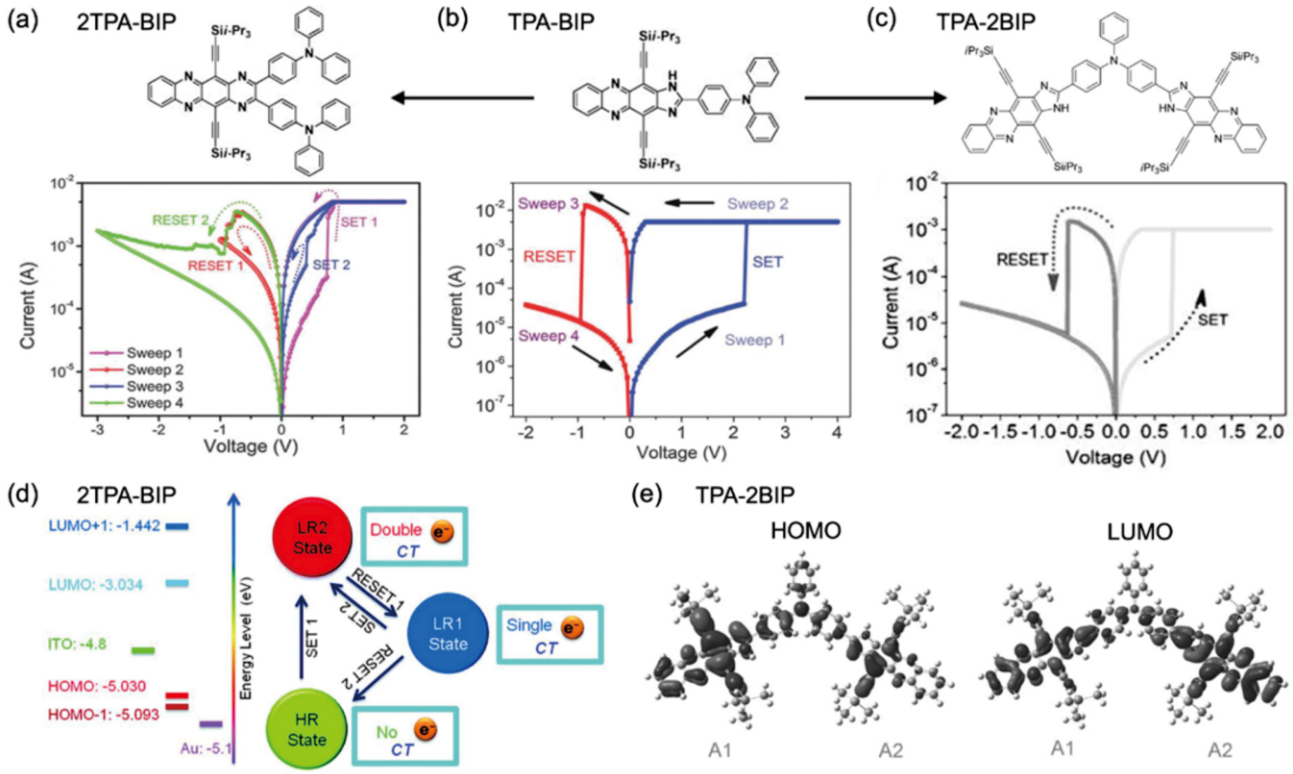

Fig. 16 Chemical structures and I-V characteristics of (a) 2TPA-BIP, (b) TPA-BIP and (c) TPA-2BIP. (d) Energy diagram and schematic switching process of 2TPA-BIP. (e) HOMO and LUMO levels of TPA-2BIP. Reproduced with permission from Refs 245-247.

complexes, corresponding to WORM and rewritable type memories.[245-249] Zhang *et al* synthesized a series of D-A molecules containing different amounts of triphenylamine (TPA) donor and imidazole-[4,5-*b*]phenazine (BIP) groups.[245-247] In TPA-BIP molecule with one donor and one acceptor groups, the occurrence of single-step charge transfer gives rise to a bistable rewritable switching characteristics (Fig. 16b). The incorporation of one more donor moiety in 2TPA-BIP, on the other hand, leads to a clear ternary switching characteristics, probably due to the two-step charge transfer phenomenon (Figs. 16a&d). When two acceptor groups are present in the TPA-2BIP molecule, binary rather than ternary switching behavior is observed (Fig. 16c). Molecular simulation indicates that this may be because of the activation of only one of the acceptor moieties in a TPA-2BIP molecule. These results suggest that the switching properties of the organic small molecules can be optimized by tuning the donor/acceptor ratio in the chemical structure.

Employing different types of electron donor and/or acceptor unities may provide alternative approach for switching modulation, in particular for obtaining multilevel switching characteristics to increase the storage density of D-A systems.[249-253] For example, Lu and coworkers synthesized (p,p'-bis(2-aryl-1,3,4-oxadiazol-5-yl)diphenyl sulfone (OZA-SO) with two types of acceptor groups (namely, 3,4-oxadiazole and sulfone), which exhibit a ternary WORM type resistive switching behavior (Fig. 17a).[250] Constructed from thiophene donor and acceptor groups of benzo[c][1,2,5]thiadiazole (BTD), 1,8-naphthalimide (NI) and nitro (NO) building blocks, molecule NONIBTDT demonstrates quaternary resistive switching behavior (Fig. 17b).[249] Based on molecular simulation, these multilevel resistive switching phenomena can be ascribed to the sequential transfer of electrons to different acceptor groups with varied electron withdrawing abilities. For instance, the four-level switching behavior of NONIBTDT originates from the transfer of electrons from donor thiophene to acceptor BTD, NI and NO in sequence (Fig. 17c). Compared to the conventional bistable electrical characteristics, the three- and four-level switching behaviors can increase the storage states exponentially from 2^n to 3^n and 4^n, respectively, which is highly desired in the current era of Big Data with information explosion. Considering the portable and wearable applications, Lu *et al* also fabricated flexible ternary memory devices based on small molecule of BAzoAN and plastic poly(ethylene terephthalate) (PET) substrate (Fig. 18), which can endure 500 continuous bending cycles at the bending radius of 6.5 mm without any switching performance degradation.[254]

Although dozens of organic small molecules have been designed and synthesized for resistive switching memory devices, it is noteworthy that the switching behaviors of the small molecules reported so far are normally WORM type. Despite that stable two, three and even four level resistive switching behaviors are achieved *via* molecule design; their application scope is still limited to disposal usage because of being non-rewritable. Efforts should be devoted to the design of resistive switching organic small molecules suitable for multiple usages. One possible direction may be indicated in the very recent work by Venkatesan *et al*,[224] where rewritable switching behavior with extremely high endurance of over 10^{12} cycles was observed in the compound *mer*-$[Ru(L)_3](PF_6)_2$. The metal coordination compound is built with three bidentate ligands (L = 2(phenylazo)pyridine), each of which contains one azo (N=N) functional group (Fig. 19). *In-situ* Raman and UV-visible absorption

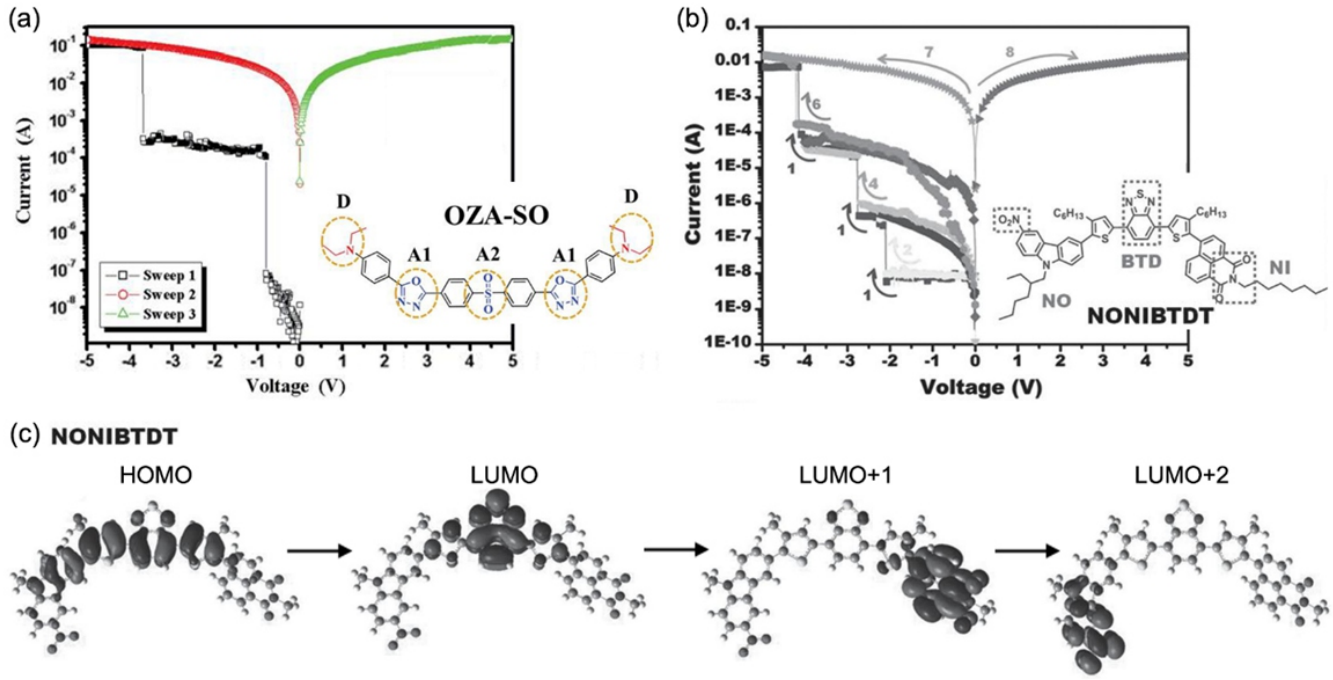

Fig. 17 Chemical structures and I-V characteristics of (a) OZA-SO and (b) NONIBTDT. (c) HOMO and LUMO levels of NONIBTDT. Reproduced with permission from Refs 248 and 249.

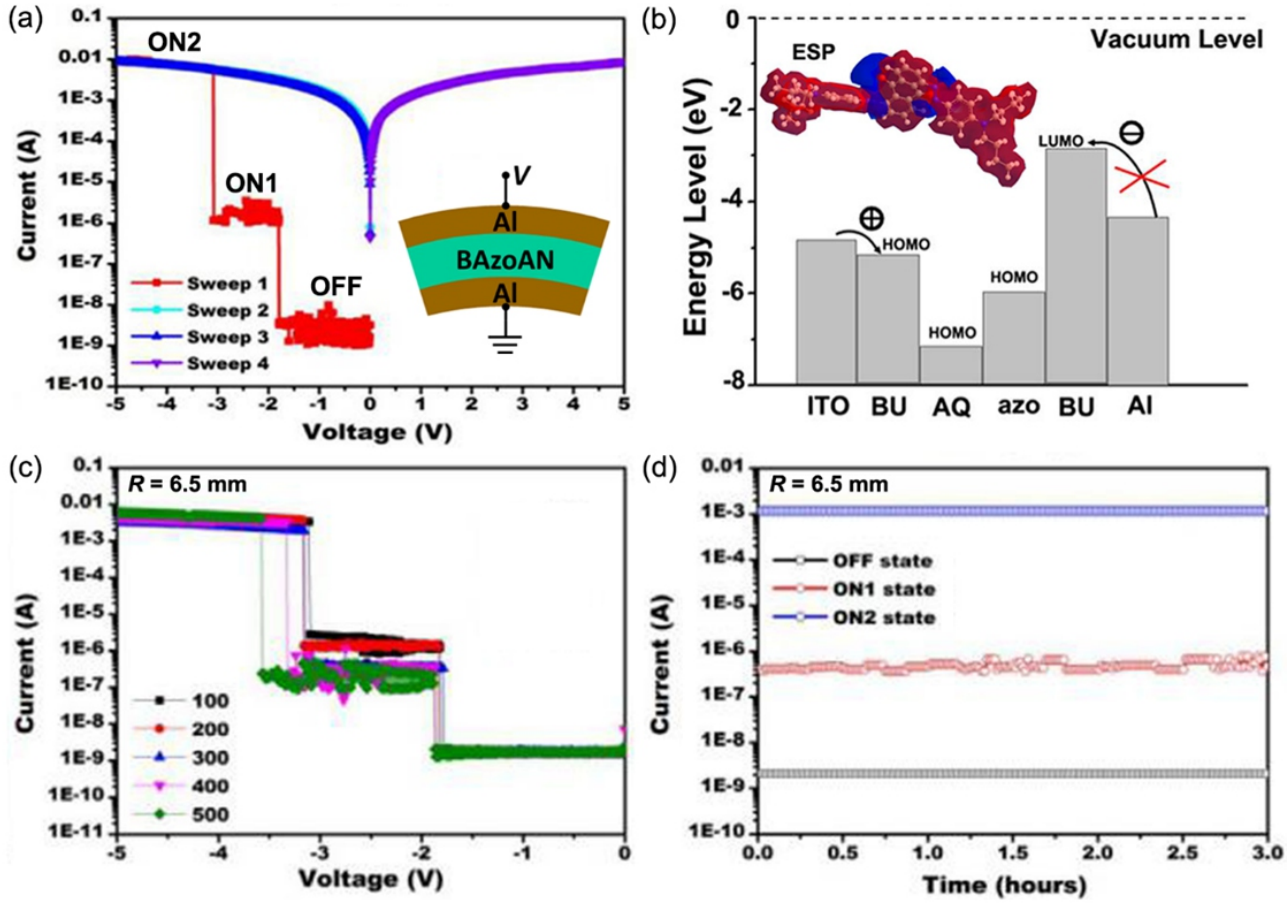

Fig. 18 (a) I-V characteristic, (b) energy level, (c) bending endurance, and (d) retention property of the BAzoAN memory device. Inset in (b): Molecular electrostatic potential (ESP) of BAzoAN. Reproduced with permission from Ref 235.

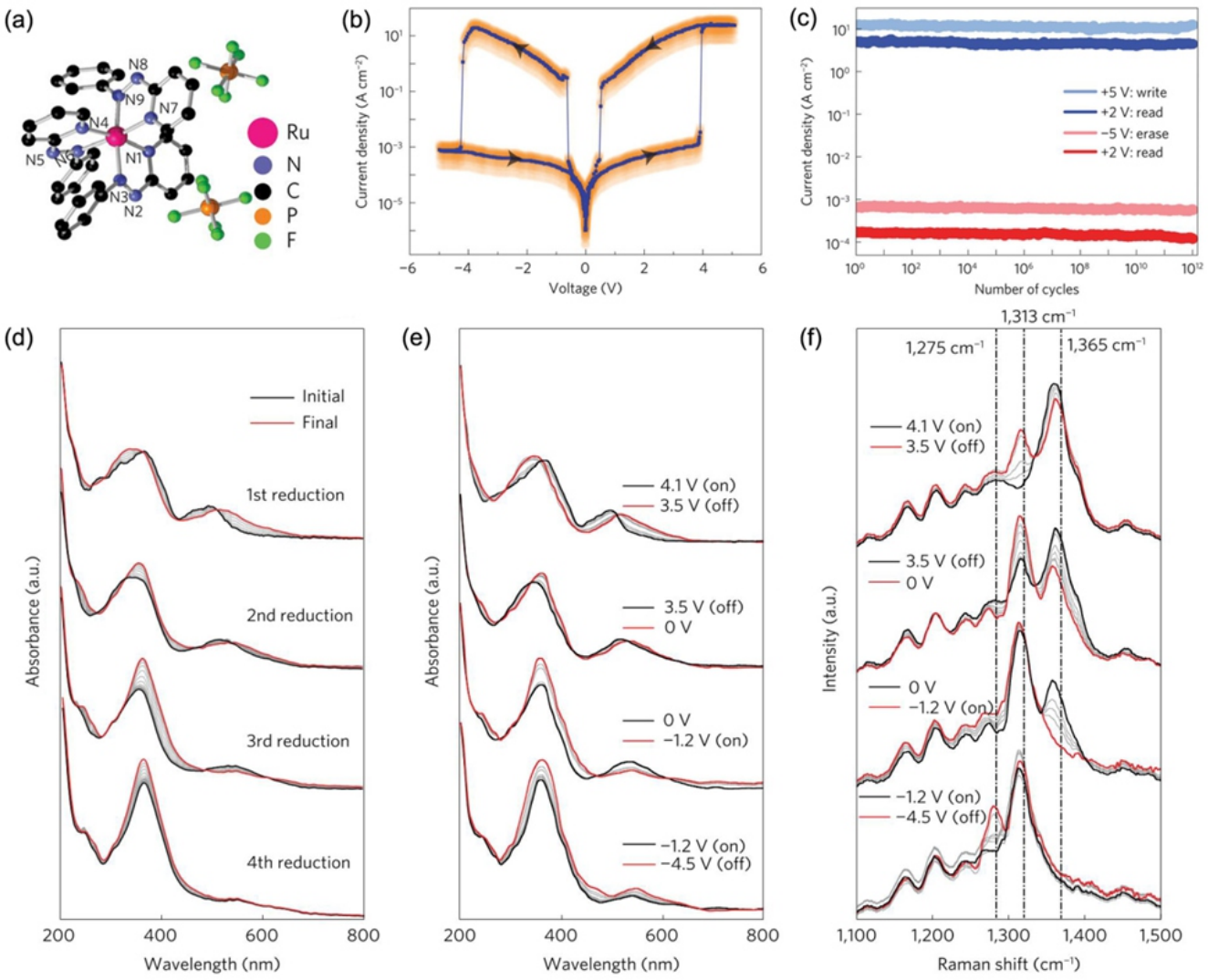

Fig. 19 (a) Molecule structure, (b) I-V characteristic, and (c) switching endurance of *mer*-$[Ru(L)_3](PF_6)_2$. (d) *In situ* UV-Visible absorption spectra of the various redox states of the molecule in solution. *In situ* (e) UV-Visible and (f) Raman spectra of the molecule in thin film state. Reproduced with permission from Ref 205.

spectroscopy, together with spectroelectro chemistry and quantum chemical calculations suggest that the switching states of the device is determined by the redox states of the bidentate ligands, while the hysteresis of the I-V curves is controlled through the counter-ions. Substitution of the ligands and the ruthenium center with other similar organic species and transition metal respectively may result in analogue resistive switching properties and thus provide a versatile platform for designing robust resistive switching devices with organic materials. Nevertheless, the fabrication of organic small molecules is usually carried out through elaborate thermal evaporation under reduced pressures. The resultant thin films crystallize easily in vacuum during sample preparation, which may hinder their direct application for flexible memory and needs to be deeply considered in future works.

3.3 Polymer Resistive Switching Materials for Memory and In-Memory Computing

In comparison to the inorganic and organic small molecule counterparts, polymer material shows higher intrinsic flexibility and ease for solution processing. The solution processing capability allows them to be handled *via* low-cost techniques of dip coating, blade casting, spray coating, spin coating, roller-coating and even ink-jet printing, making the fabrication procedure of memory devices potentially more economical without the involvement of vacuum deposition procedure.[26,255-257] Various polymer materials, including single-component electroactive polymers, polymer blends or mixtures with small molecules, nanoparticles or inorganic compounds, as well as biomacromolecules, have been investigated for resistive switching devices.

(1) Polymer-based Blends or Mixtures

In the pioneering studies of polymer memories, blends or mixtures of polymers with other materials are often used as the switching media. The obtained polymer composites may benefit from the advantages of both components and thus feature improved physical properties including electronic property, processability and mechanical flexibility. The first polymer based resistive switching memory, as reported by Forrest *et al* in 2003,[258-261] was obtained by using polyethylene dioxythiophene:polystyrene sulfonic acid (PEODT:PSS)

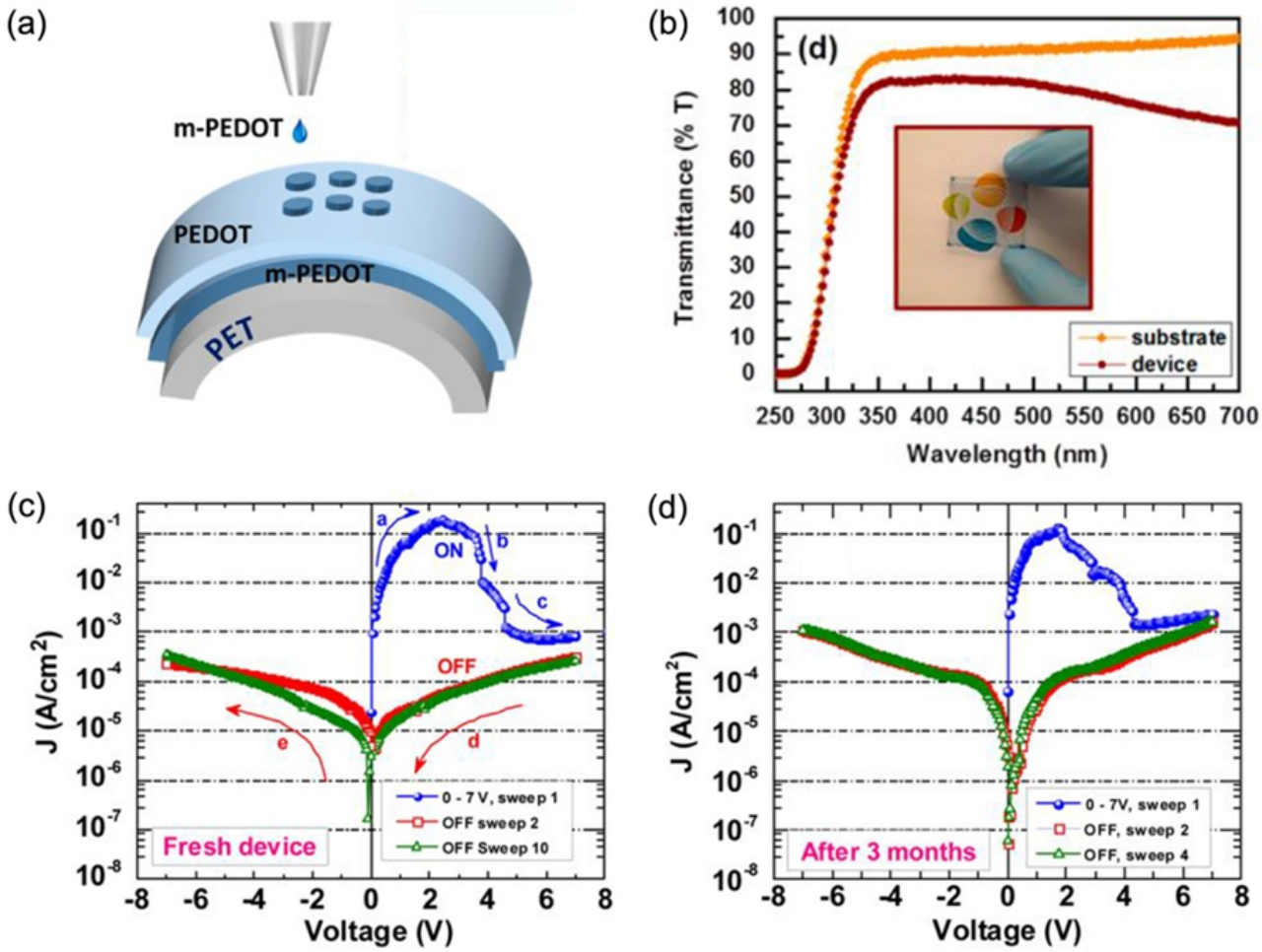

Fig. 20 (a) Schematic structure and (b) transparent property of the all-PEDOT:PSS memory device. *I-V* characteristics of the device (c) in fresh state and (d) after storage for 3 months. Reproduced with permission from Ref 243.

as the active layer. The resistive switching is attributed to the permanent reduction of $PEDOT^+$ into $PEDOT^0$ under the applied electric field, as evidenced by the x-ray photoelectron spectroscopy and temperature induced conductivity measurements. Facilitated by the aggregation of the insulating PSS^- chains near the electrode/polymer interface, charge injection from the cathode into the conducting $PEDOT^+$:PSS^- grains, as well as the bulk conduction through the reduced $PEDOT^0$ segments, are permanent prevented, thus leading to WORM type memory behavior suitable for large-scale archival storage of massive data. By using highly conductive PEDOT:PSS (with 4 wt% dimethyl sulfoxide, or DMSO dopants; conductivity: >900 S/cm) as soft electrodes on PET substrate, robust, flexible and transparent all-PEDOT:PSS resistive switching memory are demonstrated recently (Fig. 20).[262]

Other than interacting with the mixed components, polymer materials can also be used as inert matrix for nanoparticles and inorganic compounds, which was initiated by Yang *et al* in 2004 with the hope to develop single-layer, solution-processable and rewritable two-terminal memory devices.[215] Due to the ultrafast electric field-induced charge transfer between the 1-dodecanethiol-protected Au nanoparticles (Au-DT NPs) and 8-hydroxyquinoline (8HQ) in an insulating polystyrene thin film, the Al/Au-DT+8HQ+PS/Al structure undergoes a reversible transition with an ON/OFF ratio of ~ 10^4 and a switching time of less than 25 ns. Inspired by this work, a large amount of polymer-inorganic composites based on low-dimensional fillers have been explored for resistive switching memory applications. Starting from the Au nanoparticles, plenty of zero-dimensional (0D) metal/semiconducting nanoparticles or quantum dots (QDs), including Ag,[25] fullerene and its derivatives,[263-266] Cu_2O,[267] TiO_2,[268] ZnO,[269,270] CdS[271] and etc, have been explored for resistive switching memories. Quantum dots (QDs) of layered materials such as graphene,[272-274] black phosphorus (BP),[213,275] $MoSe_2$,[276] WS_2[276] and $NbSe_2$[276] are also used. When being incorporated into insulating polymer matrixes such as polyvinylpyrrolidone (PVP),[263] polyimide,[264] polystyrene,[265] poly(vinyl alcohol) (PVA),[277] poly(ethylene -*co*-vinyl acetate) (PEVA)[278] and poly(methyl methacrylate) (PMMA),[211] these nanoparticles or QDs can trap charge carriers injected from the electrodes and thus lead to resistive switching behaviors. For instance, Han *et al* synthesized uniform and high-quality BP QDs with an average size of 2.7 nm *via* sonication assisted liquid exfoliation and incorporated them as charge trapping enters in the Al/PMMA/BP QDs/PMMA/Al device on a plastic PET substrate (Figs. 21a-d).[275] The device exhibit bipolar resistive switching behavior with ultra-high ON/OFF ratio of $>10^7$, good switching endurance of >100 cycles, and stable data retention of $>10^4$ s (Figs. 21e-g). By controlling the compliance current presets, reliable multilevel memory characteristics are also observed (Figs. 21h&i). Moreover, almost no degradation is found in the ON/OFF radio (Fig. 21j) after bending the device for 500 times at

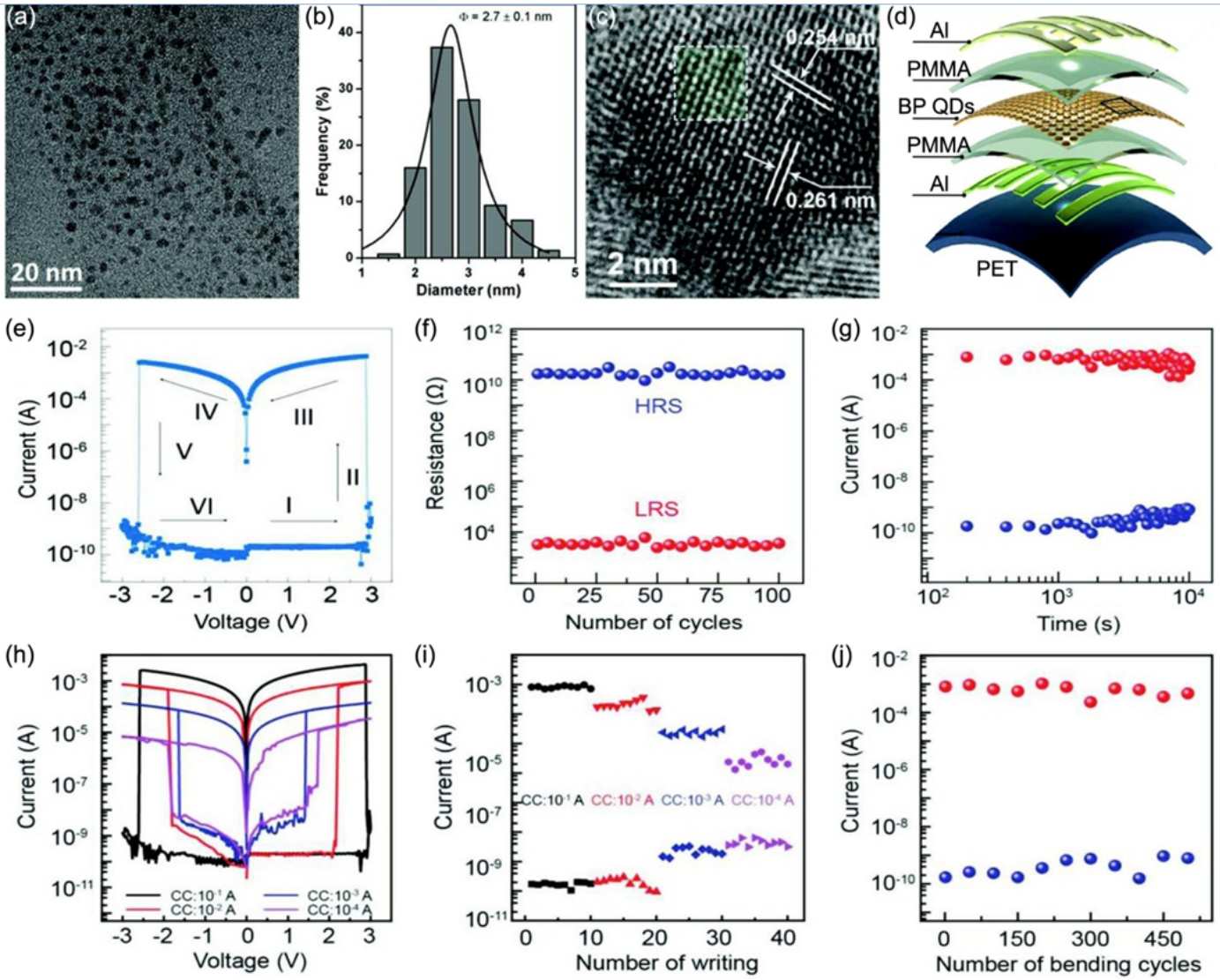

Fig. 21 (a) Low-magnification TEM image, (b) statistical size analysis, and (c) high-resolution TEM image of BP QDs. (c) Schematic structure, (d) I-V characteristic, (e) switching endurance, (f) retention property, and (h,i) multilevel switching behavior of the Al/PMMA/BP QDs/PMMA/Al memory device. (j) Bending endurance of the device at 15 mm radius. Reproduced with permission from Ref 256.

the bending radius of 15 mm.

Layered materials are also used in their original two-dimensional form for polymer resistive switching blends, with both metallic graphene and semiconducting MoS_2 nanosheets acting as trapping centers in a polymer matrix.[276-283] In 2012, Shang *et al* reported a resistive switching memory with PVK as matrix and graphene nanosheets as electron trapping centers,[279] which was found to exhibit WORM and bipolar resistive switching behaviors with 2 and 4 wt% graphene nanosheets, respectively. Compared to metallic graphene, the intrinsic bandgap, high mobility and large specific surface area allow semiconducting MoS_2 for high performance field-effect transistor, gas sensors, light emitting diodes, lithium ion batteries and etc.[284-286] Due to its appropriate quantum confinement and available energy states, MoS_2 is also considered more suitable as trapping centers. Choi *et al* fabricated a resistive switching memory with MoS_2 nanosheet- doped PVA as the active layer and Ag as both top and bottom electrodes on plastic PET substrate (Fig. 22a).[282] The branched structure of PVA is highly suitable for coating a 2D material to form uniform thin films, with cheap, non-toxic, biocompatible and environment-friendly features. Under flat state, the device exhibits bipolar resistive switching behavior with V_{set} of 2.5 V, V_{reset} of -2.6 V and high ON/OFF ratio of $>10^2$ (Fig. 22b). Good switching endurance of >1000 cycles and stable data retention of $>10^5$ s are also confirmed (Figs 22c&d). Both the ON and OFF states could be maintained when being bended for up to 1500 times with a small radius of 5 mm, while the extreme bending radius of the device is as small as ~2 mm (Figs 22e&f).

One-dimensional (1D) inorganic nanotubes or nanowires represent another group of the constitutes for the formation of polymer-inorganic resistive switching composites.[36,286-291] Carbon nanotube (CNT) with excellent carrier mobility, mechanical flexibility, compatibility with solution process and tunable electrical property has been extensively explored as 1D dopant in matrix of PVK, PVA and PS for resistive switching memories.[36,288,289] Ag and ZnO nanowires are also explored for polymer/inorganics composite memory applications, with Ag nanowires contributing to the resistive

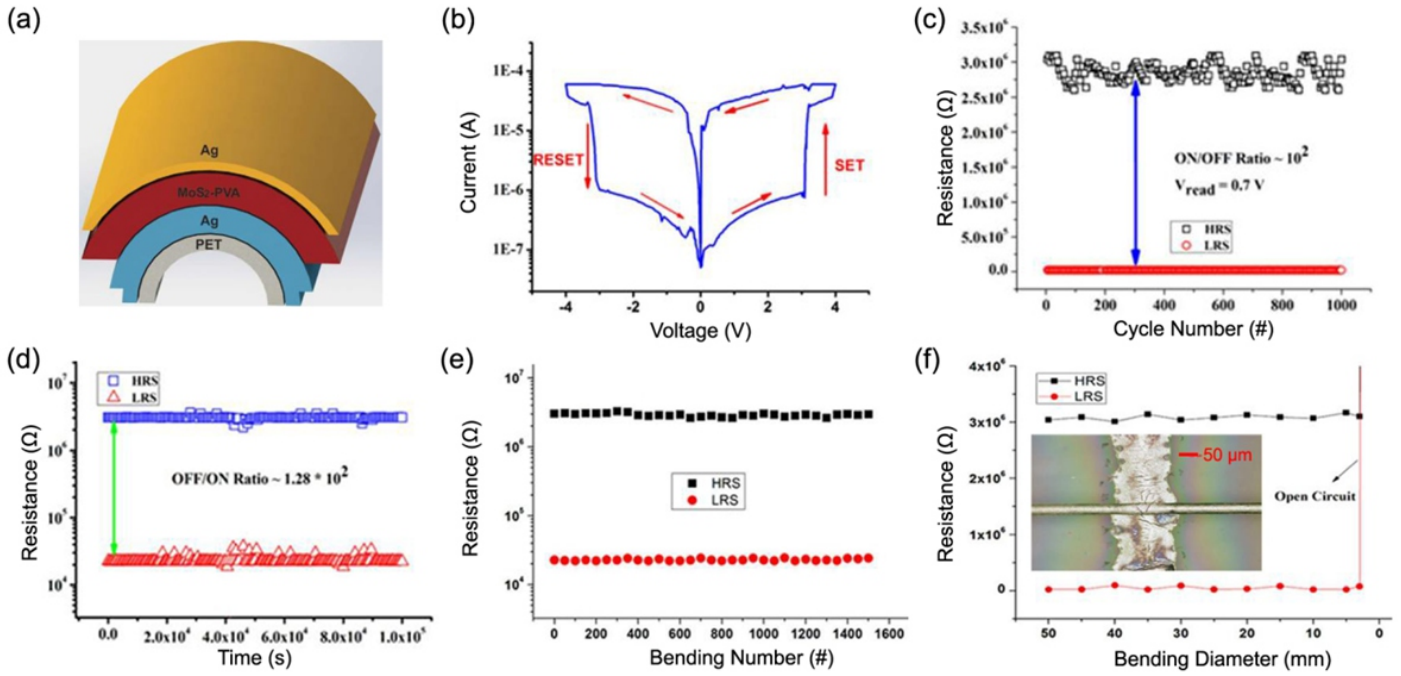

Fig. 22 (a) Schematic structure, (b) I-V characteristic, (c) switching endurance, (d) retention property, (e) bending endurance at 5 mm radius, and (f) bending performance of the Ag/PVA-MoS_2/Ag memory device. Reproduced with permission from Ref 263.

switching behavior by electroformation of silver filaments between adjacent nanowire clusters whereas ZnO nanowires acting as charge trapping centers like CNTs.[266,267] Other than serving as the matrix for metal nanoparticle and nanowire dispersion, polymers containing hetero atoms also act as chelating agent to drag metal species from the chemically active electrode into the organic layer to form conductive filaments.[216,292-294] In 2013, Pan *et al* observed directly by SEM that Ag particulated filaments can be formed in the planar Ag/PEDOT:PSS/Pt structure, which switches the device between low and high conductive states (Fig. 23).[207,208] More impressively, Huang *et al* developed a polychloro-para-xylylene (parylene-C)-based flexible resistive switching memory array through a fully CMOS-compatible process,[295] wherein the reversible of metal filament in parylene-C produces high ON/OFF ratio of $>10^4$ and good bending endurance of >500 cycles with 10 mm radius. Through deliberately controlling the formation and dissolution of Ag filaments during the set and reset processes, conductance quantization with both integer and half integer multiples of single atomic contact is also realized in polymer based memory devices by scaling down the voltage sweep speed as well as by pulse operations.[295,296]

Although the polymer blends, mixtures with organic small molecules and composites with nanoparticle, and/or inorganic compounds provide a simple yet effective strategy of fine-tuning the memory characteristics of the resistive switching devices, it is noteworthy that physical doping of polymers may not always give rise to uniform dispersion of the constituting material, especially when the two components are less compatible, therefore significantly influencing the performance of the memory devices. Much attention should be paid to controlling the composition and microstructure of the composite switching layer. Chemical modification to the dopants may be another effective approach to improve the compatibility between the polymers and doping agents with different chemical nature and geometrical dimensionality.

(2) Single-Component Electroactive Polymers

Solution-processable polymer materials that can provide superior resistive switching characteristics within a single macromolecule while possess good chemical, mechanical and morphological properties are promising candidates for information storage devices. Great efforts have been devoted to designing and synthesizing single polymer memory materials, and several comprehensive reviews have discussed thoroughly on these themes over the past fifteen years.[26,233,255-257] The pioneer work on single polymer resistive switching materials were initiated by Kang and Pal *et al*, when the first attempts were performed with photovoltaic and light emitting materials such as poly[3-(6-methoxyhexyl) thiophene] (P6OMe)[297] and etc. It was found that the memory behavior was directly related to the relaxation dynamics of the accumulated space charges.[296-301] Ling and Kang shortly adopted the concept of charge transfer from the light emitting diode and developed a series of D-A polymers for memory applications. Volatile resistive switching behavior was observed in a conjugated copolymer PFOxPy in the Al/PFOx Py/ITO structure with a high ON/OFF ratio of up to 10^6, excellent endurance of both the ON and OFF states for up to 10^8 read cycles at a read voltage of 1.0 V, and retention capability for more than 10 h under constant refreshing voltage pulses.[302] Upon optimizing the morphology of the Disperse Red 1 functionalized PVK through π-π stacking interactions of the carbazole groups in *N*,*N*-dimethylformamide (DMF, good solvent) and dichloromethane (DCM, poor solvent) mixed solvents, the resultant nanoaggregated PVDR assembles exhibit helical columnar stacks with large grain sizes which benefits the occurrence and stabilization of intermolecular charge hopping process.[31] Due to the better film crystallinity and optimized surface morphology, Al/PVDR/ITO

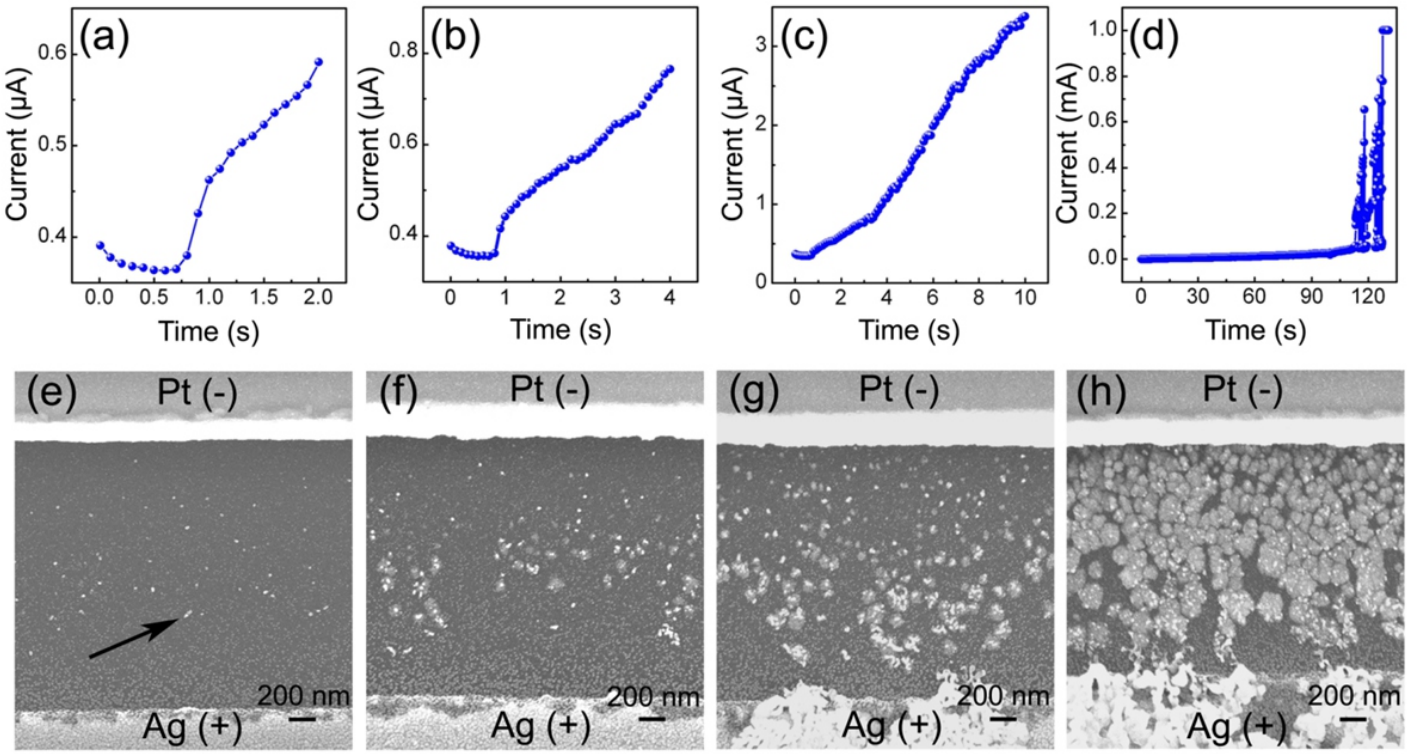

Fig. 23 (a)-(d) I–t curves of pristine Ag/PEDOT:PSS/Pt devices under constant voltage of 1 V with different periods of time and (e)-(h) corresponding SEM images. The arrow in (e) highlights one of the clusters. Reproduced with permission from Ref. 208.

devices constructed from the pre-assembled solution of PVDR showed improved WORM memory performance with much greater stability than that of the non-nanoaggregated PVDR devices (Fig. 24). This work provided an effective way to realize the high-performance polymer memory devices by controlling the polymer film morphologies.

Interestingly, the definition of electron donor and acceptor groups is not absolute. Instead, it depends on the electron withdrawing ability of the molecules under evaluation. A good example is reported by Liu *et al* in 2013,[30] when they synthesized two D-A type polyazothmine (PAM) derivatives containing triphenylamine (TPA), oxadiazole (OXD) or 3,3'-dinitro-diphenylsulfone (NPS) moieties in the conjugated polymer backbone (Fig. 25a). Sandwiched between Pt electrodes, PAM-1 shows rewritable resistive switching behavior (Fig. 25c), whereas PAM-2 exhibits WORM type switching behavior (Fig. 25d). Theoretical simulation indicates that TPA and OXD moieties in PAM-1 act respectively as donor and acceptor, while in PAM-2 the donor and acceptor are OXD and NPS moieties, respectively (Fig. 25e). The moderate electron withdrawing ability of OXD makes charge transfer interaction in TPA-OXD pair reversible, resulting in rewritable memory behavior in PAM-1. In contrast, the strong electron withdrawing ability of NPS moieties causes an irreversible charge transfer interaction in the OXD-NPS pair, which gives rist to the WORM switching behavior in PAM-2. Non-conjugated D-A polymers with relatively more flexible backbones, in comparison to the conjugated polymers with rigid skeletons, are more suitable for wearable memory applications. Chen *et al* developed triphenylamine-pyrene containing D-A polyimides for resistive switching memory applications with Al electrodes on plastic PEN substrate.[303] The polymers were prepared from 4,4'-diamino- 4''-methyltriphenylamine (AMTPA) or *N*,*N*-bis(4-aminophenyl)aminopyrene (APAP) donors and the 4,4'-(hexafluoroisopropylidene)diphthalic anhydride (6FDA) acceptor units. Through tuning the molar content of APAP and AMTPA units in the pendants, volatile, rewritable and WORM memory behaviors have been achieved and maintained stably during mechanical deformation.

With good redox reversibility, electron-accepting capability and easily tuned electronic and optoelectronic properties through metal center selection and polymer backbone or pendant modification, transition-metal complexes have been introduced into polymer structures for device applications.[304,305] Huang and coworkers systematically investigated the memory characteristics of iamPx series polymers containing phosphorescent Ir (III) complexes in the main-chains.[306-311] Attributed to the polarized charge-transfer state between 9,9'-dioctylfluorene moieties and cationic Ir (III) complex moieties under an applied electric field, the Al/iamPx/ITO structured devices exhibit low reading, writing and erasing voltages of -1.6 V, 2.8 V and -1.0 V, respectively, as well as a high ON/OFF ratio of more than 10^5 that can be sustained for up to 10^4 s or 10^8 read cycles. Ferrocene (Fe^{2+}) is another promising transition-metal complex for nonvolatile memory application, because of its well-studied reversible redox behavior and the stable oxidized form of ferrocenium (Fe^{3+}).[312,213] Choi *et al* inserted ferrocene into the conjugated backbone of PFT2-Fc randomly, with other redox active unities of bithiophene introduced to modulate the content and position of the ferrocene moieties.[217] When fabricated into Al/LiF/PFT2-Fc/ITO devices, rewritable memory behavior with a set/reset voltage of -1.9 V/+1.4 V, ON/OFF ratio of 10^3, endurance of more than 100 cycles and retention time longer than 7 h is achieved.

As discussed previously, two-dimensional and carbon nanomaterials have been widely used in polymer memory applications.[27,36,279-283,287-290,313-316]

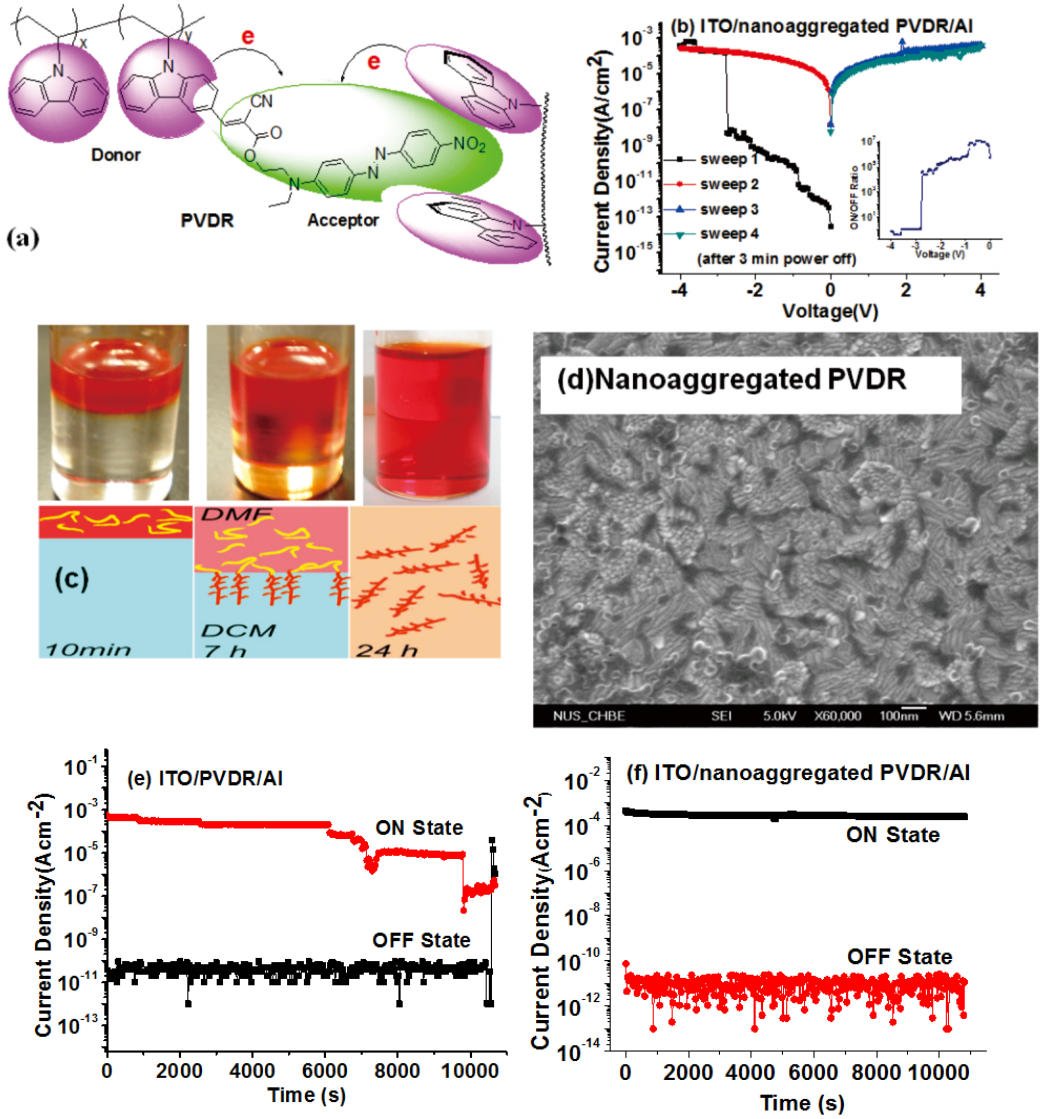

Fig. 24 (a) Chemical structure of PVDR. (b) I-V characteristics of the Al/PVDR/ITO device. (c) Schematic illustration of the interfacial self-assembly process of PVDR. The top red layer is PVDR dissolved in DMF, and the bottom layer is DCM. The volume/volume ratio of these two solvents was 1/10. (d) HRSEM image of the surface morphology of spin-coated nanoaggregated PVDR film on ITO substrate. Reproduced with permission from Ref 31.

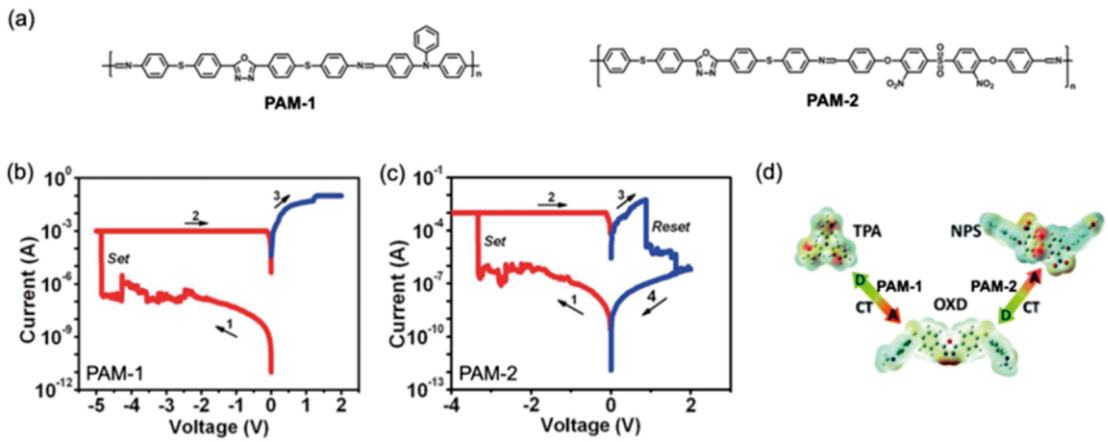

Fig. 25 (a) Chemical structures and (b,c) I-V characteristics of PAM-1 and PAM-2 (d) Charge transfer directions of PAM-1 and PAM-2. Reproduced with permission from Refs 29.

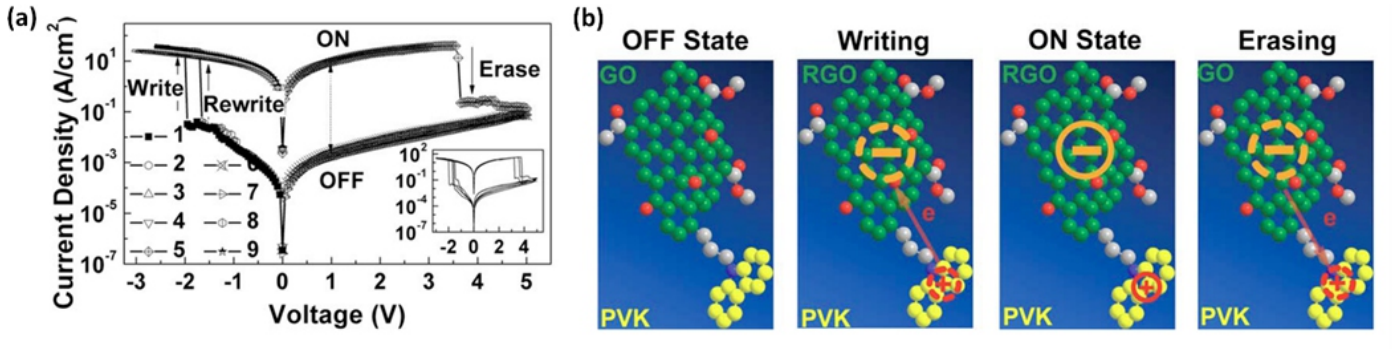

Fig. 26 (a) Resistive switching characteristics and (b) switching mechanism of GO-PVK nanocomposites. Reproduced with permission from Ref 37.

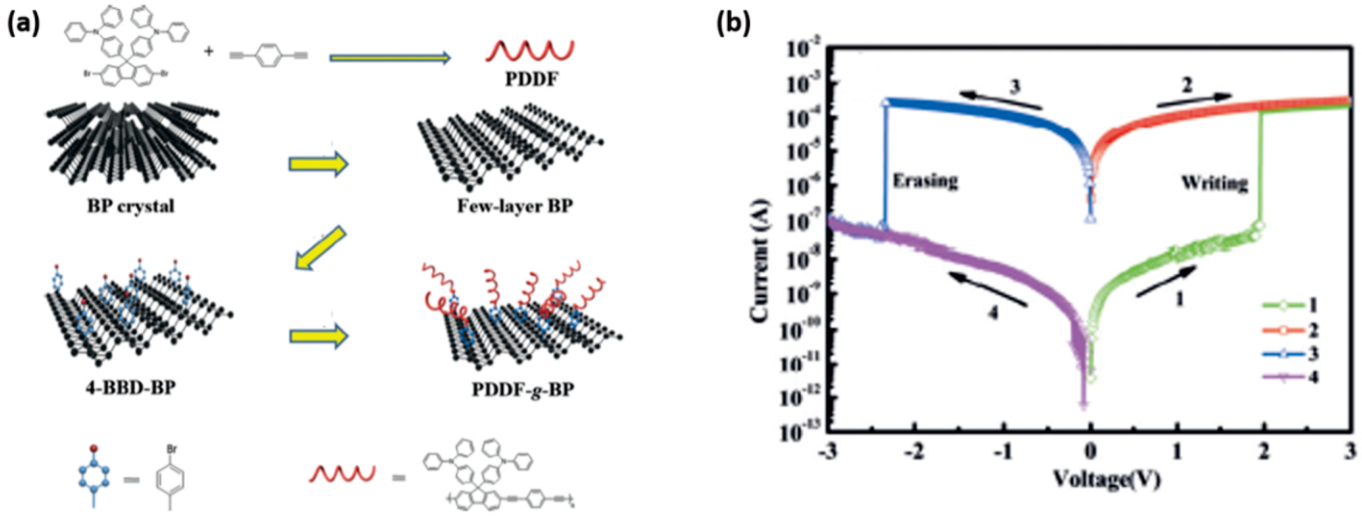

Fig. 27 (a) Synthesis of PDDF and PDDF-*g*-BP. (b) I-V characteristics of the Au/PDDF-*g*-BP/ITO device. Reproduced with permission from Ref 300.

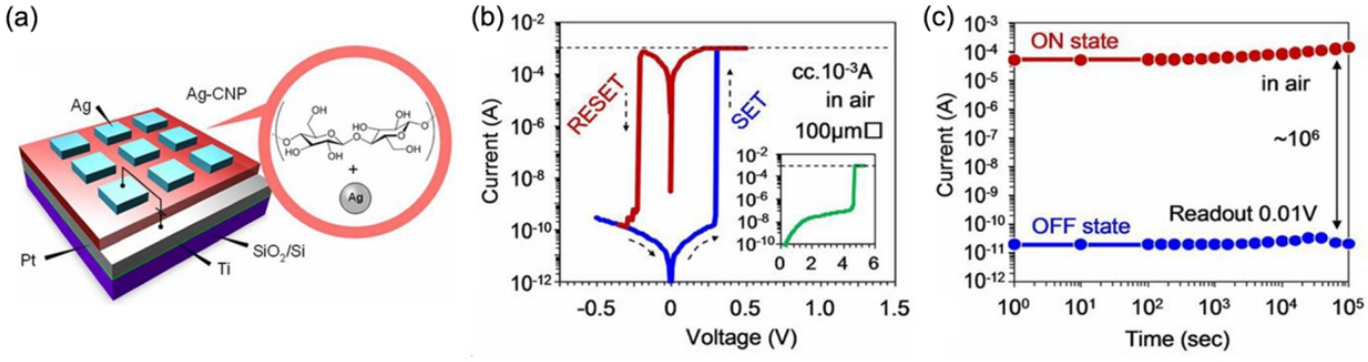

Fig. 28 Schematic structures and electrical properties of the Ag/Ag-CNP/Pt device. Reproduced with permission from Ref 305.

In order to avoid the aggregation and phase separation of foreign species in polymer matrix, as well as to improve the device performance, Chen and Kang *et al* for the first time covalently graft fullerene and graphene nanosheets onto electroactive polymer chains.[37,40-46,216,317,318] All the GO-polymer nanocomplexes are soluble and can be spin-coated into films. Arising from the charge transfer interaction between the polymer donor and graphene acceptor, good memory behaviors with ON/OFF ratio of $>10^3$ and endurance exceeding 100 million cycles are demonstrated (Fig. 26). Recently, the idea of covalent functionalization is further extended to black phosphorus, which shows both poor air-stability and solubility in common organic solvents. By tethering BP nanosheets with a TPA donor-containing polyfluorene derivative (PDDF), the resultant PDDF-*g*-BP exhibit bipolar resistive switching behavior with a turn-on and turn-off voltages of +1.95V and -2.34V, and an ON/OFF current ratio of 10^4 (Fig. 27).[319] More importantly, the device currents in both the ON and OFF states remain unchanged after 200 switching cycles in ambient environment.

(3) Resistive Switching Biomacromolecules

Extracting from living organisms, biomaterials possess the unrivalled advantages of being renewable, environmentally friendly and biocompatible. They are also flexible, inexpensive, solution processable and possible for implantable electronics.[320,321] Yang *et al* reported the first resistive switching memory made of biomacromolecules.[322,323] By attaching Pt nanoparticles onto the surface of a RNA virus tobacco mosaic virus (TMV), the resultant TMV-Pt composite dispersed in a PVA matrix exhibits bipolar resistive switching behavior with an ON/OFF ratio of ~ 10^3. Polysaccharides such as cellulose and chitosan are also explored for nonvolatile memory applications.[324-328] Yanagida and coworkers fabricated and characterized a cellulose-based resistive switching memory with Ag/Ag-decorated cellulose nanofiber paper (Ag-CNP)/Pt sandwitch structure (Figs. 28a-c).[324] Due to the reversible formation/rupture of Ag filaments, the device exhibits bipolar resistive switching behavior with small operation voltage of <0.5 V, high ON/OFF ratio of $>10^6$ and long retention up to 10^5 s that can be maintained at the bending radius of 2.5 mm (Figs. 28a-c).

Proteins are another family of biomacromolecules consisting of one or more amino acid residue chains. One particular example is the ferritin, which is the main intracellular iron storage protein with a nearly spherical shell (diameter: ~12 nm) and an active mineral core of hydrous ferric oxide (Fe(III)O·OH). In 2011, Chen *et al* mounted a bundle of ferritin in a Au nanogap etched by on-wire lithography (Fig. 29a),[329] and for the first time observed bipolar resistive switching behavior in protein materials (Fig. 29b). Increase in the Fe concentration of the ferritin can increase the ON/OFF ratio while removal of the metal oxide can annihilate the memory performance, suggesting that the electrochemical processes of the mineral core played a crucial role in the observed resistive switching behavior. It is believed that the reversible redox transition of the iron atom between ferric and ferrous states under external electric field modifies the energy structure and electrical conductance of ferritin, accounting for the resistive switching between ON and OFF states of the device (Fig. 29c). By controlling the compliance current preset, it is also possible to convert the switching behavior of the ferritin device between nonvolatile memory switching and volatile threshold switching.[54] Silk protein derived from *Bombyx mori* cocoons (e.g. fibroin),[330-335] chicken egg albumen[336] and etc also demonstrate resistive switching characteristics in flexible devices. In particular, due to their biodegradable and nontoxic nature, biomaterials are promising candidates for fabricating transient memory devices that can physically

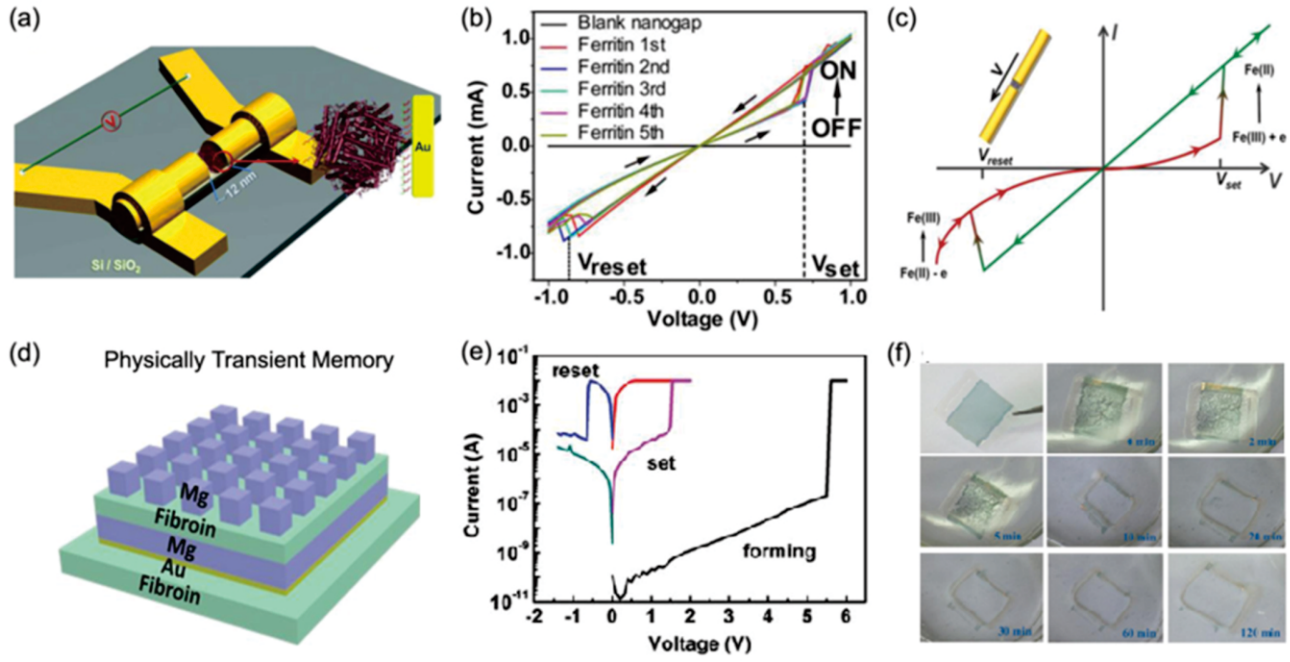

Fig. 29 (a) Schematic structure, (b) I-V characteristic, and (c) switching mechanism of the Au/ferritin/Au memory device. (d) Schematic structure, (e) I-V characteristics, and (f) dissolution process of the fibroin-based physically transient memory device in water. Reproduced with permission from Refs 329 and 334.

disappear on demand, in whole or in part, for specific applications in information security, implantable biomedical diagnostics and therapeutics and etc. To develop physically transient memories, Chen *et al* designed a resistive switching device with fibroin as the switching layer and water-dissolvable magnesium (Mg) as electrodes on home-made fibroin substrate (Fig. 29d).[222] The device showed bipolar resistive switching behavior (Fig. 29e) and can be gradually dissolved in water within 2 hours (Fig. 29f). Nevertheless, the present efforts are limited in searching protein materials that exhibit resistive switching characteristics, while less attention has been paid to the rational selection of protein towards specific end applications. Even though it is clear that water soluble biomaterials can be used in physically transient devices for biodegradable and information security applications, a stringent criterion has not be established for materials selection. Special concerns should be addressed on this in the future to select or even design suitable biomaterials for resistive switching memory devices.

(4) Resistive Switching Polymers for In-Memory Computing

Since 2008, it is demonstrated that emulation of the physiological functions of biological synapses and construction of neuromorphic computers can be made possible with the resistive switching memristors. To date, tremendous amount of efforts have been devoted to developing inorganic material based memristors.[8,11] Recently, memristive behavior was observed for the first time in soluble organic materials containing both electron donating and accepting units (PFD-4CN and PFD-8CN).[49,50,222] In addition to the bistable switching behavior that shows self-rectifying effect, nonlinear transmission characteristics of a biological synapse are achieved through consecutive multilevel conductance switching. The history-dependent memristive behaviors meet the fundamental requirements for mimicking the potentiation and depression processes of a biological synapse. Consequently, synaptic behaviors (Fig. 30), including the spike-rate-dependent and spike-timing-dependent plasticity (SRDP and STDP) characteristics, the transition from short-term memory (STM) to long-term memory (LTM), as well as the Ebbinghaus forgetting process, are realized in $EV(ClO_4)_2$/BTPA-F bilayer structure,[51-54] which may offer new opportunities for the construction of molecular electronics that can greatly enhance the performance of modern computer systems.

4. Organic-Inorganic Hybrid Resistive Switching Materials

It is common sense that the polymer materials usually shows uniform resistive switching behavior, promising mechanical flexibility but poor thermal stability, while the inorganic counterparts on the contrary carry good thermal stability but relatively smaller ON/OFF ratio and poor mechanical flexibility. With the aim to develop flexible resistive switching memories exhibiting juggled electrical and mechanical properties, the use of organic-inorganic

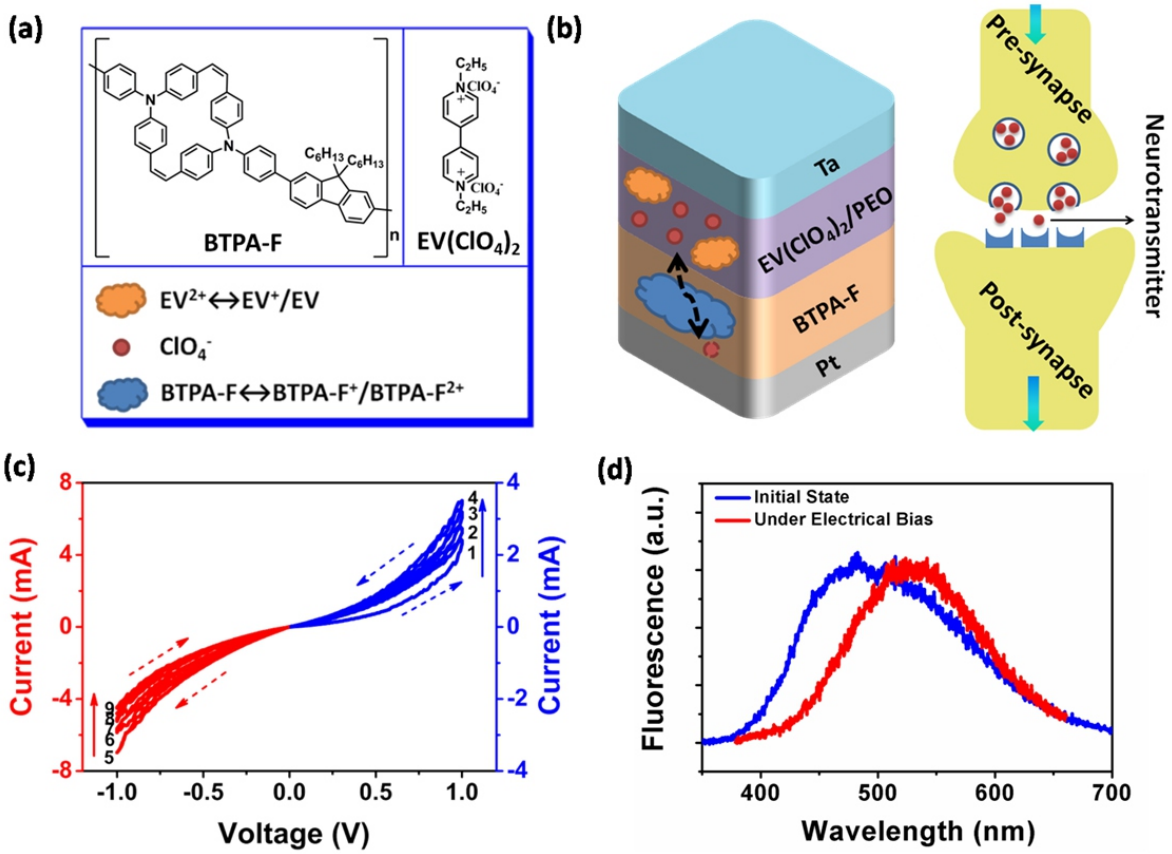

Fig. 30 (a) Chemical structures of BTPA-F and $EV(ClO_4)_2$, as well as the electrochemical redox reaction of the $EV(ClO_4)_2$/BTPA-F bilayer structure. (b) Schematic illustration of the Ta/$EV(ClO_4)_2$/BTPA-F/Pt memristor and the biological synapse. (c) The current-voltage characteristics of the Ta/$EV(ClO_4)_2$/BTPA-F/Pt memristor showing non-linear transmission behavior similar to that of a biological synapse. (d) The fluorescence of the $EV(ClO_4)_2$/BTPA-F bilayer structure in the initial state and under electrical bias. Reproduced with permission from Ref 51.

hybrid materials that can inherit the advantages of both intrinsic deformability from the organic constitutes and established electronic properties of the inorganic building blocks appears a promising strategy to implement nonvolatile memory devices with superior electromechanical performance.

4.1 Metal-Organic Framework Resistive Switching Materials

Metal-organic frameworks (MOFs) are a unique class of hybrid crystalline porous material with supermolecular structures constructed from metal cations and multitopic organic ligands, demonstrating great versatility in their physicochemical properties and three dimensional periodicity achieved through the versatile coordination synthesis chemistry.[337,338] Due to the synergetic interplay between the metal nodes and the organic linkers, as well as the host-guest interactions between the absorbed guest molecules and solid framework, deliberate tuning of the electronic and magnetic properties of the MOFs can be made possible. The presence of the soft organic linkers, moderate coordination bond strength that chelates the metal and organic species, and the large void space inside the one, two or three dimensional ordered pores, in addition provide an opportunity for mounting intrinsically flexible electronic and spintronic devices.

The initial efforts of developing MOF-based resistive switching memories were contributed individually yet simultaneously by Grzybowski and Pan *et al*.[47,339] Grzybowski used a cubic shaped millimeter size Rb-CD-MOF bulk crystal as the switching material (Fig. 31a), wherein the electric field-induced self-limiting oxidation of the anodic Ag metal leads to a clear hysteresis in the I-V loops (Fig. 31b). The as observed resistive switching characteristics are extrinsic to the use of MOF materials, while the ON state conductance decays quickly with time (Fig. 31c). On the other hand, Pan *et al* used a micrometer scale hexagonal prism RSMOF-1 crystal with the chemical formula of $[InC_{16}H_{11}N_2O_8]\cdot 1.5H_2O$ for resistive switching memory applications (Fig. 31d). The W/RSMOF-1/Pt structure device exhibits a highly uniform resistive switching behavior that can be retained over 6000 s (Figs. 31e&f), which originating from the ferroelectric transition of the N···H-O···H-N bridge-structured dipoles formed between the guest water molecules and the amino-tethered MOF nanochannel.

Confirming that MOF materials can be used for resistive switching memories, Pan and coworkers started the new mission of integrating them into thin film devices.[48] Towards this target, they developed a modified laboratory-scale liquid-phase epitaxy (LPE) facility, through which high quality thin MOF films can be prepared automatically and continuously in N_2 atmosphere without being exposed to contamination from the ambient condition. The second generation MOF film of HKUST-1 (($Cu_3(BTC)_2$, BTC = benzene-1,3,5-tricarboxylic acid, Fig. 32a) with thickness of ~130 nm and roughness of ~4 nm was successfully prepared on flexible Au-coated PET substrates. Uniform and reproducible resistive switching effect, which can be sustained under the strain of as high as 2.8%, and over the wide temperature range of -70 °C to +70 °C, has been observed for the first time in the all solid-state Au/HKUST-1/Au/PET thin film devices and explained in terms of copper ions migration and subsequent formation of sp^2-hybridized carbon conductive filaments (Figs. 32b&c). Under the strain level of 2.0%, these devices showed a highly uniform switching behavior for 300 continuous operation cycles (Fig. 32d) or 160 bending cycles (Fig. 32e), with excellent endurance $>10^7$ cycles (Fig. 32f) and stable data retention exceeding 10^4 s (Fig. 32g), providing promising material candidates for the development of flexible or even wearable information storage techniques.

Flexible resistive switching memory with the structure of Al/ZIF-8/Au on PET substrate was also fabricated through a dip-coating approach.[340] Chen *et al* prepared a Ag/ZIF-8/Si structured device and found that the formation of Ag nanoparticles inside the ZIF-8 insulating layer and the carrier hopping between these nanoparticles can cause bipolar resistive switching behavior with external voltage applied to the Ag top electrode under ambient conditions (Fig. 33a).[341] When the device is infiltrated and saturated with methanol vapor, its HRS resistance decreases dramatically to give a much lower ON/OFF ratio of $\sim 10^4$ (Fig. 33b). This phenomenon is fully reversible and robust (Fig. 33c), which is arising from the ordered packing mode and the hydrogen bonding system of the guest molecules adsorbed in MOF crystals (Fig. 32d). With their intrinsic high porosity and excellent ability for gas adsorption, MOF-based devices demonstrate great potential of MOF-based device for chemically mediated multilevel information storage with integrated and environment-responsive sensing applications.

4.2 Organic-Inorganic Hybrid Perovskite Resistive Switching Materials

Organic-inorganic hybrid perovskites with chemical structure of $MAPbX_3$ ($MA = CH_3NH_3^+$; $X = I^-$, Br^-, Cl^-) are organic analogue of the inorganic ABO_3 perovskite-type oxide materials, comprised of an extended framework of corner-sharing PbX_6 octahedral, with the methyl ammonium cation $CH_3NH_3^+$ occupying the central A site and surrounded by 12 nearest-neighbor halide ions (Fig. 34a).[342] These materials are featured with strong optical absorption, tunable band gap, ambipolar charge transport, and long electron-hole diffusion length, thus suitable for solar cells, light-emitting diodes and thin-film transistors applications. The mobile halide anions also make conductance tuning of these hybrid perovskite possible for resistive switching memory applications.

Choi *et al* reported the first Au/$CH_3NH_3PbI_{3-x}Cl_x$/FTO resistive switching memory in 2015, which shows bipolar resistive switching behavior with ON/OFF ratio of >3 over 100 cycles and data retention of $>10^4$ s (Figs. 34b&c).[343] Given the solution and large area processable feature of $MAPbX_3$, Gu and Lee successfully fabricated flexible Au/$CH_3NH_3PbI_3$/ITO on PET substrate.[344] The perovskite device shows bipolar switching behavior with operation voltage of <1 V and ON/OFF ratio of >10 in flat state, while maintains its electrical performance under tensile or compressive bending with radius of 15 mm (Figs. 34d&e). Intentional addition of hydroiodic acid in the precursor solution of perovskite can reduce the grain size and surface roughness of the $CH_3NH_3PbI_3$ film significantly, which in turn enables the Ag/$CH_3NH_3PbI_3$/Pt memory device to work free of cracks when being bended with a small radius of 5 mm.[345] The observed low voltage switching behavior is ascribed to the reversible formation and rupture of iodide vacancy based filaments (Fig. 34f), and is recently confirmed experimentally by energy-dispersive X-ray spectroscopy (EDX) analysis.[346] In the meanwhile, vapor-based and CMOS-compatible deposition of $MAPbX_3$ films has been developed by Lee *et al* on wafers perforated with 250 nm via-holes (Fig. 35a).[347] Through sequential deposition of the PbI_2 and CH_3NH_3I constituents *via* sublimation into the via-holes pre-defined by SiO_2 on Pt-coated silicon wafer, a complete formation of $CH_3NH_3PbI_3$ layer is achieved as revealed by the change of film color from yellow to brown. Nanoscale Au/$CH_3NH_3PbI_3$/Pt devices, integrated into a 16×16 cross-point memory array with line width of 300 μm, exhibit bipolar switching behavior with V_{set} of 1 V, V_{reset} of -1V and a high

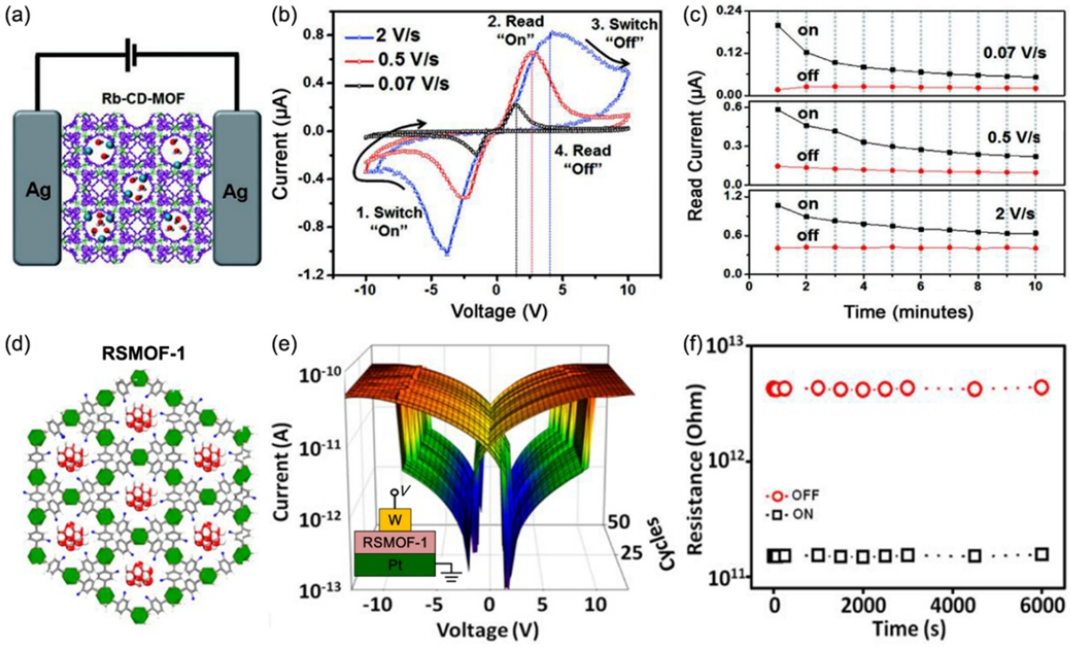

Fig. 31 Chemical structures, I-V characteristics, and retention properties of (a-c) Rb-CD-MOF and (d-f) RSMOF-1 bulk materials. Reproduced with permission from Refs 47 and 339.

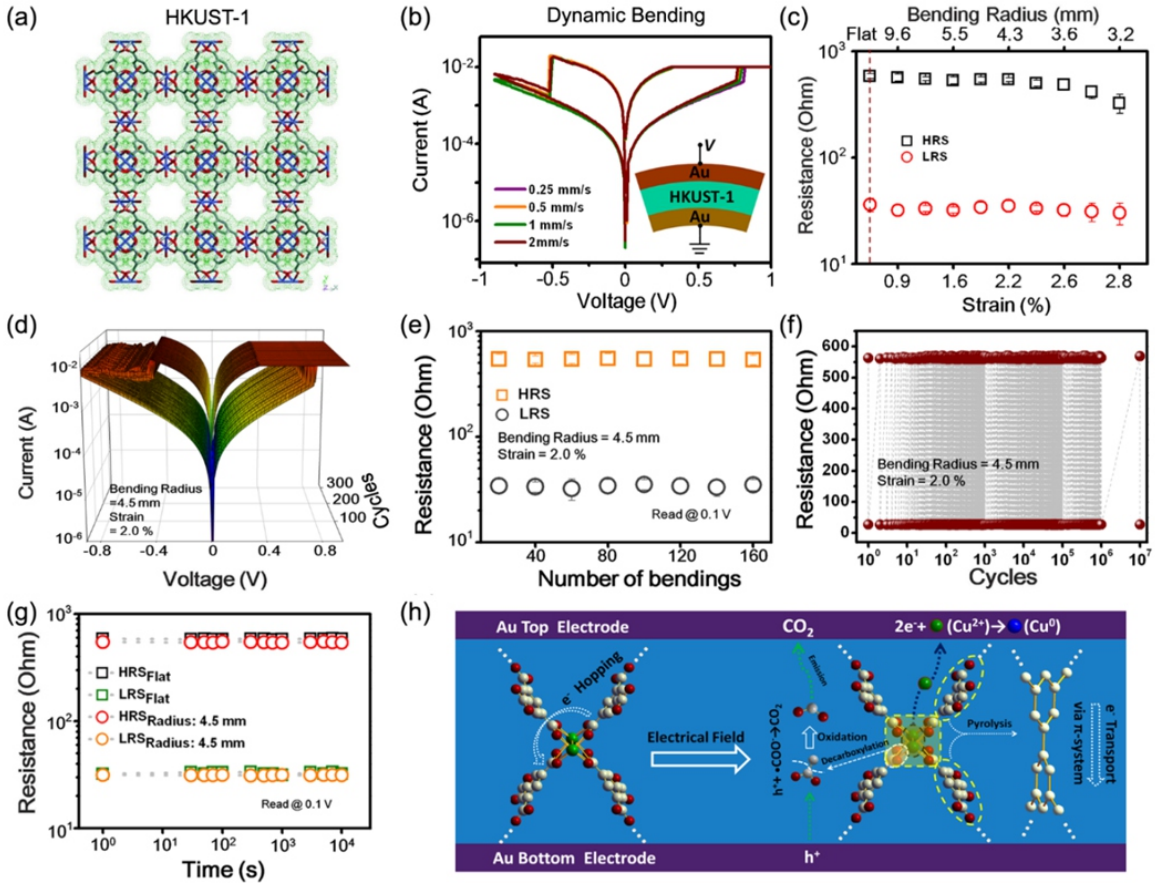

Fig. 32 (a) Chemical structure of HKUST-1. (b) *I-V* characteristic under dynamic bending and (c) static bending performance of the Au/HKUST-1/Au memory device. (d) *I-V* characteristic, (e) bending endurance, (f) switching endurance, and (g) retention property of the device under bending with 4.5 mm radius. (h) Schematic switching mechanism of the device. Reproduced with permission from Ref. 48.

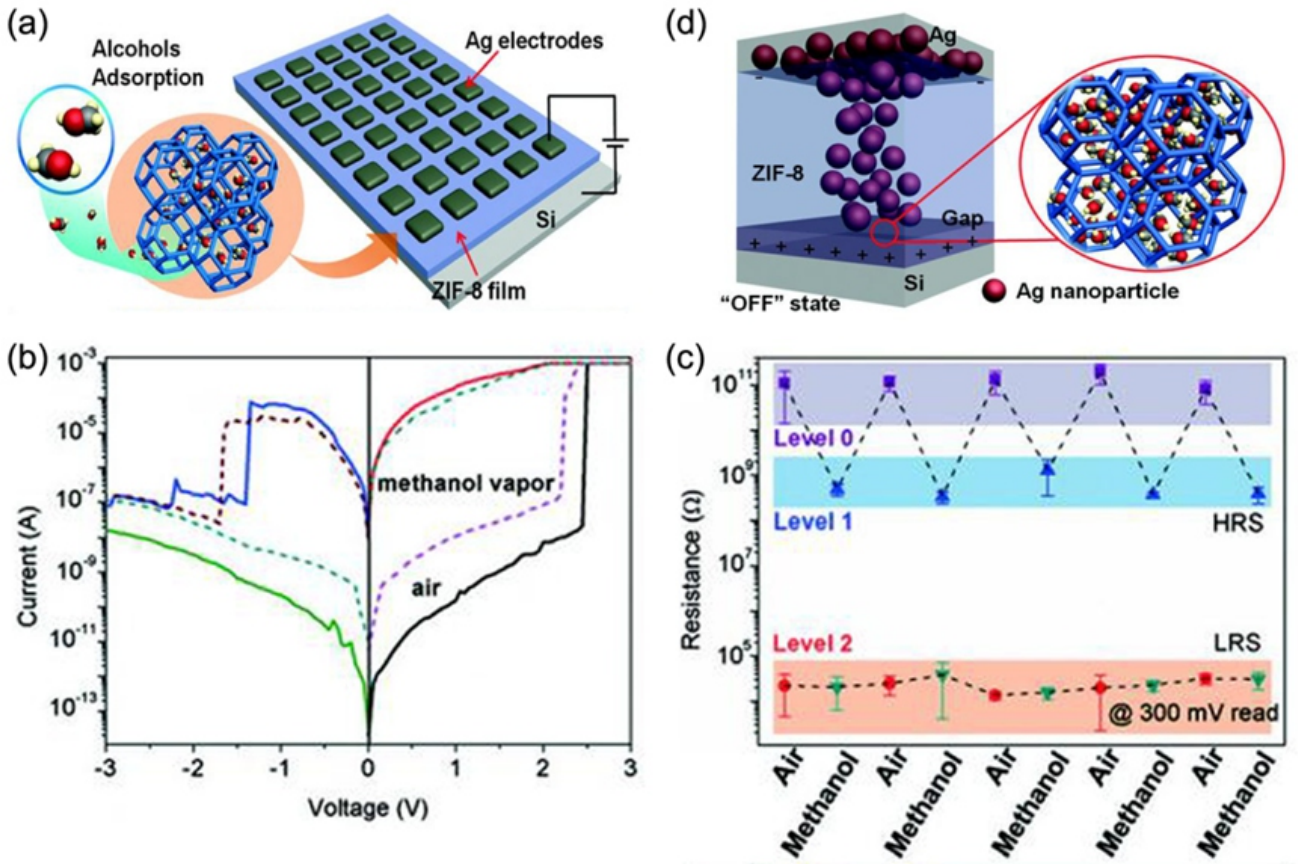

Fig. 33 (a) Schematic structure of the Ag/ZIF-8/Si memory device. (b) I–V characteristics of the device in air and saturated methanol vapor. (c) Repeated cycles of the device in air and saturated methanol vapor. (d) Schematic mechanism of the alcohol-mediated HRS resistance. Reproduced with permission from Ref 322.

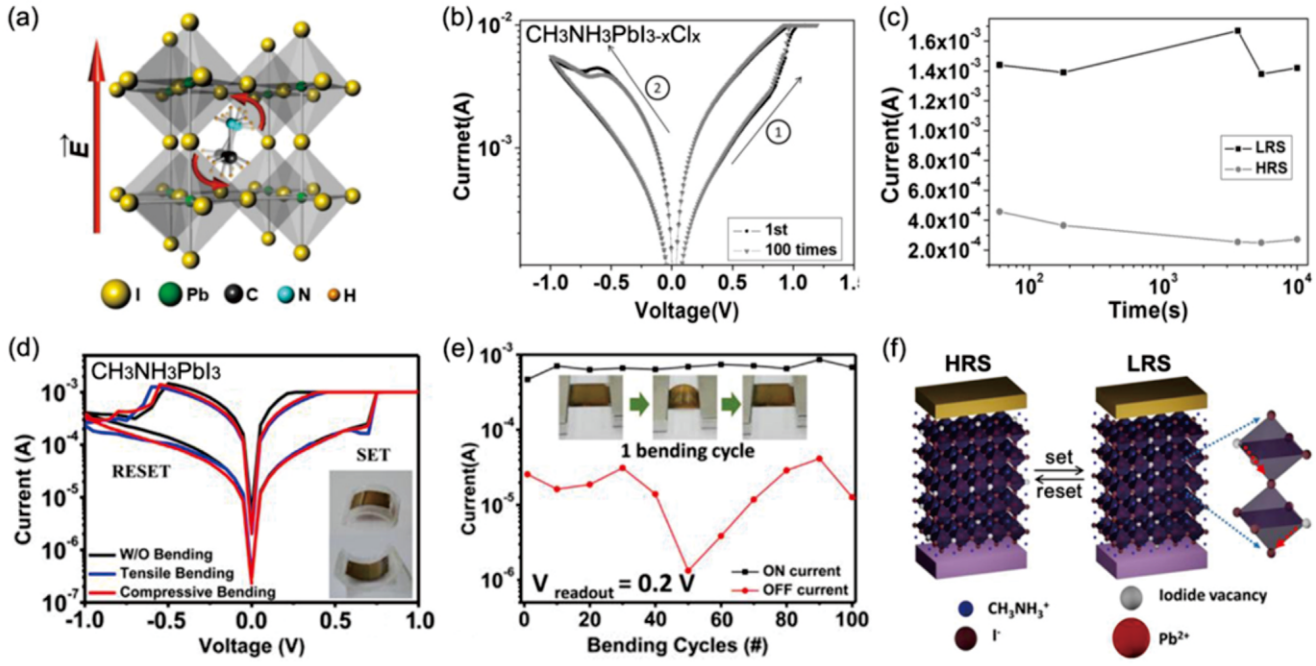

Fig. 34 (a) Chemical structure of $MAPbX_3$. (b,c) I–V characteristic and retention property of the Au/$CH_3NH_3PbI_{3-x}Cl_x$/FTO memory device. (d-f) I–V characteristics under various bending conditions, bending endurance at 15 mm radius, and switching mechanism of the Au/$CH_3NH_3PbI_3$/ITO memory device. Reproduced with permission from Refs 342-344.

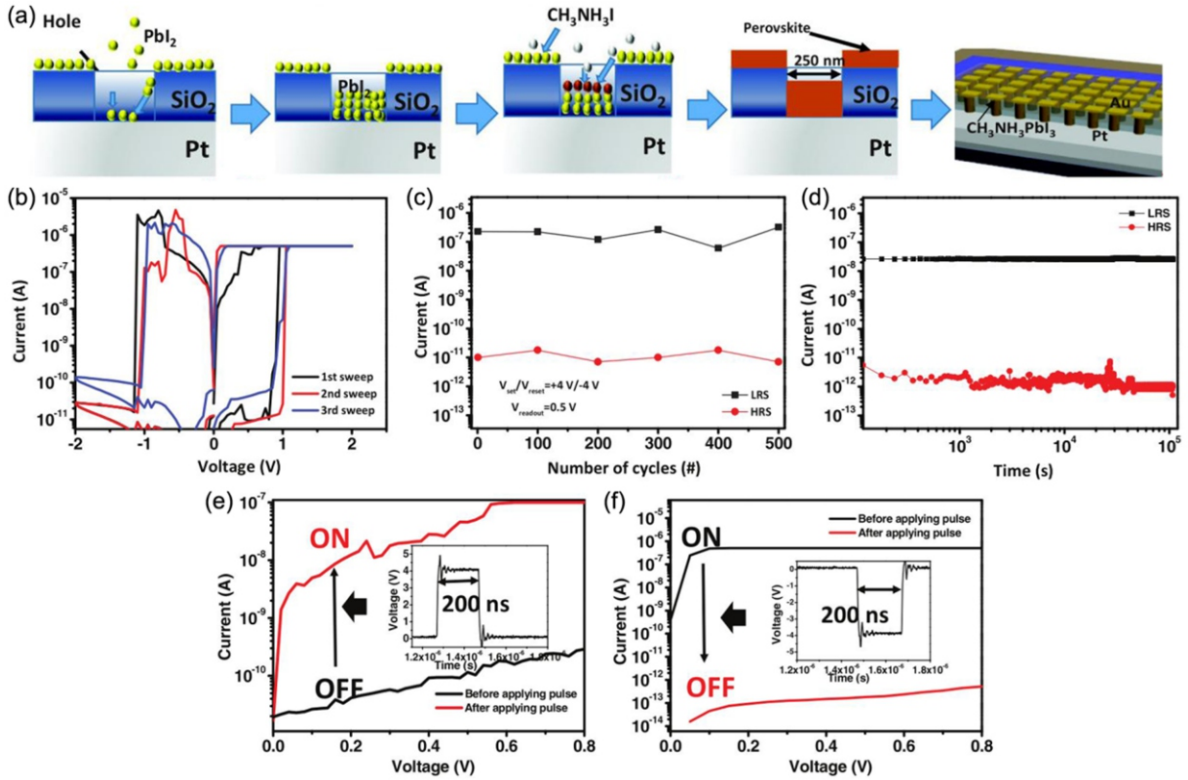

Fig. 35 (a) Fabrication procedure of the Au/$CH_3NH_3PbI_3$/Pt memory device with 250 nm via-hole structure *via* vapor method. (b) I-V characteristic, (c) switching endurance, (d) retention property, and (e,f) pulse operations of the device. Reproduced with permission from Ref 328.

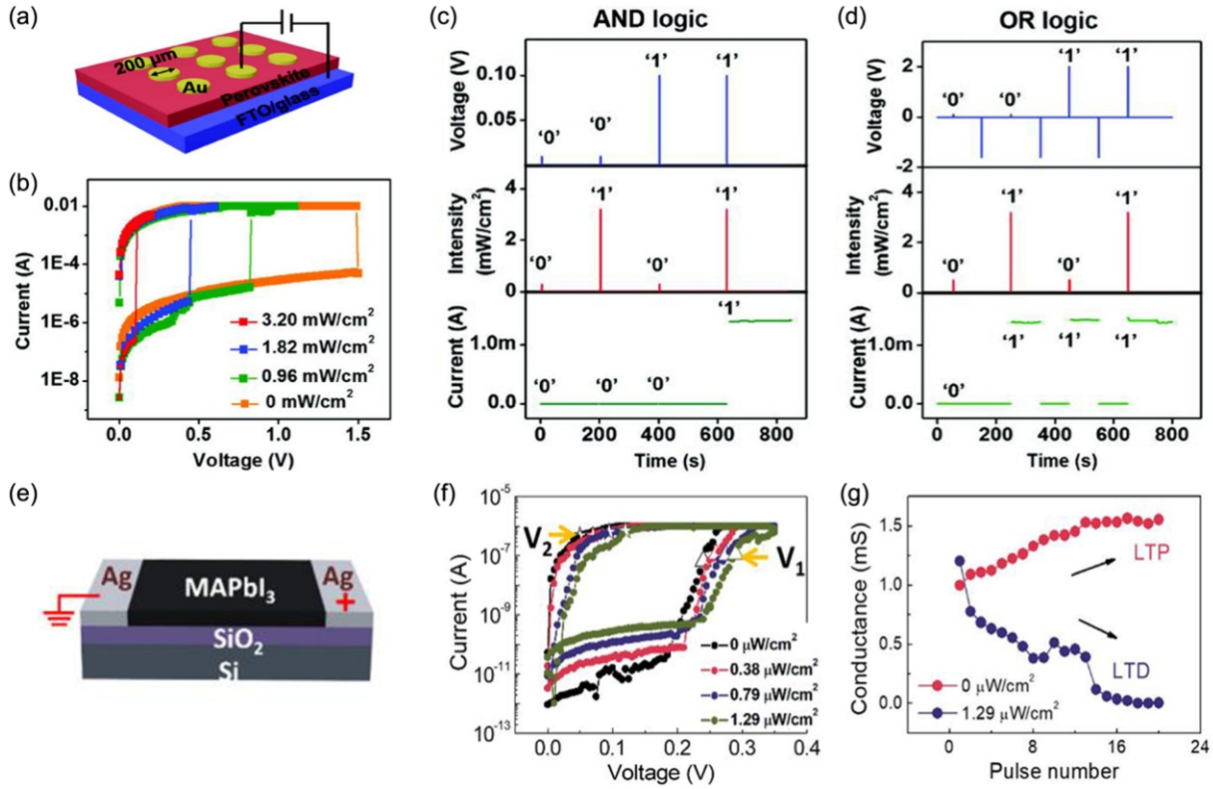

Fig. 36 (a) Schematic structure, (b) I-V characteristic, and (c,d) nonvolatile logic applications of the vertical Au/$CH_3NH_3PbI_{3-x}Cl_x$/FTO optoelectronic memory device. (e) Schematic structure, (f) I-V characteristic, and (g) light-induced change in synaptic functions of the planar structured Ag/$CH_3NH_3PbI_3$/Ag optoelectronic memory device. Reproduced with permission from Refs 348 and 349.

ON/OFF ratio of $>10^3$ during 500 consecutive switching cycles or a retention test period of $>10^5$ s (Figs. 35b-f).

Considering the photo responsive nature of the organic-inorganic hybrid perovskite materials, many efforts have been made to develop $MAPbX_3$-based optoelectronic memories that can integrate the functions of light sensing, data storage, and data processing into one single device to widen its application scope.[348,349] It is observed that due to the light-assisted hole injection into the perovskite/Au interfacial trapping centers and subsequent energy barrier modulation, the writing voltage vertical $Au/CH_3NH_3PbI_{3-x}Cl_x/FTO$ device can be greatly lowered under light illumination (Figs. 36a &b).[348] By defining light and voltage pulses with proper intensity and duration as the optical and electrical logic input "1" and "0", and HRS and LRS of the device defined as output logic "0" and output logic "1", respectively, nonvolatile AND and OR logic operations are realized with the $Au/CH_3NH_3PbI_{3-x}Cl_x/FTO$ device (Figs. 36c &d). With the continuous modulation of the $Ag/CH_3NH_3PbI_3/Ag$ device conductance under optical illumination with increasing intensities (Fis. 36e&f),[348] associated with the optical and electric dual field controlled iodine vacancy generation, optogenetic processes in biological synapses has been emulated with perovskite resistive switching devices for neuromorphic computing applications (Fig. 36g).

5. Summary and Outlook

Over the past decade, great efforts have been devoted to the development of resistive switching materials and devices. Bistable modulation of the device resistance, as well as the binary coding and storage of the digital information, are realized with both inorganic and organic resistive switching materials. Nevertheless, the kinetics of the resistive switching phenomena under ultrahigh frequency (exceeding GHz) in ultra-small scale (less than 10 nm) of practical devices are obviously different from that tested in the laboratory. In order to realize the very large scale integration of the memory with the CPU in the same chip, as well as to further implement the in-memory computing through memristor with the incremental modulation of device conductance, comprehensive and deep insight into the electrochemistry at electrode/switching medium interface on nanoscale or ever at the atomic level, the migration and aggregation behaviors of the mobile species in both the bulk switching layer, the charge transfer and redox activities involved in organic medium, and the charge transport across the storage thin film, is still necessary at the moment. CMOS compatible resistive switching materials, for both the organic small molecules polymers and organic-inorganic hybrid materials, should be developed for industrial inclusion and fabrication. Regarding the flexible and wearable applications, these materials should be made into single or few layer two-dimensional nanosheets with the aim to minimize their own thickness on the deformation capability. The stability again environmental high and low temperatures, moisture and human sweats, as well as radiation from the other equipments including the mobile phones, laptop computers and etc should also be improved for practical applications. With the rapid growth of IoT (internet of things) and wearable electronic techniques, more and more concerns should be paid on the development and application of flexible and even stretchable resistive switching materials and devices.

Acknowledgment

The authors acknowledge the financial support from the National Natural Science Foundation of China (61722407, 51333002, 61774161, 61674153, 51525103, 11474295, 21404037), the National Key R&D Program of China (2017YFB0405604), the Research Fund for the Doctoral Program of Higher Education of China (20120074110004), the State Key Laboratory of ASIC & System of Fudan University (11KF007), the State Key Project of Fundamental Research of China (973 Program, 2012CB933004), the Fundamental Research Funds for the Central Universities (WJ1514311), K. C. Wong Education Foundation (RCZX0800), Natural Science Foundation of Zhejiang Province (LR17E020001), and Ningbo Science and Technology Innovation Team (2015B11001).

References

1. G. Burr, B. Kurdi, J. Scott, C. Lam, K. Gopalakrishnan, R. Shenoy, Overview of Candidate Device Technologies for Storage-Class Memory. IBM, 2008.
2. A. Chung, J. Deen, J. Lee, *Nanotechnology*, 2010, **21**, 412001.
3. J. Von Neumann, First Draft of a Report on the EDVAC 1945.
4. P. Kogge, *ExaScale Computing Study: Technology Challenges in Achieving Exascale Systems*; DARPA Information Processing Technique Office, 2008.
5. S. Borkar, A. Chien, *Commun. Assoc. Comput. Machin.*, 2011, **54**, 67-77.
6. S. Liu, N. Wu, A. Ignatiev, *Appl. Phys. Lett.*, 2000, **76**, 2749-2751.
7. R. Waser, M. Aono, *Nature Mater.*, 2007, **6**, 833-840.
8. F. Pan, S. Gao, C. Chen, C. Song, F. Zeng, *Mater. Sci. Eng. R*, 2014, **83**, 1-59.
9. H. Wong, S. Salahuddin, *Nature Nanotech.*, 2015, **10**, 191-194.
10. http://www.itrs.net/Links/2009ITRS/2009Chapters_2009Tables/2009_Execsum.pdf
11. J. Borghetti, G. Snider, P. Kuekes, J. Yang, D. Stewart, R. Williams, *Nature*, 2010, **464**, 873-876.
12. X. Zhu, J. Shang, R. Li, *Front. Mater. Sci.*, 2012, **6**, 183-206.
13. X. Zhu, J. Shang, G. Liu, R. Li, *Chin. Sci. Bul.*, 2014, **59**, 2363-2382.
14. D. Jeong, R. Thomas, R. Katiyar, J. Scott, H. Kohlstedt, A. Petraru, C. Hwang, *Rep. Prog. Phys.*, 2012, **75**, 076502.
15. K. Yin, M. Li, Y. W. Liu, C. He, F. Zhuge, B. Chen, W. Lu, X. Q. Pan, R. Li, *Appl. Phys. Lett.*, 2010, **97**, 042101.
16. M. Li, F. Zhuge, X. Zhu, K. Yin, J. Wang, Y. Liu, C. He, B. Chen, R. Li, *Nanotechnology*, 2010, ***21***, 425202.
17. X. Zhu, F. Zhuge, M. Li, K. Yin, Y. Liu, Z. Zuo, B. Chen, R. Li, *J. Phys. D: Appl. Phys.*, 2011, **44**, 415104.
18. S. Peng, F. Zhuge, X. Chen, X. Zhu, B. Hu, L. Pan, B. Chen, R. Li, *Appl. Phys. Lett.*, 2012, **100**, 072101.
19. X. Zhu, C. Ong, X. Xu, B. Hu, J. Shang, H. Yang, S. Katlakunta, Y. Liu, X. Chen, L. Pan, J. Ding, R. Li, *Sci. Rep-UK.*, 2013, **3**, 1084.
20. X. Zhu, W. Su, Y. Liu, B. Hu, L. Pan, W. Lu, J. Zhang, R. Li, *Adv. Mater.*, 2012, **24**, 3941-3946.
21. Z. Yang, Q. Zhan, Y. Liu, G. Dai, H. Yang, Z. Zuo, B. Chen, B. Wang, Y. Zhang, X. Rong, R. Li, *Euro. Phys. Lett.*, 2014, **108**, 58004.
22. W. Xue, W. Xiao, X. Chen, X. Zhu, J. Shang, L. Pan, H. W. Tan, G. Liu, X. H. Xu, J. Ding, R. W. Li, *Nanotechnology*, 2014, **25**, 425204.
23. J. Shang, G. Liu, H. Yang, X. Zhu, X. Chen, H. Tan, B. Hu, L.

Pan, W. Xue, R. Li, *Adv. Funct. Mater.*, 2014, **24**, 2171-2179.
24. X. Chen, X. Zhu, W. Xiao, G. Liu, Y. Feng, J. Ding, R. Li, *ACS Nano*, 2015, **9**, 4210-4218.
25. J. J. Yang, D. B. Strukov, D. R. Stewart, *Nature Nanotech.*, 2013, **8**, 13-23.
26. Y. Chen, G. Liu, C. Wang, W. B. Zhang, R.-W. Li, B. Zhang, *Mater. Horiz.*, 2014, **1**, 489-506.
27. Y. Chen, B. Zhang, G. Liu, X. D. Zhuang, E. T. Kang, *Chem. Soc. Rev.*, 2012, **41**, 4688-4707.
28. L. J. Zeng, G. Liu, B. Zhang, J. Chen, Y. Chen, E. T. Kang, *Polym. J.*, 2011, **44**, 257-263.
29. L. Pan, B. L. Hu, X. J. Zhu, X. X. Chen, J. Shang, H. W. Tan, W. H. Xue, Y. J. Zhu, G. Liu, R.-W. Li, *J. Mater. Chem. C*, 2013, **1**, 4556-4564.
30. K. L. Wang, G. Liu, P. H. Chen, L. Pan, H. L. Tsai, *Org. Electron.*, 2014, **15**, 322-336.
31. X. D. Zhuang, Y. Chen, G. Liu, B. Zhang, K. G. Neoh, E. T. Kang, C. X. Zhu, Y. X. Li and L. J. Niu, *Adv. Funct. Mater.*, 2010, **20**, 2916-2922.
32. G. Liu, B. Zhang, Y. Chen, C. X. Zhu, L. J. Zeng, D. S. H. Chan, K. G. Neoh, E. T. Kang, *J. Mater. Chem.*, 2011, **21**, 6027-6033.
33. B. Zhang, G. Liu, Y. Chen, C. Wang, K. G. Neoh, T. Bai, E. T. Kang, *ChemPlusChem*, 2012, **77**, 74-81.
34. G. Liu, D. J. Liaw, W. Y. Lee, Q. D. Ling, C. X. Zhu, D. S. H. Chan, E. T. Kang, K. G. Neoh, *Phil. Trans. R. Soc. A*, 2009, **367**, 4203-4214.
35. B. L. Hu, X. J. Zhu, X. X. Chen, L. Pan, S. S. Peng, Y. Z. Wu, J. Shang, G. Liu, Q. Yan, R. W. Li, *J. Am. Chem. Soc.,* 2012, **134**, 17408-17411.
36. G. Liu, Q. D. Ling, E. Y. H. Teo, C. X. Zhu, D. S. H. Chan, K. G. Neoh, E. T. Kang, *ACS Nano,* 2009, **3**, 1929-1937.
37. G. Liu, X. D. Zhuang, Y. Chen, B. Zhang, J. H. Zhu, C. X. Zhu, K. G. Neoh, E. T. Kang, *Appl. Phys. Lett.,* 2009, **95**, Art. No. 253301.
38. C. L. He, F. Zhuge, X. F. Zou, M. Li, G. C. Zhou, Y. W. Liu, J. Z. Wang, B. Chen, W. J. Su, Z. P. Liu, Y. H. Wu, P. Cui, R. W. Li, *Appl. Phys. Lett.,* 2009, **95**, 232101.
39. B. L. Hu, R. Quhe, C. Chen, F. Zhuge, X. J. Zhu, S. S. Peng, X. X. Chen, L. Pan, Y. Z. Wu, W. G. Zheng, Q. Yan, J. Lu, R. W. Li, *J. Mater. Chem.,* 2012, **22**, 16422-16430.
40. X. D. Zhuang, Y. Chen, G. Liu, P. P. Li, C. X. Zhu, E. T. Kang, K. G. Neoh, B. Zhang, J. H. Zhu, Y. X. Li, *Adv. Mater.,* 2010, **22**, 1731-1735.
41. B. Zhang, Y. Chen, X. D. Zhuang, G. Liu, B. Yu, E. T. Kang, J. H. Zhu, Y. X. Li, *J. Polym. Sci Part A: Polym. Chem*., 2010, **48**, 2642-2649.
42. B. Zhang, Y. Chen, Y. Ren, L. Xu, G. Liu, E. T. Kang, C. Wang, C. X. Zhu, K. G. Neoh, *Chem. Eur. J.,* 2013, **19**, 6265-6273.
43. G. L. Li, G. Liu, M. Li, D. Wan, K. G. Neoh, E. T. Kang, *J. Phys. Chem. C,* 2010, **114**, 12742-12748.
44. B. Zhang, Y. Chen, G. Liu, L. Q. Xu, L. J. Zeng, C. X. Zhu, K. G. Neoh, E. T. Kang, *J. Polym. Sci. Part A: Polym. Chem.,* 2011, **50**, 378-387.
45. B. Zhang, G. Liu, Y. Chen, L. J. Zeng, C. X. Zhu, K. G. Neoh, C. Wang, E. T. Kang, *Chem. Eur. J.,* 2011, **17**, 13646-13652.
46. G. Liu, Y. Chen, B. Zhang, R. W. Li, E. T. Kang, *ChemElectroChem,* 2014, **1**, 514-519.
47. L. Pan, G. Liu, H. Li, S. Meng, L. Han, J. Shang, B. Chen, A. E. Platero-Prats, W. Lu, X. Zou and R. W. Li, *J. Am. Chem. Soc.,* 2014, **136**, 17477-17483.
48. L. Pan, Z. Ji, X. Yi, X. Zhu, X. Chen, J. Shang, G. Liu and R. W. Li, *Adv. Funct. Mater.,* 2015, **25**, 2677-2685.
49. C. Wang, G. Liu, Y. Chen, S. S. Liu, Q. B. Chen, R. W. Li, B. Zhang, *ChemPlusChem,* 2014, **79**, 1263-1270.
50. C. Wang, G. Liu, Y. Chen, R. W. Li, W. B. Zhang, L. X. Wang, B. Zhang, *J. Mater. Chem. C,* 2015, **3**, 664-673.
51. G. Liu, C. Wang, W. B. Zhang, L. Pan, C. C. Zhang, X. Yang, F. Fan, Y. Chen, R. W. Li, *Adv. Electron. Mater.,* 2016, **2**, 1500298.
52. C. C. Zhang, Y. T. Tai, J. Shang, G. Liu, K. L. Wang, C. W. Hsu, X. H. Yi, X. Yang, W. H. Xue, H. W. Tan, S. S. Guo, L. Pan, R.-W. Li, *J. Mater. Chem. C,* 2016, **4**, 3217-3223.
53. X. Yang, C. Wang, J. Shang, C. C. Zhang, H. W. Tan, X. H. Yi, L. Pan, W. B. Zhang, F. Fan, Y. Q. Liu, Y. Chen, G. Liu, R. W. Li, *RSC Adv.,* 2016, **6**, 25179-25184.
54. C. Zhang, J. Shang, W. Xue, H. Tan, L. Pan, X. Yang, S. Guo, J. Hao, G. Liu and R. W. Li, *Chem. Commun.,* 2016, **52**, 4828-4831.
55. I. Valov, I. Sapezanskaia, A. Nayak, T. Tsuruoka, T. Bredow, T. Hasegawa, G. Staikov, M. Aono, R. Waser, *Nature Mater.,* 2012, **11**, 530-535.
56. J. R. Jameson, N. Gilbert, F. Koushan, J. Saenz, J. Wang, S. Holmer, M. N. Kozicki, *Appl. Phys. Lett.,* 2011, **99**, 063506.
57. S. Tappertzhofen, H. Mündelein, I. Valov, R. Waser, *Nanoscale,* 2012, **4**, 3040-3043.
58. T. Sakamoto, K. Lister, N. Banno, T. Hasegawa, Tebera, T. M. Aono, *Appl. Phys. Lett.,* 2007, **91**, 092110.
59. B. Yang, X. F. Liang, H. X. Guo, K. B. Yin, J. Yin, Z. G. Liu, *J. Appl. Phys. D.-Appl. Phys.,* 2008, **41**, 115304.
60. J. Yao, L. Zhong, Z. Zhang, T. He, Z. Jin, P. J. Wheeler, D. Natelson, J. M. Tour, *Small,* 2009, **5**, 2910-2915.
61. S. Tappertzhofen, I. Valov, R. Waser, *Nanotechnology,* 2012, **23**, 145703.
62. I. Valov, M/ N. Kozicki, *J. Appl. Phys. D.-Appl. Phys.,* 2013, **46**, 074005.
63. R. Waser, R. Dittmann, G. Staikov, K. Szot, *Adv. Mater.,* 2009, **21**, 2632-2663.
64. I. Valov, R. Waser, J. R. Jameson, M. N. Kozicki, *Nanotechnology,* 2012, **22**, 254003.
65. I. Valov, E. Linn, S. Tappertzhofen, S. Schmelzer, J. v. d. Hurk, F. Lentz, R. Waser, *Nature Commun.,* **2013**, *4*, 1771.
66. M. Lübben, S. Wiefels, R. Waser, I. Valov, *Adv. Electron. Mater.,* 2018, **4**, 1700458.
67. M. N. Kozicki, M. Park, M. Mitkova, *IEEE Trans. Nanotechnology*, 2005, **4**, 331-338.
68. C. Schindler, M. Merier, R. Waser, M. N. Kozicki, In *Proc. IEEE Non-Volatile Memory Technology Symp.,* 2007, 82-85.
69. K. Szot, W. Speier, G. Bihlmayer, R. Waser, *Nature Mater.,* 2006, **5**, 312-320.
70. A. Sawa, T. Fujii, M. Kawasaki, Y. Tokura, *Appl. Phys. Lett.,* 2006, **88**, 232112.
71. J. J. Yang, M. D. Pickett, X. Li, D. A. A. Ohlberg, D. R. Stewart, R. S. Williams, *Nature Nanotech.,* 2008, **3**, 429-433.
72. D. H. Kwon, K. M. Kim, J. H. Jang, J. M. Jeon, M. H. Lee, G. H. Kim, X. S. Li, G. S. Park, B. Lee, S. Han, M. Kim and C. S. Hwang, *Nature Nanotech.,* 2010, **5**, 148-153.
73. M. J. Lee, C. B. Lee, D. S. Lee, S. R. Lee, M. Chang, J. H. Hur, Y. B. Kim, C. J. Kim, D. H. Seo, S. Seo, U. I. Chang, I. K. Yoo and K. Kim, *Nature Mater.,* 2011, **10**, 625-630.
74. S. J. Choi, G. S. Park, K. H. Kim, S. Cho, W. Y. Yang, X. S. Li, J. H. Moon, K. J. Lee, K. Kim, *Adv. Mater.,* 2011, **23**, 3272-3277.

75. Y. Yang, P. Gao, S. Gaba, T. Chang, X. Q. Pan, W. Lu, *Nature Commun.,* 2012, **3**, 732.
76. G. S. Park,Y. B. Kim, S. Y. Park, X. Shu, Li, S. Heo, M. J. Lee, M. Chang, J. H. Kwon, M. Kim, UI. Chung, R. Dittmann, R. Waser, K. Kim, *Nature Commun.,* 2013, **4**, 2382.
77. S. Kumar, Z. Wang, N. Davila, N. Kumari, K. J. Norris, X. Huang, J. P. Strachan, D. Vine, A. L. D. Kilcoyne, Y. Nishi, R. S. Williams, *Nature Commun.,* 2017, **8**, 658.
78. Y. Yang, X. Zhang, L. Qin, Q. Zeng, X. Qiu, R. Huang, *Nature Commun.,* 2017, **8**, 15173.
79. D. S. Shan, S. Lei, J. R. Sun, B. G. Shen, *J. Appl. Phys.,* 2012, **111**, 053504.
80. X. Guo, C. Schindler, S. Menzel, R. Waser, *Appl. Phys. Lett.,* 2007, **91**, 133513.
81. Y. Yang, P. Gao, L. Li, X. Q. Pan, S. Tappertzhofen, S. Choi, R. Waser, I. Valov, W. Lu, *Nature Commun.,* 2014, **5**, 4232.
82. X. Wu, S. Mei, M. Bosman, N. Raghavan, X. Zhang, D. Cha, K. Li, K. L. Pey, *Adv. Electron. Mater.,* 2015, **1**, 1500130
83. L. H. Li, E. J. G. Santos, T. Xing, E. Cappelluti, R. Roldan, Y. Chen, K. Watanabe, T. Taniguchi, *Nano Lett.,* 2015, **15**, 218-223.
84. M. Hempel, A. Y. Lu, F. Hui, T. Kpulun, M. Lanza, G. Harris, T. Palacios, J. Kong, *Nanoscale,* 2018, **10**, 5522-5531.
85. E. Yalon, S. Cohen, A. Gavrilov, D. Ritter, *Nanotechnology,* 2012, **23**, 465201.
86. M. Witzleben, K. Fleck, C. Funck, B. Baumköter, M. Zuric, A. Idt, T. Breuer, R. Waser, U. Bötger, S. Menzel, *Adv. Electron. Mater.,* 2017, **3**, 1700294.
87. E. Yalon, A. A. Sharma, M. Skowronski, J. A. Bain, D. Ritter, I. V. Karpov, *IEEE Trans. Electron Device,* 2015, **69**, 2972-1977.
88. A. Majumdar, *Annu. Rev. Mater. Sci.,* 1999, **29**, 505-585.
89. E. Yalon, S. Deshmukh, M. M. Rojo, F. Lian, C. M. Neumann, F. Xiong, E. Pop, *Sci. Rep.,* 2017, **7**, 15360.
90. M. A. Villena, F. Jimenez- Molinos, J. B. Roldan, J. Sune, S. Long, X. Lian, F. Gamiz, M. Liu, J. Appl. Phys., 2013, **114**, 144505.
91. S. Menzel, P. Kaupmann, R. Waser, *Nanoscale,* 2015, **7**, 12673-12681.
92. G. González-Cordero, J. B. Roldan, F. Jiménez-Molinos, J. Suñé, S. Long, M. Liu, *Semicond. Sci. Technol.,* 2016, **31**, 115013.
93. Y. C. Yang, W. D. Lu, *IEEE Trans. Nanotechnol.,* 2016, *15*, 465-472.
94. W. A. Hubbard, A. Kerelsky, G. Jasmin, E. R. White, J. Lodico,M. Mecklenburg, B. C. Regan, *Nano Lett.,* 2015, **15,** 3983-3987.
95. Y. Song, B. Magyari-Kope, Y. Lin, Y. Nishi, *IEEE International Memory Workshop,* 2017, **1**, https://doi.org/10.1109/IMW.2017.7939089.
96. J. L. Gavartin, D. M. Ramo, A. L. Shluger, *Appl. Phys. Lett.,* 2006, **89**, 082908.
97. A. Padovani, L. Larcher, O. Pirrotta, L. Vandelli, G. Bersuker, *IEEE Trans. Electron Devices,* 2015, **62**, 1998-2006.
98. D. Ielmini, F. Nardi, C. Cagli, *IEEE Trans. Electron Devices,* 2011, **58**, 3246-3253.
99. M. Bocquet, D. Deleruyelle, C. Muller, J.-M. Portal, *Appl. Phys. Lett.,* 2011, **98**, 263507.
100. M. Lanza, H. S. P. Wong, E. Pop, D. Ielmini, D. Strukov, B. C. Regan, L. Larcher, M. A. Villena, J. J. Yang, L. Goux, *Adv. Electron. Mater.,* 2018, **4**, 1800143.
101. D. S. Hong, Y. S. Chen, Y. Li, H. W. Yang, L. L. Wei, B. G. Shen, J. R. Sun, *Sci. Rep-UK.,* 2014, **4**, 4058.
102. J. Y. Chen, C. W. Huang, C. H. Chiu, Y. T. Huang, W. W. Wu, *Adv. Mater.,* 2015, **27**, 5028-5033.
103. C. Li, B. Gao, Y. Yao, X. Guan, X. Chen, Y. Wang, P. Huang, L. Liu, X. Liu, J. Li, C. Gu, J. Kang, R. Yu, *Adv. Mater.,* 2017, **29**, 1602976.
104. Y. C. Yang, F. Pan, Q. Liu, M. Liu, F. Zeng, *Nano Lett.,* 2009, **9**, 1636-1643.
105. Q. Liu, J. Sun, H. Lv, S. Long, K. Yin, N. Wan, Y. Li, L. Sun, M. Liu, *Adv. Mater., 2012*, **24**, 1844-1849.
106. J. Y. Chen, C. L. Hsin, C. W. Huang, C. H. Chiu, Y. T. Huang, S. J. Lin, W. W. Wu, L. J. Chen, *Nano Lett.,* 2013, **13**, 3671-3677.
107. Y. Yao, V. Li, Z. L. Huo, M. Liu, C. X. Zhu, C. G. Gu, X. F. Duan, Y. G. Wang, L. Gu, R. Yu, *Nature Commun.,* 2013, **4**, 2764.
108. F. Miao, J. P. Strachan, J. J. Yang, M.-X. Zhang, I. Goldfarb, A. C. Torrezan, P. Eschbach, R. D. Kelley, C. Medeiros-Ribeiro, R. S. Williams, *Adv. Mater.,* 2011, **23**, 5633-5640.
109. Z. Wang, H. Jiang, M. H. Jang, P. Lin, A. Ribbe, Q. Xia, J. J. Yang, *Nanoscale,* 2016, **8**, 14023-14030.
110. S. Privitera, B. Bersuker, B. Butcher, A. Kalantarian, S. Lombardo, C. Bongiorno, R. Geer, D. C. Gilmer, P. D. Kirsch, *Microelectron. Eng.,* 2013, **109**, 75-78.
111. S. Kumar, C. E. Graves, J. P. Strachan, E. M. Grafals, A. L. D. Kilcoyne, T. Tyliszczak, J. N. Weker, Y. Nishi, R. S. Williams, *Adv. Mater.,* 2016, **28**, 2772-2776.
112. J. Shang, W. H. Xue, Z. H. Ji, G. Liu, X. H. Niu, X. H. Yi, L. Pan, Q. F. Zhan, X. H. Xu, R. W. Li, *Nanoscale,* 2017, 9, 7037-7046.
113. D. Copper, C. Baeumer, N. Bernier, A. Marchewka, C. L. Torre, R. E. Bunin-Borowski, S. Menzel, R. Waser, R. Dittmann, *Adv. Mater.,* 2017, **29**, 1700212.
114. B. J. Choi, A. C. Torrezan, J. P. Strachan, P. G. Kotula, A. J. Lohn, M. J. Marinella, Z. Li, R. S. Williams, J. J. Yang, *Adv. Funct. Mater.,* 2016, **26**, 5290-5296.
115. I. Valvo, ChemElectroChem, 2014, **1**, 26-36.
116. S. C. Chae, J. S. Lee, S. Kim, S. B. Lee, S. H. Chang, C. Liu, B. Kahng, H. Shin, D.-W. Kim, C. U. Jung, S. Seo, M.-J. Lee, T. W. Noh, *Adv. Mater.,* 2008, **20**, 1154-1159.
117. K. Skaja, C. Bäumer, O. Peters, S. Menzel, M. Moors, H. Du, M. Bornhöfft, C. Schmitz, V. Feyer, C.-L. Jia, C. M. Schneider, J. Mayer, R. Waser, R. Dittmann, *Adv. Funct. Mater.*, 2015, **25**, 7154-7162.
118. U. Celano, L. Goux, R. Degraeve, A. Fantini, O. Richard, H. Bender, M. Jurczak, W. Vandervorst, *Nano Lett.,* 2015, **15**, 7970-7975.
119. R. Waser, *Microelectron. Eng.,* 2009, **86**, 1925-1928.
120. H. S. P. Wong, H. Y. Lee, S. Yu, T. S. Chen, Y. Wu, P. S. Chen, B. Lee, F. T. Chen, M. J. Tsai, *Proc. IEEE,* 2012, **100**, 1951-1970.
121. C. S. Hwang, *Adv. Electron. Mater.,* 2015, **1**, 1400056.
122. D. Ielmini, R. Waser, Ed: Resistive Switching, Wiley-VCH, **2016**.
123. D. G. Schlom, J. H. Haeni, *MRS Bull.,* 2002, **27**, 198-204.
124. J. Robertson, *Rep. Prog. Phys.,* 2006, **69**, 327-396.
125. S. G. Lim, S. Kriventsov, T. N. Jackson, J. H. Haeni, D. G. Schlom, A. M. Balbashov, R. Uecker, P. Reich, J. L. Freeouf, G. Lucovsky, *J. Appl. Phys.,* 2002, **91**, 4500-4505.
126. M. Alvisi, M. Di Giulio, S. G. Marrone, M. R. Perrone, M. L. Protopapa, A. Valentini, L. Vasanelli, *Thin Solid Films,* 2000, **358**, 250-258.

127. P. Rauwel, E. rauwel, C. Persson, M. F. Sunding, A. Galeckas, *J. Appl. Phys.,* 2012, **112**, 104107.
128. X. Y. Zhao, D. Vanderbilt, *Phys. Rev. B,* 2002, **65**, 233106.
129. F. Miao, Y. We, I. Goldfarb, J. J. Yang, M.-X. Zhang, M. D. Pickett, J. P. Strachan, G. Medeiros-Ribeiro, R. S. Williams, *ACS Nano,* 2012, **6**, 2312-2318.
130. K. Terabe, T. Hasegawa, T. Nakayama, M. Aono, *Science*, 2005, **433**, 47-50.
131. C. Chen, S. Gao, F. Zeng, G. Y. Wang, S. Z. Li, C. Song, F. Pan, *Appl. Phys. Lett.,* 2013, **103**, 043510.
132. S. Gao, F. Zeng, C. Chen, G. Tang, Y. Lin, Z. Zheng, C. Song, F. Pan, *Nanotechnology,* 2013, **24**, 335201.
133. A. Mehonic, A. Vrajitoarea, S. Cueff, S. Hudziak, H. Howe, C. Labbé, R. Rizk, M. Pepper, A. J. Kenyon, *Sci. Rep-UK.,* 2013, **3**, 2708.
134. S. B. Long, L. Perniola, C. Cagli, J. Buckley, X. Lian, E. Miranda, F. Pan, M. Liu, J. Suňé, *Sci. Rep-UK.,* 2013, **3**, 2929.
135. S. B. Long, X. Lian, C. Cagli, X. Cartoixà, R. Rurali, E. Miranda, D. Jiménz, L. Perniola, M. Liu, J. Suňé, *Appl. Phys. Lett.,* 2013, **102**, 183505.
136. C. Hu, M. D. McDaniel, A. Posadas, A. A. Demkov, J. G. Ekerdt, E. T. Yu, *Nano Lett.,* 2014, **14**, 4360-4367.
137. A. Wedig, M. Luebben, D.-Y. Cho, M. Moors, K. Skaja, V. Rana, T. Hasegawa, K. K. Adepalli, B. Yildiz, R. Waser, I. Valov, *Nature Nanotechnol.,* **2016**, *11*, 67-74.
138. W. Yi, S. E. Savel'ev, G. Medeiros-Ribeiro, F. Miao, M.-X. Zhang, J. J. Yang, A. M. Bratkovsky, R. S. Williams, *Nature Commun.,* **2016**, *7*, 11142.
139. S. U. Sharath, S. Vogel, L. Molina-Luna, E. Hildebrnandt, C. Wenger, J. Kurian, M. Duerrschnabel, T. Niermann, G. Niu, P. Calka, M. Lehmann, H. J. Kleebe, T. Schroeder, L. Alff, *Adv. Funct. Mater.,* 2017, **27**, 1700432.
140. E. Scheer, N. Agrait, J. C. Cuevas, A. L. Yeyati, B. Ludoph, A. Martín-Rodero, G. R. Bollinger, J. M. van Ruitenbeek, C. Urbina, *Nature,* 1989, **394**, 154-157.
141. D. P. E. Smith, *Science,* 1995, **269**, 371-373.
142. N. Agraït, *Phys. Rep.,* 2003, **377**, 81-279.
143. D. B. Strukov, R. S. Williams, *Proc. Natl. Acad. Sci.,* 2009, **106**, 20155-20158.
144. S. Yu, H.-Y. Chen, B. Gao, J. Kang, H.-S. P. Wong, *ACS Nano,* 2013, **7**, 2320-2325.
145. J. Y. Seok, S. J. Song, J. H. Yoon, K. J. Yoon, T. H. Park, D. E. Kwon, H. Lim, G. H. Lim, D. S. Jeong, C. S. Hwang, *Adv. Funct. Mater.,* 2014, **24**, 5316-5339.
146. S. Kim, J. Zhou, W. Lu, *IEEE Trans. Electron Dev.,* 2014, **61**, 2820-2826.
147. J. Zhou, K. H. Kim, W. Lu, *IEEE Trans. Electron Dev.,* 2014, **61**, 1369-1376.
148. M. Liu, H. Y. Hwang, H. Tao, A. C. Strikwerda, K. Fan, G. R. Keiser, A. J. Sternbach, K. G. West, S. Kittwatanakul, J. Lu, S. A. Wolf, F. G. Omenetto, X. Zhang, K. A. Nelson, R. D. Averitt, *Nature,* 2012, **487**, 345-348.
149. M. M. Qazilbash, M. Brehm, B.-G. Chae, P.-C. Ho, G. O. Andreev, B.-J. Kim, S. J. Yun, A. V. Balatsky, M. B. Maple, F. Keilmann, H. T. Kim, D. N. Basov, *Science,* 2007, **318**, 1750-1753.
150. N. Manca, T. Kanki, H. Tanaka, D. Marré, L. Pellegrino, *Appl. Phys. Lett.,* 2015, **107**, 143509.
151. H. Madan, M. Jerry, A. Pogrebnyakov, T. Mayer, S. Datta, *ACS Nano,* 2015, **9**, 2009-2017.
152. W. H. Xue, G. Liu, Z. Zhong, Y. Dai, J. Shang, Y. Liu, H. Yang, X. Yi, H. Tan, L. Pan, S. Gao, J. Ding, X.-H. Xu and R.-W. Li, *Adv. Mater.,* 2017, **29**, 1702162.
153. R. Midya, Z. Wang, J. Zhang, S. E. Savel'ev, C. Li, M. Rao, M. H. Jang, S. Joshi, H. Jiang, P. Lin, K. Norris, N. Ge, Q. Wu, M. Barnell, Z. Li, H. L. Xin, R. S. Williams, Q. Xia, J. J. Yang, *Adv. Mater.,* 2017, **29**, 1604457.
154. Z. Wang, S. Joshi, S. E. Savel'ev, J. Jiang, R. Midya, P. Lin, M. Hu, N. Ge, J. P. Strachan, Z. Li, Q. Wu, M. Barnell, G.-L. Lin, H. L. Xin, R. S. Williams, Q. Xia, J. J. Yang, *Nature Mater.,* 2017, **16**, 101-108.
155. Z. Wang, M. Rao, R. Midya, S. Joghi, H. Jiang, P. Lin, W. Song, S. Asapu, Y. Zhuo, C. Li, H. Wu, Q. Xia, J. J. Yang, *Adv. Funct. Mater.,* 2018, **28**, 1704862.
156. X. Zhao, J. Ma, X. Xiao, Q. Liu, L. Shao, D. Chen, S. Liu, J. Niu, X. Zhang, Y. Wang, R. Cao, W. Wang, Z. Di, H. Lv, S. Long, M. Liu, *Adv. Mater.,* 2018, **30**, 1705193.
157. S. Liu, N. Lu, X. Zhao, H. Xu, W. Banerjee, H. L, S. Long, Q. Li, Q. Liu, M. Liu, *Adv. Mater., 2016*, **28**, 10623-10629.
158. L. O. Chua, *IEEE Trans. Circuit Theory,* 1971, **18**, 507-519.
159. L. O. Chua, S. M. Kang, *Proc. IEEE,* 1976, **64**, 209-223.
160. D. B. Strukov, G. S. Snider, D. R. Stewart and R. S. Williams, *Nature,* 2008, **453**, 80-83.
161. Y. Yang, W. Lu, *Nanoscale,* 2013, **5**, 10076-10092.
162. A. Sawa, *Mater. Today,* 2008, **11**, 28-36.
163. J. J. Yang, M. X. Zhang, J. P. Strachan, F. Miao, M. d. Pickett, R. D. Kelley, G. Medeiros-Ribeiro and R. S. Williams, *Appl. Phys. Lett.,* 2010, **97**, 232102.
164. J. Yao, L. Zhong, D. Natelson, J. M. Tour, *J. Am. Chem. Soc.,* 2011, **133**, 941-948.
165. C. Chen, Y. C. Yang, F. Zeng and F. Pan, *Appl. Phys. Lett.,* 2010, **97**, 083502.
166. M. Wuttig, N. Yamada, *Nature Mater.,* 2007, **6**, 824-832.
167. L. O. Chua, *Appl. Phys. A,* 2011, **102**, 765-783.
168. L. O. Chua, *Proc. IEEE*, 2012, **100**, 1920-1927.
169. T. Prodromakis, C. Toumazou, L. Chua, *Nature Mater.,* 2012, **11**, 478.
170. F. Alibart, S. Pleutin, D. Guérin, C. Noembre, S. Lenfant, K. Lmimouni, C. Camrat, D. Vuillaume, *Adv. Funct. Mater.,* 2010, **20**, 330-337.
171. S. H. Jo, T. Chang, I. Ebong, B. B. Bhadviya, P. Mazumder, W. Lu, *Nano Lett.,* 2010, **10**, 1297-1301.
172. T. Chang, S. H. Jo, W. Lu, *ACS Nano,* 2011, **5**, 7669-7676.
173. D. Kuzum, R. G. D. Jeyasingh, B. Lee, H. S. P. Wong, *Nano Lett.,* 2012, ***12***, 2179-2186.
174. Z. Q. Wang, H. Y. Xu, X. H. Li, H. Yu, Y. C. Liu, X. J. Zhu, *Adv. Funct. Mater.,* 2012, **22**, 2759-2765.
175. P. Huang, J. Kang, Y. Zhao, S. Chen, R. Han, Z. Zhou, Z. Chen, W. Ma, M. Li, L. Liu, X. Liu, *Adv. Mater.,* 2016, **28**, 9758.
176. J. Lee, W. Lu, *Adv. Mater.,* 2017, **29**, 1702770.
177. M. Hu, C. E. Graves, C. Li, Y. Li, N. Ge, E. Montgomery, M. Davila, H. Jiang, R. S. Williams, J. J. Yang, Q. Xia, J. P. Strachan, *Adv. Mater.,* 2018, **30**, 1705914.
178. Z. Sun, E. Ambrosi, A. Bricalli, D. Ielmini, *Adv. Mater.,* 2018, **30**, 1802554.
179. B. C. Jang, Y. Nam, B. J. Koo, J. Choi, S. G. Im, S. H. K. Park, S. Y. Choi, *Adv. Funct. Mater.,* 2018, **28**, 1704725.
180. X. Yan, J. Zhao, S. Liu, Z. Zhou, Q. Liu, J. Chen, X. Y. Liu, *Adv. Funt. Mater.,* 2018, **28**, 1705320.

181. N. Xu, K. J. Yoon, K. M. Kim, L. Fang, C. S. Hwang, *Adv. Electron. Mater.,* 2018, 1800189.
182. M. A. Zidan, J. P. Strachan, W. Lu, *Nature. Electron., 2018*, **1**, 22.
183. Z. Wang, S. Joshi, S. Savel'ev, W. Song, R. Midya, Y. Li, M. Rao, P. Yan, S. Asapu, Y. Zhuo, H. Jiang, P. Lin, C. Li, J. H. Yoon, N. K. Upadhyay, J. Zhang, M. H, J. P. Strachan, M. Barnell, Q. Wu, H. Wu, R. S. Stanley, Q. Xia, J. J. Yang, *Nature Electron.,* 2018, **1**, 137.
184. M. A. Zidan, Y. J. Jeong, J. Lee, B. Chen, S. Huang, M. J. Kushner, W. Lu, *Nature Electron.,* 2018, **1**, 411-420.
185. S. Yu, Y. Wu, R. Jeyasungh, D. Kuzum, H.-S. P. Wong, *IEEE Trans. Dev. Lett.,* 2011, **58**, 2729-2737.
186. T. Ohno, T. Hasegawa, T. Tsuruoka, K. Terabe, J. K. Gimzewski, M. Aono, *Nature Mater.,* 2011, **10**, 591-595.
187. Y. V. Pershin, M. Di Ventra, *Proc. IEEE,* 2012, **100**, 2071-2080.
188. H. Lim, I. Kim, J. S. Kim, C. S. Hwang, D. S. Jeong, *Nanotechnology,* 2013, **24**, 384005.
189. M. Prezioso, F. Merrikh-Bayat, B. D. Hoskins, G. C. Adam, K. K. Likharev, D. B. Strukov, *Nature,* 2015, **521**, 61-64.
190. A. Serb, J. Bill, A. Khiat, R. Berdan, R. Legenstein, T. Prodromakis, *Nature Commun.,* 2016, **7**, 12611.
191. M. Al-Shedivat, R. Naous, G. Cauwenberghs, K. N. Salama, *IEEE Trans. Emerg. Sel. Top. Circuit Syst.,* 2015, **5**, 242-253.
192. A. Mehonic, A. J. Kenyon, *Front. Neurosci.,* 2016, **10**, 57.
193. I. Gupta, A. Serb, A. Khiat, R. Zeitler, S. Vassanelli, T. Prodromakis, *Nature Commun.,* **2016**, *7*, 12805.
194. J. C. Magee, *Nature Rev. Neurosci.,* 2000, **1**, 181-190.
195. H. Simon, T. Zacharia, R. Stevens, *Modeling and Simulation at the Exascale for Energy and the Environment* (Department of Energy Technical Report), 2007.
196. T. Palmer, *Nature,* 2015, **526**, 32-33.
197. N. Aage, E. Andereassen, B. S. Lazarov, O. Sigmund, *Nature,* 2017, **550**, 84-86.
198. P. Bauer, G. Brunet, *Nature,* 2015, **525**, 47-55.
199. Y. Achdou, F. J. Buera, J.-M. Lasry, P.-L. Lions, B. Moll, *Philos. Trans. R. Soc. A,* 2014, **372**, 20130397.
200. S. kvtinsky, G. Satat, N. Wald, E. G. Friedman, A. Kolodny, U. C. Weiser, *IEEE Trans. Very Large Scale Integ. Syst.,* 2014, **22**, 2054-2066.
201. B. Chen, F. Cai, J. Zhou, W. Ma, P. Sheridan, W. Lu, *IEDM Tech. Dig.,* 2015, *17.5.1.*
202. S. Balatti, S. Ambrogio, D. Ielmini, *IEEE Trans. Electron. Dev.,* 2015, **62**, 1831-1838.
203. L. F. Pender and R. J. Fleming, *J. Appl. Phys.,* 1975, **46**, 3426-3431.
204. Y. Segui, B. Ai and H. Carchano, *J. Appl. Phys.*, 1976, **47**, 140-143.
205. B. H. Lee, H. Bae, H. Seong, D. I. Lee, H. Park, Y. J. Choi, S.-G. Im, S. O. Kim and Y.-K. Choi, *ACS Nano,* 2015, **9**, 7306-7313.
206. B. Cho, J. M. Yun, S. Song, Y. Ji, D.-Y. Kim and T. Lee, *Adv. Funct. Mater.,* 2011, **21**, 3976-3981.
207. S. Gao, C. Song, C. Chen, F. Zeng and F. Pan, *J. Phys. Chem. C,* 2012, **116**, 17955-17959.
208. S. Gao, C. Song, C. Chen, F. Zeng and F. Pan, *Appl. Phys. Lett.,* 2013, **102**, 141606.
209. K. Krishnan, T. Tsuruoka, C. Mannequin and M. Aono, *Adv. Mater.,* 2016, **28**, 640-648.
210. S. K. Kim, J. Y. Kim, B. C. Jang, M. S. Cho, S. Y. Choi, J. Y. Lee and H. Y. Jeong, *Adv. Funct. Mater.,* 2016, **26**, 7406-7414.
211. W. T. Kim, J. H. Jung, T. W. Kim and D. I. Son, *Appl. Phys. Lett.,* 2010, **96**, 253301.
212. D. I. Son, D. H. Park, J. B. Kim, J. W. Choi, T. W. Kim, B. Angadi, Y. Yi and W. K. Choi, *J. Phys. Chem. C,* 2011, **115**, 2341-2348.
213. X. Zhang, H. Xie, Z. Liu, C. Tan, Z. Luo, H. Li, J. Lin, L. Sun, W. Chen, Z. Xu, L. Xie, W. Huang and H. Zhang, *Angew. Chem. Int. Ed.,* 2015, **54**, 3653-3657.
214. P. Zhang, B. Xu, C. Gao, G. Chen and M. Gao, *ACS Appi. Mater. Interfaces,* 2016, **8**, 30336-30343.
215. J. Ouyang, C. W. Chu, C. R. Szmanda, L. Ma and Y. Yang, *Nature Mater.,* 2004, **3**, 918-922.
216. Q. D. Ling, S. L. Lim, Y. Song, C. X. Zhu, D. S. H. Chan, E. T. Kang and K. G. Neoh, *Langmuir,* 2007, **23**, 312-319.
217. T. L. Choi, K. H. Lee, W. J. Joo, S. Lee, T. W. Lee and M. Y. Chae, *J. Am. Chem. Soc.,* 2007, **129**, 9842-9843.
218. W. Zhang, C. Wang, G. Liu, X. Zhu, X. Chen, L. Pan, H. Tan, W. Xue, Z. Ji, J. Wang, Y. Chen and R. W. Li, *Chem. Commun.,* 2014, **50**, 11856-11858.
219. S. L. Lim, Q. Ling, E. Y. H. Teo, C. X. Zhu, D. S. H. Chan, E. T. Kang, K. G. Neoh, *Chem. Mater.,* 2007, **19**, 5148.
220. L. H. Xie, Q. D. Ling, X. Y. Hou and W. Huang, *J. Am. Chem. Soc.,* 2008, **130**, 2120-2121.
221. B. C. Das and A. J. Pal, *Org. Electron.,* 2008, **9**, 39-44.
222. A. Bandyopadhyay, S. Sahu, M. Higuchi, *J. Am. Chem. Soc.,* 2011, **133**, 1168-1171.
223. R. Kumar, R. G. Pillai, N. Pekas, Y. Wu, R. L. McCreery, *J. Am. Chem. Soc.,* 2012, **134**, 14869-14876.
224. S. Goswami, A. J. Matula, S. P. Rath, S. Hedström, S. Saha, M. Annamalai, D. Sengupta, A. Patra, S. Ghosh, H. Jani, S. Sarkar, M. R. Motapothula, C. A. Nijhuis, J. Martin, S. Goswami, V. S. Batista, T. Venkatesan, *Nature Mater.,* 2017, **16**, 1216-1225.
225. K. Hattori, J. Y. Wada, *J. Polym. Sci. Polym. Phys.,* 1975, **13**, 1863-1869.
226. J. V. Grazelevivues, P. Strohrirgl, J. Pielichowski, K. Pielichowski, *Prog. Polym. Sci.,* 2003, **28**, 1297-1353.
227. Y. D. Zhang, T. Wada, H. Sasabe, *J. Mater. Chem.,* 1998, **8**, 809-828.
228. J. Vandendriessche, P. Palmans, S. Topet, N. Boens, F. C. De Schryver, H. Masuhara, *J. Am. Chem. Soc.,* 1984, **106**, 8057-8064.
229. J. Y. Oh, S. Rondeau-Gagné, Y. C. Chiu, A. Chortos, F. Lissel, G. J. N. Wang, B. C. Schroeder, T. Kurosawa, J. Lopez, T. Katsumata, J. Xu, C. Zhu, X. Gu, W. G. Bae, Y. Kim, L. Jin, J. W. Chung, J. B. H. Tok, Z. Bao, *Nature,* 2016, **539**, 411-415.
230. J. Xu, S. Wang, G. J. N. Wang, C. Zhu, S. Luo, L. Jin, X. Gu, S. Chen, V. R. Feig, J. W. F. To, S. Rondeau-Gagné, J. Park, B. C. Schroeder, C. Lu, J. Y. Oh, Y. Wang, Y. H. Kim, H. Yan, R. Sinclair, D. Zhou, G. Xue, B. Murmann, C. Linder, W. Cai, J. B. H. Tok, J. W. Chung, Z. Bao, *Science,* 2017, **355**, 59-64.
231. S. Wang, J. Xu, W. Wang, G. J. N. Wang, R. Rastak, F. Molina-Lopez, J. W. Chung, S. Niu, V. R. Feig, J. Lopez, T. Lei, S.-K. Kwon, Y. Kim, A. M. Foudeh, A. Ehrlich, A. Gasperini, Y. Yun, B. Murmann, J. B. H. Tok, Z. Bao. *Nature,* 2018, **555**, 83-88.
232. J. C. Scott, L. D. Bozano, *Adv. Mater.,* **2007**, **19**, 1452-1463.
233. B. Cho, S. Song, Y. Ji, T. W. Kim, T. Lee, *Adv. Funct. Mater.,* 2011, **21**, 2806-2829.
234. L. P. Ma, J. Liu, Y. Yang, *Appl. Phys. Lett.,* 2002, **80**, 2997-

2999.
235. L. Ma, S. Pyo, J. Ouyang, Q. Xu, Y. Yang, *Appl. Phys. Lett.,* **2003**, **82**, 1419-1421.
236. Y. Yang, J. Ouyang, L. Ma, R. J. H. Tseng, C. W. Chu, *Adv. Funct. Mater.,* 2006, **16**, 1001-1014.
237. L. D. Bozano, B. W. Kean, V. R. Deline, J. R. Salem, J. C. Scott, *Appl. Phys. Lett.,* 2004, 84, 607-609.
238. J. G. Park, W. S. Nam, S. H. Seo, Y. G. Kim, Y. H. Oh, G. S. Lee, U. G. Park, *Nano Lett.,* 2009, **9**, 1713-1719.
239. D. Tondelier, K. Lmimouni, D. Vuillaume, C. Fery, G. Haas, *Appl. Phys. Lett.,* 2004, **85**, 5763-5765.
240. J. Chen, D. Ma, *Appl. Phys. Lett.,* 2005, **87**, 023505.
241. J. Chen, L. Xu, J. Lin, Y. Geng, L. Wang, D. Ma, *Appl. Phys. Lett.,* 2006, **89**, 083514.
242. J. Chen, D. Ma, *J. Appl. Phys.,* 2006, **100**, 034512.
243. J. Chen, L. Xu, J. Lin, Y. Geng, L. Wang, D. Ma, *Semicond. Sci. Technol.,* 2006, **21**, 1121-1124.
244. J. Lin, D. Ma, *Org. Electron.,* 2009, **10**, 275-279.
245. C. Wang, J. Wang, P. Z. Li, J. Gao, S. Y. Tan, W. W. Xiong, B. Hu, P. S. Lee, Y. Zhao, Q. Zhang, *Chem. Asian J.,* 2014, **9**, 779-783.
246. C. Wang, M. Yamashita, B. Hu, Y. Zhou, J. Wang, J. Wu, F. Huo, P. S. Lee, N.Aratani, H. Yamada, Q. Zhang, *Chem. Asian J., 2015*, **10**, 116-119.
247. C. Wang, B. Hu, J. Wang, J. Gao, G.Li, W. W. Xiong, B. Zou, M. Suzuki, N. Aratani, H. Yamada, F. Huo, P. S. Lee, Q. Zhang, *Asian J. Org. Chem.,* 2015, **4**, 646-651.
248. Q. F. Gu, J. H. He, D. Y. Chen, H. L. Dong, Y. Y. Li, H. Li, Q. F. Xu, J. M. Lu, *Adv. Mater.,* 2015, **27**, 5968-5973.
249. Q. Zhang, J. H. He, H. Zhuang, H. Li, N. J. Li, Q. F. Xu, D. Y. Chen, J. M. Lu, *Adv. Funct. Mater.,* 2016, **26**, 146-154.
250. H. Li, Q. Xu, N. J. Li, R. Sun, J. Ge, J. M. Lu, H. Gu, F. Yan, *J. Am. Chem. Soc.,* 2010, **132**, 5542-5543.
251. S. Miao, H. Li, Q. F. Xu, Y. Y. Li, S. Ji, N. Li, L. Wang, J. Zheng, J M. Lu, *Adv. Mater.,* 2012, **24**, 6210-6215.
252. P. Y. Gu, J. Gao, C. J. Lu, W. Chen, C. Wang, G. Li, F. Zhou, Q. F. Xu, J. M. Lu ,Q. Zhang. *Mater. Horiz.,* 2014, **1**, 446-451.
253. Z. Liu, J. H. He, H. Li, Q. F. Xu, N. Li, D. Y. Chen, L. Wang, X. Chen, K. Zhang, J. M. Lu. *Adv. Electron. Mater.,* 2016, **2**, 1500474.
254. Q. J. Zhang, J. H. He, H. Zhuang, H. Li, N. J. Li, Q. F. Xu, D. Y. Chen, J. M. Lu. *Chem. Asian J.* 2016, **11**, 1624-1630.
255. Q. D. Ling, D. J. Liaw, C. Zhu, D. S. H. Chan, E. T. Kang, K.-G. Neoh, *Prog. Polym. Sci.,* 2008, **33**, 917-978.
256. W. P. Lin, S. J. Liu, T. Gong, Q. Zhao, W. Huang, *Adv. Mater.,* 2014, **26**, 570-606.
257. C. L. Liu, W. C. Chen, *Polym. Chem.,* 2011, **2**, 2169-2174.
258. S. Möller, C. Perlov, W. Jackson, C. Taussig, S. R. Forrest, *Nature,* 2003, **426**, 166-169.
259. S. Möller, S. R. Forrest, C. Perlov, W. Jackson, C. Taussig, *J. Appl. Phys.,* 2003, **94**, 7811-7819.
260. S. Smith, S. R. Forrest, *Appl. Phys. Lett.* 2004, **84**, 5019-5021.
261. X. Xu, R. A. Register,S. R. Forrest, *Appl. Phys. Lett.,* 2006, **89**, 142109.
262. U. S. Bhansali, M. A. Khan, D. Cha, M. N. AlMadhoun, R. Li, L. Chen, A. Amassian, I. N. Odeh, H. N. Alshareef, *ACS Nano,* 2013, **7**, 10518-10524.
263. S. Paul, A. Kanwal, M. Chhowalla, *Nanotechnology,* 2006, **17**, 145-151.
264. Y. Ji, S. Lee, B. Cho, S. Song, T. Lee. *ACS Nano,* 2011, **5**, 5995-6000.
265. H. Jo, J. Ko, J. A. Lim, H. J. Chang, Y. S. Kim, *Macromol. Rapid Commun.,* 2013, **34**, 355-361.
266. Y. Ji, D. F. Zeigler, D. S. Lee, H. Choi, A. K. Y. Jen, H. C. Ko, T. W. Kim, *Nature Commun.,* 2013, **4**, 2707.
267. J. H. Jung, J. H. Kim, T. W. Kim, M. S. Song, Y.-H. Kim, S. Jin. *Appl. Phys. Lett.,* 2006, **89**, 122110.
268. B. Cho, T. W. Kim, M. Choe, G. Wang, S. Song, T. Lee, *Org. Electron.,* 2009, **10**, 473-477.
269. K. Onlaor, T. Thiwawong, B. Tunhoo, *Org. Electron.,* 2014, **15**, 1254-1262.
270. Y. Sun, D. Wen, X. Bai, *Phys.Chem.Chem.Phys., 2018*, **20**, 5771-5779.
271. B. C. Das, A. J. Pal, *ACS Nano,* 2008, **2**, 1930-1938.
272. S. Ali, J. Bae, C. H. Lee, K. H. Choi, Y. H. Doh, *Org. Electron.,* 2015, **25**, 225-231.
273. J. Ali, G.U.D. Siddiqui, Y. J. Yang, K. T. Lee, K. Um, K. H. Choi, *RSC Adv.,* 2016, **6**, 5068-5078.
274. D. H. Kim, W. K. Kim, S. J. Woo, C. Wu, T. W. Kim, *Org. Electron.,* 2017, **51**, 156-161.
275. S.T. Han, L. Hu, X. Wang, Y. Zhou, Y. J. Zeng, S. Ruan, C. Pan, Z. Peng, *Adv. Sci.,* 2017, **4**, 1600435.
276. X. Zhang, Z. Lai, Z. Liu, C. Tan, Y. Huang, B. Li, M. Zhao, L. Xie, W. Huang, H. Zhang, *Angew. Chem.,* 2015, **127**, 5515-5518.
277. L. Meng, M. Lan, L. Guo, L. Xie, W. Hui, J. Ge, W. Liu, Y. Wang and P. Wang. *RSC Adv.,* 2015, **5**, 26886-26890.
278. K. Onlaor, T. Thiwawong, B. Tunhoo, *Org. Electron.,* 2016, **31**, 19-24.
279. Q. Zhang, J. Pan, X. Yi, L. Li, S. Shang, *Org. Electron.,* 2012, **13**, 1289-1295.
280. J. Liu, Z. Zeng, X. Cao, G. Lu, L.-H. Wang, Q. L. Fan, W. Huang, H. Zhang, *Small,* 2012, **8**, 3517-3522.
281. P. Zhang, C. Gao, B. Xu, L. Qi, C. Jiang, M. Gao, D. Xue, *Small, 2016*, **12**, 2077-2084.
282. M. M. Rehman, G. U. Siddiqui, J. Z. Gul, S. W. Kim, J. H. Lim, K. H. Choi, *Sci. Rep-UK.,* 2016, **6**, 36195.
283. G. U. Siddiqui, M. M. Rehman, Y. J. Yang, K. H. Choi, *J. Mater. Chem. C,* 2017, **5**, 862-871.
284. J. N. Coleman, M. Lotya, A. O'Neill, S. D. Bergin, P. J. King, U. Khan, K. Young, A. Gaucher, S. De, R. J. Smith, I. V. Shvets, S. K. Arora, G. Stanton, H. Kim, K. Lee, G. T. Kim, G. S. Duesberg, T. Hallam, J. J. Boland, J. Wang, J. F. Donegan, J. C. Grunlan, G. Moriarty, A. Shmeliov, R. J. Nicholls, J. Perkins, E. M. Grieveson, K. Theuwissen, D. W. McComb, P. D. Nellist, V. Nicolosi. *Science,* 2011, **331**, 568-571.
285. B. Radisavljevic, A. Radenovic, J. Brivio, V. Giacometti, A. Kis, *Nature Nanotech.,* 2011, **6**, 147-150.
286. G. Eda, H. Yamaguchi, D. Voiry, T. Fujita, M. Chen, M. Chhowalla, *Nano Lett.,* 2011, **11**, 5111-5116.
287. S. K. Hwang, J. M. Lee, S. Kim, J. S. Park, H. I. Park, C. W. Ahn, K. J. Lee, T. Lee, S. O. Kim, *Nano Lett.,* 2012, **12**, 2217-2221.
288. S. K. Hwang, J. R. Choi, I. Bae, I. Hwang, S. M. Cho, J. Huh, C. Park, *Small,* 2013, **9**, 831-837.
289. S. C. Kishore, A. Pandurangan, *RSC Adv.,* 2014, **4**, 9905-9911.
290. S. I. White, P. M. Vora, J. M. Kikkawa, K. I. Winey, *Adv. Funct. Mater.,* 2011, **21**, 233-240.
291. J. Jang, W. Park, K. Cho, H. Song, T. Lee, *Curr. Appl. Phys.,* 2013, **13**, 1237-1240.

292. W. J. Woo, T. L. Choi, J. Lee, S. K. Lee, M. S. Jung, N. Kim, J. M. Kim, *J. Phys. Chem. B,* 2006, **110**, 23812-23816.
293. W. J. Joo, T. L. Choi, K. H. Lee, Y. Chung, *J. Phys. Chem. B,* 2007, **111**, 7756-7760.
294. H. Ling, M. Yi, M. Nagai, L. Xie, L. Wang, B. Hu, W. Huang. *Adv. Mater.,* **2017**, *29*, 1701333.
295. Y. Cai, J. Tan, L. Y. Fan, M. Lin, R. Huang. *Nanotechnology,* 2016, **27**, 275206.
296. K. Krishnan, M. Muruganathan, T. Tsuruoka, H. Mizuta, M. Aono, *Adv. Funct. Mater.,* 2017, **27**, 1605104.
297. H. S. Majumdar, A. Bandyopadhyay, A. Bolognesi, A. J. Pal, *J. Appl. Phys.,* 2002, **91**, 2433-2437.
298. H. S. Majumdar, A. Bolognesi, A. J. Pal, *Thin Solid Film,* 2004, **446**, 296-300.
299. H. S. Majumdar, A. Bolognesi, A. J. Pal, *Synth. Met.,* 2004, **140**, 203-206.
300. H. S. Majumdar, C. Botta, A. Bolognesi, A. J. Pal, *Synth. Met.,* **2005**, **148**, 175-178.
301. S. K. Majee, H. S. Majumdar, A. Bolognesi, A. J. Pal. *Synth. Met.,* 2006, **156**, 828-832.
302. Q. D. Ling, Y. Song, S. L. Lim, E. Y. H. Teo, Y. P. Tan, C. X. Zhu, D. S. H. Chan, D. L. Kwong, E. T. Kang, K. G. Neoh, *Angew. Chem. Int. Ed.,* 2006, **45**, 2947-2951.
303. A.D. Yu, T. Kurosawa, Y.C. Lai, T. Higashihara, M. Ueda, C.L. Liu, W.C. Chen, *J. Mater. Chem.,* 2012, **22**, 20754-20763.
304. S. J. Liu, Q. Zhao, W. Huang, *Macromol. Rapid. Commun.,* 2010, **31**, 794-807.
305. S. J. Liu, Y. Chen, W. J. Xu, Q. Zhao, W. Huang, *Macromol. Rapid Commun.,* 2012, **33**, 461-480.
306. S. J. Liu, Z. H. Lin, Q. Zhao, Y. Ma, H. F. Shi, M. D. Yi, Q. D. Ling, Q. L. Fan, C. X. Zhu, E. T. Kang, W. Huang, *Adv. Funct. Mater.,* 2011, **21**, 979-985.
307. S. J. Liu, P. Wang, Q. Zhao, H. Y. Yang, J. Wong, H. B. Sun, X. D. Chen, W. P. Lin, W. Huang, *Adv. Mater.,* 2012, **24**, 2901-2905.
308. P. Wang, S. J. Liu, Z. H. Lin, X. C. Dong, Q. Zhao, W. P. Lin, M. D. Yi, S. H. Ye, C. X. Zhu, W. Huang, *J. Mater. Chem.,* 2012, **22**, 9576-9583.
309. S. J. Liu, W. P. Lin, M. D. Yi, W. J. Xu, C. Tang, Q. Zhao, S. H. Ye, X. M. Liu, W. Huang, *J. Mater. Chem.,* 2012, **22**, 22964-22970.
310. W. P. Lin, H. B. Sun, S. J. Liu, H. R. Yang, S. H. Ye, W. J. Xu, Q. Zhao, X. M. Liu, W. Huang, *Macromol. Chem. Phys.,* 2012, **213**, 2472-2478.
311. H. Shi, H. Sun, H. Yang, S. J. Liu, G. Jenkins, W. Feng, F. Li, B. Liu, W. Huang, *Adv. Funct. Mater.,* 2013, **23**, 3268-3276.
312. R. Rulkens, R. Resendes, A. Verma, I. Manners, K. Murti, E. Fossum, P. Miller, K. Matyjaszewski, *Macromolecules,* 1997, **30**, 8165-8171.
313. P. W. Cyr, M. Tzolov, I. Manners, E. H. Sargent, *Macromol. Chem. Phys.,* 2003, **204**, 915-921.
314. B. Padhan, S. K. Batabyal, A. J. Pal, *J. Phys. Chem. B,* 2006, **110**, 8274-8277.
315. J. Liu, Z. Yin, X. Cao, F. Zhao, A. Lin, L. Xie, Q. Fan, F. Boey, H. Zhang, W. Huang, *ACS Nano,* 2010, **4**, 3987-3992.
316. L. Li, Q. D. Ling, C. X. Zhu, D. S. H. Chan, E. T. Kang, K. G. Neoh, *J. Electrochem. Soc.,* 2008, **155**, H205-H209.
317. B. Zhang, Y. L. Liu, Y. Chen, K. G. Neoh, Y. X. Li, C. X. Zhu, E. S. Tok, E. T. Kang, *Chem. Eur. J.,* 2011, **17**, 10304-10311.
318. B. Zhang, Y. Chen, L. Xu, L. Zeng, Y. He, E. T. Kang, J. Zhang, *J. Polym. Sci. A: Polym. Chem.,* 2011, **49**, 2043-2050.
319. Y. Cao, X. Tian, J. Gu, B. Liu, B. Zhang, S. Song, F. Fan, Y. Chen, *Angew. Chem. Int. Ed., 2018*, **57**, 4543-4548.
320. S. Mühl, B. Beyer, *Electronics,* 2014, **3**, 444-461.
321. Z. Lv, Y. Zhou, S. T. Han, V. A. L. Roy, *Mater. Today,* 2018, **21**, 537-552.
322. R. J. Tseng, C. L. Tsai, L. P. Ma, J. Y. Ouyang, C. S. Ozkan, Y. Yang, *Nature Nanotech.,* 2006, **1**, 72-77.
323. N. G. Portney, R. J. Tseng, G. Destito, E. Strable, Y. Yang, *Appl. Phys. Lett.,* 2007, **90**, 214104.
324. K. Nagashima, H. Koga, U. Celano, F. Zhuge, M. Kanai, S. Rahong, G. Meng, Y. He, J. De Boeck, M. Jurczak, W. Vandervorst, T. Kitaoka, M. Nogi, T. Yanagida, *Sci. Rep-UK.,* 2014, **4**, 5532.
325. U. Celano, K. Nagashima, H. Koga, M. Nogi, F. Zhuge, G. Meng, Y. He, J. De Boeck, M. Jurczak, W. Vandervorst, T. Yanagida, *NPG Asia Mater.,* 2016, **8**, e310.
326. N. Raeis-Hosseini, J.S. Lee, *ACS Nano* 2015, **9**, 419-426.
327. N. Raeis-Hosseini, J.S. Lee, *Adv. Funct. Mater.,* 2015, **25**, 5586-5592.
328. N. Raeis-Hosseini, J.S. Lee. *ACS Appl. Mater. Interfaces,* 2016, **8**, 7326-7332.
329. F. Meng, L. Jiang, K. Zheng, C. F. Goh, S. Lim, H. H. Hong, J. Ma, F. Boey, X. Chen, *Small,* 2011, **7**, 3016-3020.
330. M. K. Hota, M. K. Bera, B. Kundu, S. C. Kundu, C. K. Maiti, *Adv. Funct. Mater.,* 2012, **22**, 4493-4499.
331. H. Wang, F. Meng, Y. Cai, L. Zheng, Y. Li, Y. Liu, Y. Jiang, X. Wang, X. Chen, *Adv. Mater.,* 2013, **25**, 5498-5503.
332. H. Wang, Y. Du, Y. Li, B. Zhu, W. R. Leow, Y. Li, J. Pan, T. Wu, X. Chen. *Adv. Funct. Mater.,* 2015, **25**, 3825-3831.
333. H. Wang, Z. Bowen, W. Hua, M. Xiaohua, H. Yue, X. Chen, *Small,* 2016, **12**, 3360-3365.
334. H. Wang, B. Zhu, X. Ma, Y. Hao, X. Chen, *Small,* 2016, **12**, 2715-2719.
335. Y. Xing, C. Shi, J. Zhao, W. Qiu, N. Lin, J. Wang, X. B. Yan, W. D. Yu, X. Y. Liu, *Small,* 2017, **13**, 1702390.
336. J. X. Zhu, W. L. Zhou, Z. Q. Wang, H. Y. Xu, Y. Lin, W. Z. Liu, J. G. Ma, Y. C. Liu, *RSC Adv,*. 2017, **7**, 32114-32119.
337. H. Furukawa, K. E. Cordova, M. O'Keeffe, O. M. Yaghi, *Science,* 2013, **341**, 974-987.
338. S. S.Y. Chui, S. M.F. Lo, J. P. H. Charmant, A. G. Orpen, I. D. Williams, *Science,* 1999, **283**, 1148-1150.
339. S. M. Yoon, S. C. Warren, B. A. Grzybowski *Angew. Chem., Int. Ed.,* 2014, **53**, 4437-4441.
340. M. J. Park, J. S. Lee. *RSC Adv.,* 2017, **7**, 21045-21049.
341. Y. Liu, H. Wang, W. Shi, W. Zhang, J. Yu, B. K. Chandran, C. Cui, B. Zhu, Z. Liu, B. Li, C. Xu, Z. Xu, S. Li, W. Huang, F. Huo, X. Chen, *Angew. Chem., Int. Ed.,* 2016, **55**, 8884-8888.
342. J. Choi, S. Park, J. Lee, K. Hong, D.H. Kim, C. W. Moon, G. D. Park, J. Suh, J. Hwang, S. Y. Kim, H. S. Jung, N.-G. Park, S. Han, K. T. Nam, H. W. Jang, *Adv. Mater.,* 2016, **28**, 6562-6567.
343. E. J. Yoo, M. Lyu, J.H. Yun, C. J. Kang, Y. J. Choi, L. Wang, *Adv. Mater.,* 2015, **27**, 6170-6175.
344. C. Gu, J. S. Lee, *ACS Nano,* 2016, **10**, 5413-5418.
345. J. Choi, Q. V. Le, K. Hong, C. W. Moon, J. S. Han, K. C. Kwon, P. R. Cha, Y. Kwon, S. Y. Kim, H. W. Jang, *ACS Appl. Mater. Interfaces,* 2017, **9**, 30764-30771.
346. X. J. Zhu, J. Lee, W. Lee, *Adv. Mater.,* 2017, **29**, 1700527.
347. B. Hwang, J.S. Lee, *Adv. Mater.,* 2017, ***29***, 1701048.
348. F. Zhou, Y. Liu, X. Shen, M. Wang, F. Yuan, Y. Chai, *Adv.*

Funct. Mater., **2018**, *28*, 1800080.

349. X. J. Zhu, W. Lu, *ACS Nano,* 2018, **12**, 1242-1249.